Introduction to

Computational Neuroscience

Hermann Riecke

Engineering Sciences and Applied Mathematics

Northwestern University

h-riecke@northwestern.edu

June 8, 2011

©2011 Hermann Riecke

These notes are based to a large extent on the book *Theoretical Neuroscience* by P. Dayan and L.F. Abbott (MIT Press).

To avoid copyright issues this version of the lecture notes does not include any of the figures.

Contents

Recommended Books:

Available online at the library:

- P. Dayan and L.F. Abbott, *Theoretical Neuroscience*, MIT Press, 2001.`http://cognet.mit.edu.turing.library.northwestern.edu/library/books/view?isbn=0262041995`

- G.B. Ermentrout and D. Terman, *Foundations of Mathematical Neuroscience*, 2010. `https://wamprod1.itcs.northwestern.edu/amserver/cdcservlet?TARGET=https%3A%2F%2Fsesame.library.northwestern.edu%3A443%2Fcgi-bin%2FssoEzpCheck.pl%3Furl%3Dezp.2aHR0cDovL2R4LmRvaS5vcmcvMTAuMTAwNy85NzgtMC0zODctODc3MDgtMg--&Requ`1232338061&MinorVersion=0&ProviderID=http%3A%2F%2Fsesame.library.northwestern.edu%3A80%2Famagent&MajorVersion=1&IssueInstant=2011-03-28T19%3A47%3A47Z`

References

[1] B. Bathellier, D.L. Buhl, R. Accolla, and A. Carleton. Dynamic ensemble odor coding in the mammalian olfactory bulb: sensory information at different timescales. *Neuron*, 57(4):586–598, Feb 2008.

[2] R. Ben-Yishai, R. L. Bar-Or, and H. Sompolinsky. Theory of orientation tuning in visual cortex. *Proc. Natl. Acad. Sci.*, 92:3844, 1995.

[3] P. R. Brotchie, R. A. Andersen, L. H. Snyder, and S. J. Goodman. Head position signals used by parietal neurons to encode locations of visual-stimuli. *Nature*, 375(6528):232–235, May 1995.

[4] J. J. Bussgang. Crosscorrelation functions of amplitude-distorted gaussian signals. Technical report, MIT, 1952.

[5] M. V. Chafee and P. S. Goldman-Rakic. Matching patterns of activity in primate prefrontal area 8a and parietal area 7ip neurons during a spatial working memory task. *J. Neurophysiol.*, 79(6):2919–2940, June 1998.

[6] E. J. Chichilnisky. A simple white noise analysis of neuronal light responses. *Network*, 12(2):199–213, May 2001.

[7] P. S. Churchland and T. J. Sejnowski. *The computational brain*. MIT, 1999.

[8] J. A. Connor and C. F. Stevens. Voltage clamp studies of a transient outward membrane current in gastropod neural somata. *J. Physiol.*, 213(1):21, 1971.

[9] J. A. Connor, D. Walter, and R. Mckown. Neural repetitive firing - modifications of hodgkin-huxley axon suggested by experimental results from crustacean axons. *Biophys. J.*, 18(1):81–102, 1977.

[10] P. Dayan and L. F. Abbott. *Theoretical Neuroscience*. MIT Press, 2001.

[11] G. C. DeAngelis, I. Ohzawa, and R. D. Freeman. Receptive-field dynamics in the central visual pathways. *Trends Neurosci.*, 18(10):451–458, October 1995.

[12] A. Destexhe, D. Contreras, M. Steriade, T. J. Sejnowski, and J. R. Huguenard. In vivo, in vitro and computational analysis of dendritic calcium currents in thalamic reticular neurons. *J. Neurosci.*, 16:169, 1996.

[13] A. Destexhe, Z.F. Mainen, and T.J. Sejnowski. Synthesis of models for excitable membranes, synaptic transmission and neuromodulation using a common kinetic formalism. *J Comput Neurosci*, 1(3):195–230, Aug 1994.

[14] G. B. Ermentrout and N. Kopell. Parabolic bursting in an excitable system coupled with a slow oscillation. *SIAM J. Appl. Math.*, 46(2):233–253, April 1986.

[15] G. B. Ermentrout and D. H. Terman. *Foundations of Mathematical Neuroscience*. 2010.

[16] M. O. Ernst and M. S. Banks. Humans integrate visual and haptic information in a statistically optimal fashion. *Nature*, 415(6870):429–433, Jan 2002.

[17] G. D. Field and E. J. Chichilnisky. Information processing in the primate retina: Circuitry and coding. *Annu. Rev. Neurosci.*, 30(4):1–30, 2007.

[18] I. M. Finn, N. J. Priebe, and D. Ferster. The emergence of contrast-invariant orientation tuning in simple cells of cat visual cortex. *Neuron*, 54(1):137–152, April 2007.

[19] F. Gabbiani and S. J. Cox. *Mathematics for Neuroscientists*. 2010.

[20] F. Gabbiani, W. Metzner, R. Wessel, and C. Koch. From stimulus encoding to feature extraction in weakly electric fish. *Nature*, 384(6609):564–567, Dec 1996.

[21] M. N. Geffen, De Vries S. E. J., and M. Meister. Retinal ganglion cells can rapidly change polarity from Off to ON. *PLoS Biology*, 5(3):065, March 2007.

[22] F. A. Geldard and C. E. Sherrick. The cutaneous "rabbit": a perceptual illusion. *Science*, 178(4057):178, 1972.

[23] D. Goldreich. A bayesian perceptual model replicates the cutaneous rabbit and other tactile spatiotemporal illusions. *PLoS ONE*, 3:e333, 2007.

[24] M. S. Graziano, X. T. Hu, and C. G. Gross. Visuospatial properties of ventral premotor cortex. *J. Neurophysiol.*, 77(5):2268–2292, May 1997.

[25] H. K. Hartline. Visual receptors and retinal interaction. *Science*, 164:270, 1969.

[26] H. K. Hartline and F. Ratliff. Inhibitory interaction of receptor units in the eye of limulus. *J. Gen. Physiol.*, 40(3):357–376, 1957.

[27] J. Hertz, A. Krogh, and R. G. Palmer. *Introduction to the theory of neural computation*. Addison-Wesley, 1991.

[28] A. L. Hodgkin and A. F. Huxley. A quantitative description of membrane current and its applicaiton to conduction and excitation in nerve. *J. Physiol.*, 117:500, 1952.

[29] A. L. Hodgkin, A. F. Huxley, and B. Katz. Measurement of current-voltage relations in the membrane of the giant axon of loligo. *J. Physiol.*, 116:424, 1952.

[30] A. L. Hodgkin and B. Katz. The effect of sodium ions on the electrical activity of the giant axon of the squid. *J. Physiol.*, 108:37, 1949.

[31] J. J. Hopfield. Neural networks and physical systems with emergent collective computational abilities. *Proc. N. Acad. U.S.A*, 79(8):2554–2558, 1982.

[32] D. H. Hubel and T. N. Wiesel. Receptive fields, binocular interaction and functional architecture in cats visual cortex. *J. Physiol.*, 160(1):106, 1962.

[33] J. R. Huguenard and D. A. Mccormick. Simulation of the currents involved in rhythmic oscillations in thalamic relay neurons. *J. Neurophysiol.*, 68(4):1373–1383, October 1992.

[34] E. M. Izhikevich. Simple model of spiking neurons. *IEEE Trans. Neural Netw.*, 14(6):1569–1572, November 2003.

[35] E. M. Izhikevich. Which model to use for cortical spiking neurons? *IEEE Trans. Neural Netw.*, 15(5):1063–1070, September 2004.

[36] E. M. Izhikevich. *Dynamical Systems in Neuroscience: the geometry of excitability and bursting*. MIT Press, 2005.

[37] T. Jarsky, A. Roxin, W. L. Kath, and N. Spruston. Conditional dendritic spike propagation following distal synaptic activation of hippocampal ca1 pyramidal neurons. *Nature Neurosc.*, 8(12):1667–1676, December 2005.

[38] E. R. Kandel, J. H. Schwartz, and T. M. Jessel. *Principles of neural science*. McGraw-Hill, 2000.

[39] J. Keener and J. Sneyd. *Mathematical Physiology*. Springer, 1998.

[40] B. W. Knight, J. I. Toyoda, and F. A. Dodge. A quantitative description of dynamics of excitation and inhibition in eye of limulus. *J. Gen. Physiol.*, 56(4):421, 1970.

[41] V. I. Krinskii and IuM Kokoz. Analysis of the equations of excitable membranes. I. reduction of the Hodgkins-Huxley equations to a 2d order system. *Biofizika*, 18(3):506–511, May-Jun 1973.

[42] L. Lapicque. Quantitative investigations of electrical nerve excitation treated as polarization (translated by N. Brunel and M.C.W. van Rossum in Biol. Cyber. 97 (2007) 341). *J. Physiol. Pathol. Generale*, 9:620, 1907.

[43] H. Markram, Y. Wang, and M. Tsodyks. Differential signaling via the same axon of neocortical pyramidal neurons. *Proc Natl Acad Sci U S A*, 95(9):5323–5328, Apr 1998.

[44] D. A. Mccormick and T. Bal. Sleep and arousal: Thalamocortical mechanisms. *Annu. Rev. Neurosci.*, 20(13):185–215, July 1997.

[45] D. A. McCormick and H. C. Pape. Properties of a hyperpolarization-activated cation current and its role in rhythmic oscillation in thalamic relay neurones. *J Physiol*, 431:291–318, Dec 1990.

[46] W. S. Mcculloch and W. Pitts. A logical calculus of the ideas immanent in nervous activity (reprinted from bulletin of mathematical biophysics, vol 5, pg 115-133, 1943). *Bull. Math.Biol.*, 52(1-2):99–115, 1990.

[47] J. L. Mcfarland and A. F. Fuchs. Discharge patterns in nucleus-prepositus-hypoglossi and adjacent medial vestibular nucleus during horizontal eye-movement in behaving macaques. *J. Neurophysiol.*, 68(1):319–332, July 1992.

[48] A. M. Pastor, R. R. de la Cruz, and R. Baker. Eye position and eye velocity integrators reside in separate brain-stem nuclei. *Proc. N. Acad. U.S.A*, 91(2):807–811, January 1994.

[49] W. H. Press, S. A. Teukolsky, W. T. Vetterling, and B. P. Flannery. Numerical recipes, 2007.

[50] R. Rieke, D. Warland, R. de Ruyter van Steveninck, and W. Bialek. *Spikes. Exploring the neural code*. MIT, 1999.

[51] E. Salinas and L. F. Abbott. Transfer of coded information from sensory to motor networks. *J. Neurosci.*, 15(10):6461–6474, October 1995.

[52] H. S. Seung, D. D. Lee, B. Y. Reis, and D. W. Tank. Stability of the memory of eye position in a recurrent network of conductance-based model neurons. *Neuron*, 26(1):259–271, April 2000.

[53] M. N. Shadlen and W. T. Newsome. The variable discharge of cortical neurons: Implications for connectivity, computation, and information coding. *J. Neurosci.*, 18(10):3870–3896, May 1998.

[54] G. M. Shepherd. *Neurobiology*. Oxford University Press, 1988.

[55] S. M. Sherman. Thalamic relays and cortical functioning. In S.M. Sherman V.A. Casagrande, R.W. Guillery, editor, *Cortical function: a view from the thalamus*, page 107. Elsevier, 2005.

[56] A. P. Sripati, T. Yoshioka, P. Denchev, S. S. Hsiao, and K. O. Johnson. Spatiotemporal receptive fields of peripheral afferents and cortical area 3b and 1 neurons in the primate somatosensory system. *J. Neurosci.*, 26(7):2101–2114, February 2006.

[57] P. Stern, F. A. Edwards, and B. Sakmann. Fast and slow components of unitary epscs on stellate cells elicited by focal stimulation in slices of rat visual cortex. *J Physiol*, 449:247–278, Apr 1992.

[58] T. Trappenberg. *Fundamentals of Computational Neuroscience*. Oxford, 2009.

[59] M. Tsodyks, K. Pawelzik, and H. Markram. Neural networks with dynamic synapses. *Neural Comput.*, 10(4):821–835, May 1998.

[60] A. L. van der Meer, F. R. van der Weel, and D. N. Lee. The functional-significance of arm movements in neonates. *Science*, 267(5198):693–695, February 1995.

[61] J. Ma W, J. M Beck, P. E Latham, and A. Pouget. Bayesian inference with probabilistic population codes. *Nature Neurosci.*, 2006.

[62] K. A. Zaghloul, K. Boahen, and J. B. Demb. Contrast adaptation in subthreshold and spiking responses of mammalian y-type retinal ganglion cells. *J. Neurosci.*, 25(4):860–868, January 2005.

1   Interesting and Fun Links

Here is a list of (randomly obtained) links that are of interest for this class or just plain neural fun.

- Flash movie of ions participating in action potential
  `http://www.brainu.org/action_potential_cartoon.swf`

- Movies by Rudolph and Destexhe
  `http://cns.iaf.cnrs-gif.fr/alain_movies.html`

- Graphical Hodgkin-Huxley Simulator
  `http://www.cs.cmu.edu/~dst/HHsim/`
  this simulator is also available as Matlab source code.

- GUI for Izhikevich's Simple Model [34]
  `http://vesicle.nsi.edu/users/izhikevich/publications/whichmod.htm#izhikevich`

- Illusions:

  - Optical illusions and other visual phenomena
    `http://www.michaelbach.de/ot/index.html`
  - Animated Necker cube
    `http://www.dogfeathers.com/java/necker.html`
  - Barber Pole Illusion:
    `http://www.psychologie.tu-dresden.de/i1/kaw/diversesMaterial/www.illusionworks.com/html/barber_pole.html`
  - Moving Rhombus:
    `http://www.cs.huji.ac.il/~yweiss/Rhombus/`
  - More optical illusions:
    `http://www.purveslab.net/seeforyourself/ http://web.mit.edu/persci/index.html`
  - Best Illusion Contests:
    `http://illusioncontest.neuralcorrelate.com/`

- Many interesting aspects of the brain
  `http://www.youramazingbrain.org.uk/`
  illusions of various kinds
  `http://www.youramazingbrain.org.uk/supersenses/default.htm`

2   Introduction

What is the purpose of the brain?

- based on sensory input

    - mouse sees cat, frog sees a fly, ...

- and past experience (memory)

    - learning from experience (narrow escape, tasty), ...
      [even bees and flies can be trained: extend proboscis, flying left or right in a
      T-channel,...]

- the organism must decide what to do and then give generate motor output

    - jump, eta, run
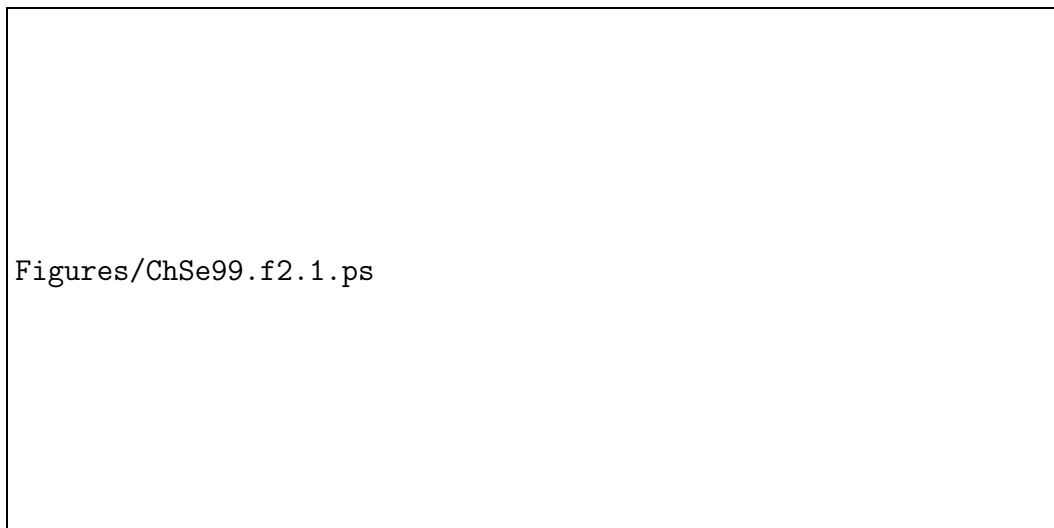

Figures/ChSe99.f2.1.ps

Figure 1: The multiple scales of the brain [54] (reproduced in [7]) .

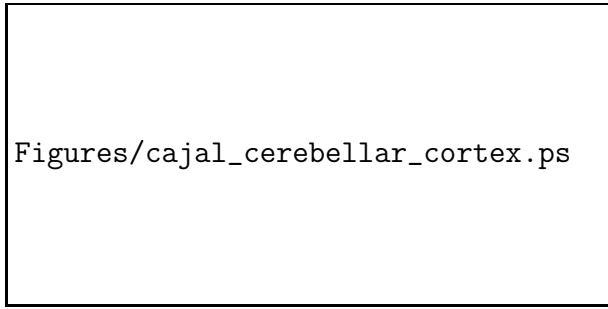Studying brain function requires studies at a wide range of scales:

- behavior of the animal

- brain regions:
  anatomy, connectivity between the regions, activities of the regions related to
  behavior (e.g. fMRI measuring blood-oxygen-level-dependent (BOLD) signal)
  note extensive feed-back between different regions (*not* marked in Fig.1)

- circuits within brain regions:
  e.g. mammalian cortex is arranged in columns (half a million, each$\sim 0.5mm$ wide, $\sim 2mm$ thick containing $\sim 50,000$ neurons)
  columns have 6 layers: input, output to other columns, to other cortical areas, to spinal cord and other areas outside of cortex
  simpler circuits controling breathing, locomotion (worms), stomach grinding (lobster),...

- individual neurons:
  wide variety of types with different characteristics: excitatory, inhibitory, wide spread in morphology
  neurons consist of

    - soma with nucleus (DNA and chemical machinery like in other cells that is needed for metabolism)

    - axon: output of information to other neurons via an electric pulse (action potential), currents are carried by ions

    - dendrite: input of information from other neurons as a result of their action potential

Figures/webvision.med.utah.edu.visualcortex.ps

Figure 2: Different neuron morphologies in visual cortex. `webvision.med.utah.edu/ VisualCortex.html`
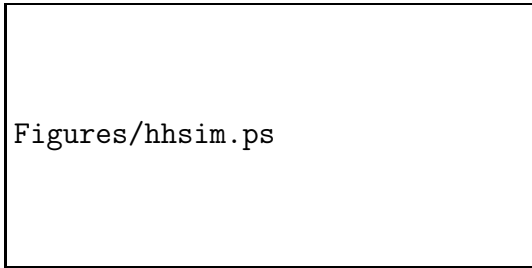
Figures/cajal_cerebellar_cortex.ps

Figure 3: Purkinje cells (A) and basket cells (B) in cerebellar cortex.

- dendrites themselves can serve as computational units: inputs can gate other inputs

- electric activity of neuron due to ion channels across the cell membrane

  - they consist of a combination of a few large molecules, e.g. 4 molecules in K^+-channel (tetramer)

  - ion concentrations are different inside and outside of the cell (e.g. Na^+ much higher outside)

  - ion channels typically permeable only to certain types of ions (e.g., Na^+ and not K^+, etc.)

  - ion channels open and close depending on voltage across membrane (voltage-gated) $\Rightarrow$ resulting currents change voltage, which affects in turn ion channels
    neurons are nonlinear devices: *excitable* by sufficiently strong external input $\Rightarrow$ action potential

Figures/hhsim.ps

Figure 4: Action potential simulation `http://www.cs.cmu.edu/~dst/HHsim/`.

- large number of synapses provide connection between different neurons, mostly between axons and dendrites (~ 2 synapses/μm of dendritic length, total $\mathcal{O}(10,000)$, can be $\mathcal{O}(100,000)$ for Purkinje cell)

  - neurotransmitters are released from pre-synaptic terminal and diffuse across the narrow synaptic cleft between the cells

- neurotransmitters activate numerous types of receptors

  - similarly to ion channels, receptors are comprised of a combination of a few large molecules, e.g. $AMPA$-receptor is a tetramer

  - binding of the neurotransmitter to the receptor opens an ion channel and modifes voltage of post-synaptic cell

- genetics

  - different cells express different sub-units of receptors or ion channels giving them different properties

Computational and theoretical approaches:

- detailed modeling at a given level/scale :
  individual ion channel, single synapse, single neuron, possibly circuit consisting of few neurons, ...
  extracting sufficiently many parameters from experiments is a challenge

- effective models to identify essential mechanisms of brain functions:
  networks of minimal models of neurons, interaction of neural populations representing brain areas
  e.g. origin of oscillations, principles of memory

- statistical approaches and information theory:
  encoding of information (e.g. sensory) in spike trains: mean firing rate, timing of individual spikes, correlation between spikes? Decoding the spike trains.
  optimality considerations: 'natural scenes' $\Rightarrow$ suggestions for brain function or architecture (e.g. early visual processing: what type of information should the retina transmit to the brain?)

3   Single Neuron

3.1   Passive, Single-Compartment Neuron[1]

Neurons are bounded by a membrane comprised of a lipid bilayer

- hydrophilic heads oriented towards electrolyte (extra- and intra-cellular fluid)

- hydrophobic tails inside the membrane

- electric insulator

---

[1]Dayan & Abbott: DA 5.2

Across the membrane a charge can build up: capacitance C

$$Q = CV \qquad C = \frac{Q}{V}$$

Units:
charge $[Q]$=Coulomb, voltage $[V]$=Volt, capacitance $[C]$=Farad

Convention:

- The potential outside the cell is defined to be 0

- Positive current is defined to be *outward*:
  positive charges flow out of the cell and decrease the potential inside the cell:
  V becomes negative

Typical voltages are in the range $-90mV$ to $+50mV$. These voltages are not far above the thermal range: at physiological temperatures T the thermal energy corresponds to a voltage

$$V_T = \frac{k_B T}{q} \sim 25mV$$

and thermal fluctuations can almost move charges aross these voltages (k_B is the Boltzmann constant, q the charge of an electron) $\Rightarrow$ expect *noisy* dynamics (i.e. even for fixed voltage, i.e. in voltage clamp, the current should be expected to fluctuate)

A change in the voltage across the layer requires a current I

$$I \equiv \frac{d}{dt} Q = C \frac{d}{dt} V$$

The capacitance increases with surface area

$$C = cA \qquad c \sim 1 \frac{\mu F}{cm^2} = 10 \frac{nF}{mm^2}$$

Typical cell areas are 0.01 to $0.1 \; mm^2$:

$$C \sim 0.1 \ldots 1 nF$$

Axial current flow in the intracellular medium enclosed by the double-layer membrane experiences a resistance R.

For a cylinder of length L and area A one has

$$R = r \frac{L}{A} \qquad r \sim 1 \ldots 3 \, k\Omega \cdot mm = 100 \ldots 300 \Omega \cdot cm$$

- Resistance increases with L (circuit of resistors in series)

- Resistance decreases with A (circuit of parallel resistors)

- $\rightarrow$ unit: $[r] = \Omega \cdot m$

Current flow *across* the membrane possible through ion channels

- proteins embedded in membrane

- allow ions to diffuse through membrane

- proteins can be selective for specific ions
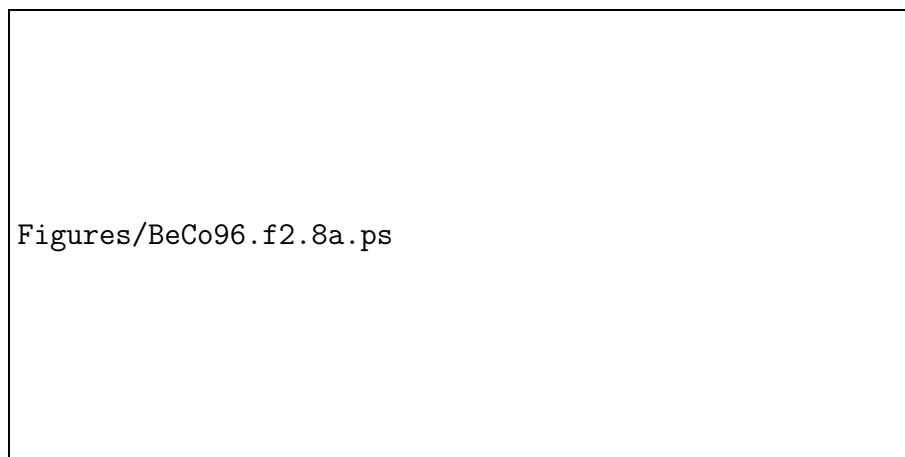 $\rightarrow$ many different types of ion channels

Figures/BeCo96.f2.8a.ps

Figure 5: Ion channels in membrane.

Estimate of channel conductance $1/R$ assuming that channel pore corresponds to a cylinder of cellular fluid:

- $L \sim 6nm$, $A \sim 0.15nm^2$: $1/R = 25pS = 25 \cdot 10^{-12}S$

- unit is *Siemens*: $1\,S\ = 1\Omega^{-1}$

- the channels cover the membrane: *conductance density* g
  unit: $[g] = pS/cm^2$

The membrane resistance depends on the density of open channels. It can vary substantially. For neuron in resting state *specific membrane resistance* r_m

$$r_m \sim 1M\Omega\,mm^2 \qquad R_m = \frac{r_m}{A} \sim 10\ldots100M\Omega$$

Unit: $[r_m] = \Omega m^2$ since channels correspond to resistors in parallel and *conductance* is proportional to membrane area.

Equivalent Circuit:

Kirchhoff's law:

the ions of the injected current I_e flow either back out of the cell via the membrane current I_m or they increase the charge on the membrane corresponding to a capacitive current I_C

$$I_e = I_m + I_C = \frac{V}{R_m} + C\frac{dV}{dt}$$

i.e.

$$\frac{dV}{dt} = -\frac{1}{R_m C}V + \frac{1}{C}I_e$$

Introducing the membrane time constant $\tau_m = R_m C$ one gets

$$\tau_m \frac{dV}{dt} = -V + R_m I_e \tag{1}$$

Steady state

$$V_{ss} = R_m I_e$$

Relaxation towards steady state[2]

$$V(t) = R_m I_e \left(1 - e^{-\frac{t}{R_m C}}\right) \qquad \text{for} \ \ V(0) = 0.$$

Exponential relaxation with time constant $\tau_m = R_m C$.
Typical value: $\tau_m \sim 1 ms$.

3.2 Ion Channels[3]

The ion flux through the ion channels depends on the ion concentrations and the voltage across the membrane.
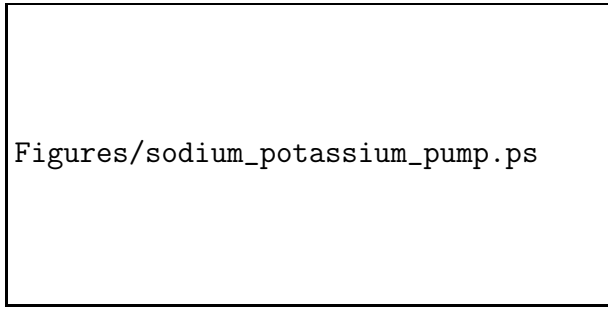
The ion concentrations inside and outside the cell are typically different:

- $[Na^+]$ and $[Ca^{2+}]$ higher outside the cell

- $[K^+]$ lower outside the cell

These differences are maintained by active ion pumps. Their activity requires metabolic energy (ATP).

---

[2]The general solution of a linear, inhomogeneous ode like (1) is given by the general solution V_h of the homogeneous equation $\tau_m dV/dt = -V$ (here $V_h = Ae^{-t/\tau_m}$) and any particular solution V_p of the inhomogeneous equation (1) (here $V_p = V_{ss}$).

[3]DA 5.2

Figure 6: Na^+-K^+-exchange pump.
Movie http://highered.mcgraw-hill.com/olc/dl/120068/bio03.swf

Combined with the semi-permeability of the membrane the concentration differences lead in the steady state to a difference in the electrical potential across the membrane: the current across the membrane vanishes for a non-zero voltage called the *reversal potential*.

Nernst equation:

Consider only single ion species, e.g. $[Na^+]$, and a single ion channel for now:

- $V = 0$

    - number of ions that enter channel from inside is proportional to $[Na^+]_{inside}$

    $$j_{out}(V = 0) = k[Na^+]_{inside}$$

    with k some constant (related to the mobility of the ions).

    - number of ions that enter channel from outside is proportional to $[Na^+]_{outside}$

    $$j_{in}(V = 0) = k[Na^+]_{outside}$$

    - for $[Na^+]_{outside} > [Na^+]_{inside}$ ions flux is inward: this flux leads to a net positive charge inside and a net negative charge outside: V becomes positive

- for $V > 0$

    - potential is *higher* inside the cell and only those Na^+ ions can enter the cell that have an enough energy (above qV) to overcome the potential energy barrier

    - probability distribution for the energy of the ions

    $$p(E)dE = Ne^{-\frac{E}{k_B T}}dE$$

    with normalization

    $$\int_0^\infty p(E)dE = 1 \qquad \Rightarrow \qquad N = \frac{1}{k_B T}$$

17

– fraction of ions with energy above $E_0 = zqV_0$

$$P(E > E_0) = \int_{E_0}^{\infty} p(E)dE = e^{-\frac{zqV_0}{k_BT}}$$

– the flux against the positive potential is therefore given by

$$j_{in}(V) = k\,[Na^+]_{outside}e^{-\frac{zqV}{k_BT}}$$

($z = 1$ for Na^+).

– ions leaving the cell need not overcome an energy barrier

$$j_{out}(V) = j_{out}(V = 0) = k[Na^+]_{inside}$$

• for a certain voltage, $V = E_{Na^+}$, the system is in *equilibrium* the two fluxes balance

$$j_{in}(V = E_{Na^+}) = j_{out}$$

The reversal potential E_{Na^+} for Na^+ is given by the Nernst equation (for Na^+ one has $z = 1$)

$$E_{Na^+} = \frac{V_T}{z} \ln\left(\frac{[Na^+]_{outside}}{[Na^+]_{inside}}\right) \qquad V_T = \frac{k_BT}{q}.$$

Notes:

• For $V < E_{Na^+}$ the electric field (potential barrier) is not strong enough to keep the Na^+ from entering the cell $\Rightarrow$ more positive charges flow into the cell and make the potential more positive, i.e. V approaches E_{Na^+} and conversely for $V > E_{Na^+}$.
$\Rightarrow$ For fixed concentrations $[Na^+]_{inside,outside}$ the ion flux pushes the voltage towards the reversal potential E_{Na^+}.

Squid	Na^+	K^+	Cl^-	Ca^{2+}
intracellular concentration	50mM	400mM	40mM	
extracellular concentration	440mM	20mM	550mM	
ratio of concentrations ext/int	8.8	0.05	14	
Nernst reversal potential	+56mV	-77mV	-68mV	

Birds/Mammals	Na^+	K^+	Cl^-	Ca^{2+}
intracellular concentration	12mM	155mM	4mM	100nM
extracellular concentration	150mM	4mM	120mM	1.5mM
ratio of concentrations ext/int	12.5	0.03	30	15,000
Nernst reversal potential	+67mV	-98mV	-90mV	130mV

Table 1: Rough values of concentrations. Birds and mammals have much lower concentrations than marine invertebrates

• Thus, opening Na^+-channels drive the potential to positive values, while $K^+-$and Cl^--channels hyperpolarize cells to negative potentials.

18

- In thermodynamic equilibrium it does not matter how ions diffuse through the channel: result is independent of the mobility k.

- If multiple ion species diffuse across the membrane, the steady state does in general *not* correspond to thermodynamic equilibrium:

  - ion fluxes can cancel each other:
    although charge flux vanishes the individual ion fluxes may be non-zero
  - the ion fluxes must be treated explicitly

Goldman-Hodgkin-Katz Equation[4]

In general:

multiple ions species diffuse across channel $\Rightarrow$ to get the steady state, i.e. the rest potential, we need the ion flux $\mathbf{j}_\phi$ driven by the electric field $\mathbf{E} = -\nabla\phi$ for each species

Planck's equation

$$\mathbf{j}_\phi = \underbrace{-zq\nabla\phi}_{\text{force on ion}} \quad \underbrace{\frac{D}{k_B T}}_{\text{drag coefficient}} \quad c = -u\frac{z}{|z|}c\nabla\phi$$

with

- z: valence of ion (zq is total charge of ion)

- u: mobility of ion: includes the magnitude of the charge, more strongly charged ions have larger u
  related to Fick's diffusion constant D

$$u = \frac{|z|q}{k_B T}\, D$$

- c: concentration of the ion species

Total ion flux

$$\mathbf{j} = -D\left(\nabla c + \frac{zq}{k_B T}\, c\nabla\phi\right)$$

In general the electric field $\nabla\phi$ depends on the charge distribution $\rho(\mathbf{r})$ through the Poisson equation

$$\nabla^2\phi = -\frac{1}{\epsilon}\,\rho(\mathbf{r}) \qquad \epsilon = \text{dielectric constant of the medium}$$

Charge density changes due to the current $\mathbf{j} \Rightarrow$ coupled equations for ϕ and $\mathbf{j}$ (Poisson-Nernst-Planck equations)
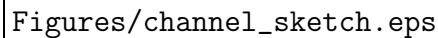
---

[4]Keener&Sneyd 2.6.2

Figure 7: Modeling one-dimensional ion channel.

Simplify for short, narrow channel:

- consider the steady state: all quantities are time-independent

- assume all quantities depend only on the x-coordinate along the channel: one-dimensional model:
$$\nabla c \rightarrow \frac{dc}{dx} \qquad \nabla \phi = \frac{d\phi}{dx}$$
choose coordinates such that inside of the cell is for $x < 0$ and outside of the cell is for $x > L$:
$$V = \phi(0) - \phi(L)$$

- assume that the electric field independent of position in the channel:
$$\frac{d\phi}{dx} = \frac{\phi(L) - \phi(0)}{L} = -\frac{V}{L}$$

This yields the differential equation
$$\frac{dc}{dx} - \alpha c + \frac{j}{D} = 0 \qquad \text{with } \alpha = \frac{zq}{k_B T} \frac{V}{L}$$

with boundary conditions
$$c(0) = c_{inside} \qquad c(L) = c_{outside}$$

Note:

- a first order differential equation has only a single free parameter: how can we satisfy *both* boundary conditions? The boundary conditions will pose an additional condition on a parameter in the equation: it will determine j.

Using integrating factor $e^{-\alpha x}$
$$e^{-\alpha x} \left(\frac{dc}{dx} - \alpha c \right) = -e^{-\alpha x} \frac{j}{D}$$

can be written as
$$\frac{d}{dx} \left(e^{-\alpha x} c(x) \right) = -e^{-\alpha x} \frac{j}{D}$$

integrating from $x = 0$ to x yields

$$e^{-\alpha x} c(x) - c(0) = \frac{1}{\alpha} \frac{j}{D} \left(e^{-\alpha x} - 1 \right)$$

with $c(0) = c_{inside}$.

To satisfies the boundary condition at $x = L$ the flux j has to satisfy the condition

$$j = \alpha D \frac{c_{inside} - e^{-\alpha L} c_{outside}}{1 - e^{-\alpha L}}$$

To get a current density j_e we need to multiply j with the charge of the ions. Measuring c in moles/volume the charge per volume is $\rho = zFc$ with F the Faraday constant (charge of 1 Mole of single-valence ions).

This yields the **Goldman-Hodgkin-Katz current equation**

$$j_e = \frac{z^2 F q}{k_B T} P V \frac{c_{inside} - e^{-\alpha L} c_{outside}}{1 - e^{-\alpha L}} \qquad \text{with} \qquad \alpha L = \frac{zq}{k_B T} V \qquad (2)$$

with membrane permeability

$$P = \frac{D}{L}$$

Notes:

- the current-voltage relationship $j_e(V)$ is nonlinear *(through α)*

- the membrane permeability in general will depend on the channel and the ion species

Now we can consider cells with multiple ion species c^i

$$j_e = \sum_i j_e^i$$

In the steady state the total current density j_e must vanish.

For simplicity consider single-valence ions, $z = \pm 1$, with concentrations $c^{i\pm}$

$$0 = \sum_{i+} P_{i+} \frac{c_{inside}^{i+} - c_{outside}^{i+} e^{-\frac{q}{k_B T} V}}{1 - e^{-\frac{q}{k_B T} V}} + \sum_{i-} P_{i-} \frac{c_{inside}^{i-} - c_{outside}^{i-} e^{\frac{q}{k_B T} V}}{1 - e^{\frac{q}{k_B T} V}}$$

rewrite it as

$$0 = \sum_{i+} P_{i+} \frac{c_{inside}^{i+} - c_{outside}^{i+} e^{-\frac{q}{k_B T} V}}{1 - e^{-\frac{q}{k_B T} V}} + \sum_{i-} P_{i-} \frac{c_{inside}^{i-} e^{-\frac{q}{k_B T} V} - c_{outside}^{i-}}{e^{-\frac{q}{k_B T} V} - 1}$$

$$0 = \sum_{i+} P_{i+} \left(c_{inside}^{i+} - c_{outside}^{i+} e^{-\frac{q}{k_B T} V} \right) - \sum_{i-} P_{i-} \left(c_{inside}^{i-} e^{-\frac{q}{k_B T} V} - c_{outside}^{i-} \right)$$

One can solve this equation for V

$$V_{GHK} = \frac{k_B T}{q} \ln \left(\frac{\sum_{i+} P_{i+} c_{outside}^{i+} + \sum_{i-} P_{i-} c_{inside}^{i-}}{\sum_{i+} P_{i+} c_{inside}^{i+} + \sum_{i-} P_{i-} c_{outside}^{i-}} \right) \tag{3}$$

Notes:

- for a single ion species V_{GHK} reduces to Nernst reversal potential[5]. For multiple species the concentrations are weighted with their respective permeability.

- at the rest potential $V = V_{GHK}$

  - the electric current across the membrane vanishes
  - the concentration currents of the various ion species do in general *not vanish*
  - the concentration differences across the membrane need to be maintained by ion pumps to maintain the steady state

- the result depends in particular on the assumption of a spatially constant electric field along the channel. Depending on the channel type this assumption may or may not be a good approximation.

- unlike the Nernst potential the GHK-result is not universal: P depends on the mobility of the various ion species in that channel

- for the standard three ion species one gets (for $z = \pm 1$)

$$V_{GHK} = \frac{k_B T}{q} \ln \left(\frac{P_{Na}[Na^+]_{outside} + P_K[K^+]_{outside} + P_{Cl}[Cl^-]_{inside}}{P_{Na}[Na^+]_{inside} + P_K[K^+]_{inside} + P_{Cl}[Cl^-]_{outside}} \right)$$

For example

	Na^+	K^+	Cl^-	Ca^{2+}
intracellular concentration	15mM	100mM	13mM	
extracellular concentration	150mM	5mM	150mM	
ratio of concentrations	10	0.05	11.5	
Nernst Potential	+62mV	-80mV	-65mV	
P/P_K	0.025	1	0.1	

Because of the high membrane permeability for K^+ the resting membrane potential is dominated by the K^+ ions with a slight depolarization by Na^+.

3.3 The Hodgkin-Huxley Model

- How do neurons function?

---

[5]Note that in the derivation of (3) we have assume $z = \pm 1$.

- What makes the action potential?

- What is a good mathematical model for it?

Bernstein:

- measured action potentials (1968)

- based on Nernst equation and knowledge of the concentration difference across membrane suggested that membrane is semi-permeable to K^+: $V_{rest} \sim -70mV$ (1912)

- speculated that during action potential membrane becomes permeable to all types of ions, which would lead to a break-down of the membrane potential.

Cole and Curtis (1940):

- establish that conductance of membrance changes significantly during action potential

Membrane currents can still not be measured directly until Cole and Marmont develop *space clamp technique* (1940's): insert very narrow electrode down the center of the axon to make voltage spatially uniform and measure associated current.

Figures/KeSn98.f4.1.ps
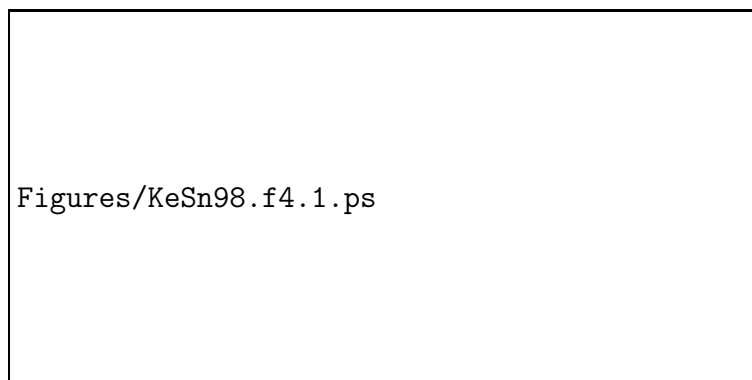
Figure 8: The giant squid axon is not an axon from the 'giant squid' (from [39])

To measure currents and action potentials in axons they used the giant axon of squid: 100 times thicker than axons in mammals, made experiments feasible.

Hodgkin and Curtis independently show that during action potential the voltage *overshoots*, i.e. crosses $V = 0$: Bernstein's suggestion of a general permeability of the membrane cannot be correct.

Hodgkin and Katz (1949):

- identify Na^+ as essential for action potential generation by reducing $NaCl$ in extracellular fluid by replacing it with some other substance like dextrose or choline chloride (membrane is impermeable to choline ions)

```
Figures/HoKa49.f4.ps
```
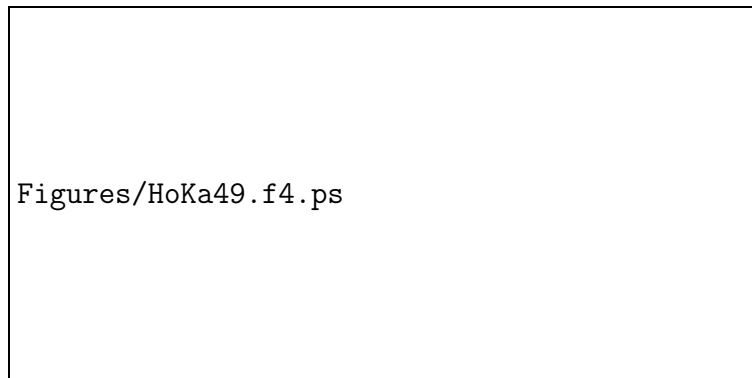
Figure 9: Reduction of action potential upon partial replacement of extracellular seawater by dextrose, reducing extracellular $[Na^+]$. a) 67% dextrose, b) 50%, c) 29%. Curve 1 and 3 (wash-out) are with seawater [30]

- this explains the overshoot, since Na^+ has positive reversal potential

- permeability of membrane must change selectively for ions: there must be a period during which the permeability for Na^+ dominates

Hodgkin and Huxley (1952, 5 papers, one with Katz)

- measure currents as a function of membrane voltage:

    – membrane is rectifying (Fig.10)
      * hyperpolarization beyond rest potential ($V < V_{rest}$) induces no current
      * depolarization induces *time-dependent* current
        · initially negative (inward) current
          the inward current *depolarizes* the membrane further
        · later positive (outward) current

```
Figures/HoHu52a.f11.ps
```
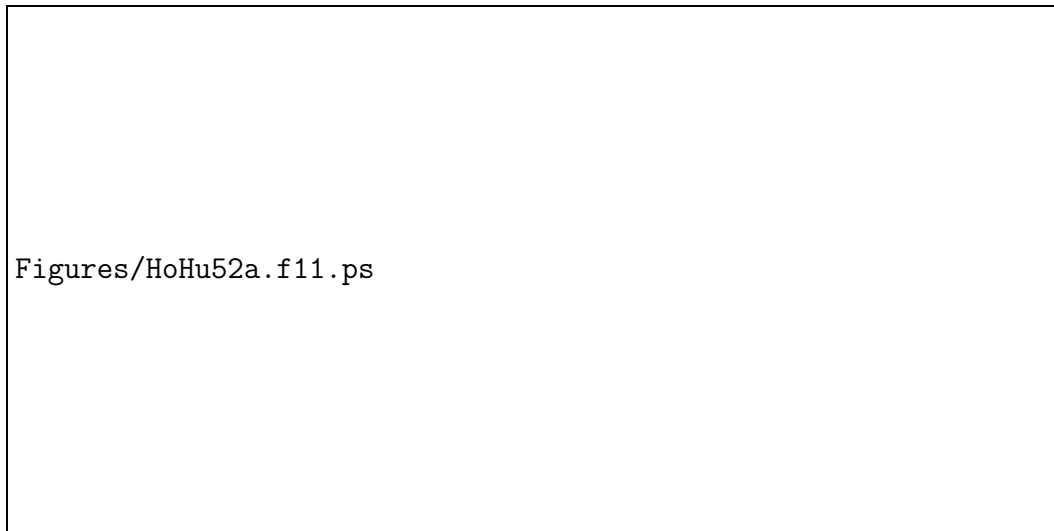
Figure 10: Channels are rectifying: no current for hyperpolarization (to -130mV, top), transient current for depolarization (to 0mV, bottom figure). Note: sign convention of current opposite to the one used nowadays. [29]

* for channels to open the membrane needs to be sufficiently depolarized
  – shape of transient depends on the voltage step (Fig.11)
    different channels open for different voltages and they have different driving forces $(V - E)$

```
Figures/HoHu52a.f12.ps
```
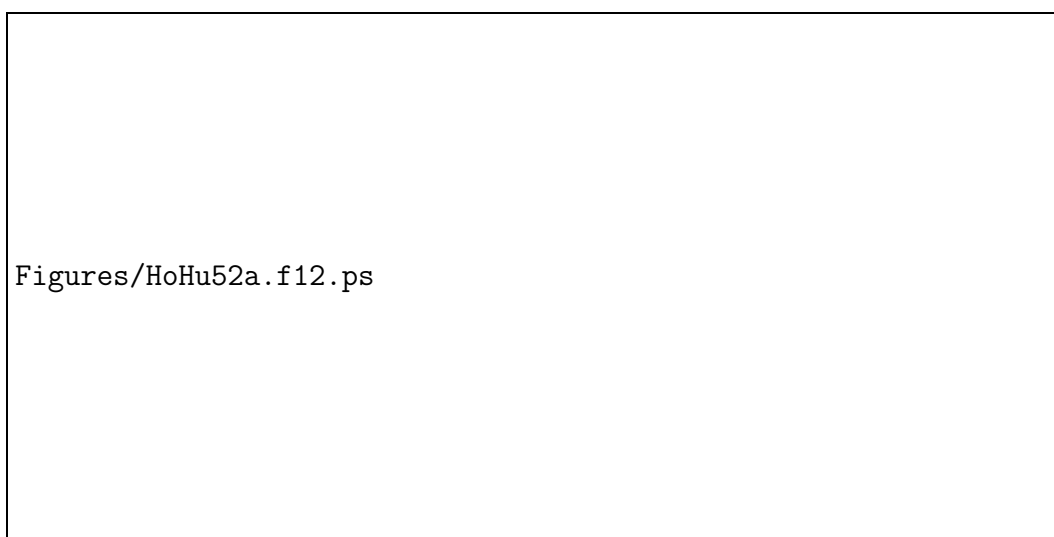
Figure 11: Shape of transient current depends on the membrane voltage.The numbers marking the curves denote hyper-polarization relative to resting potential: negative numbers indicate depolarization [29].

• extract K^+- and Na^+-current separately by replacing parts of the extracellular $NaCl$ with choline chlorid (Fig.12)

25

– Na^+-component is **transient** despite steady applied voltage

```
Figures/I_Na_separation.ps
```
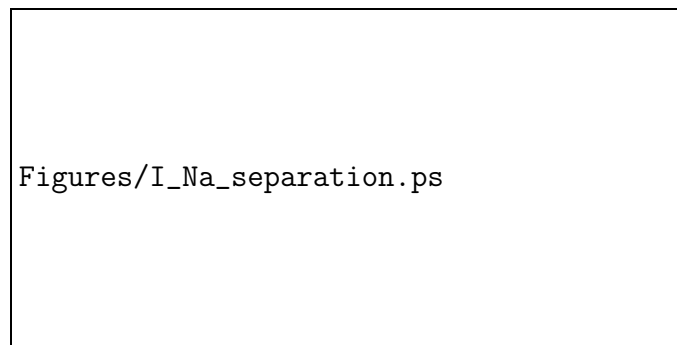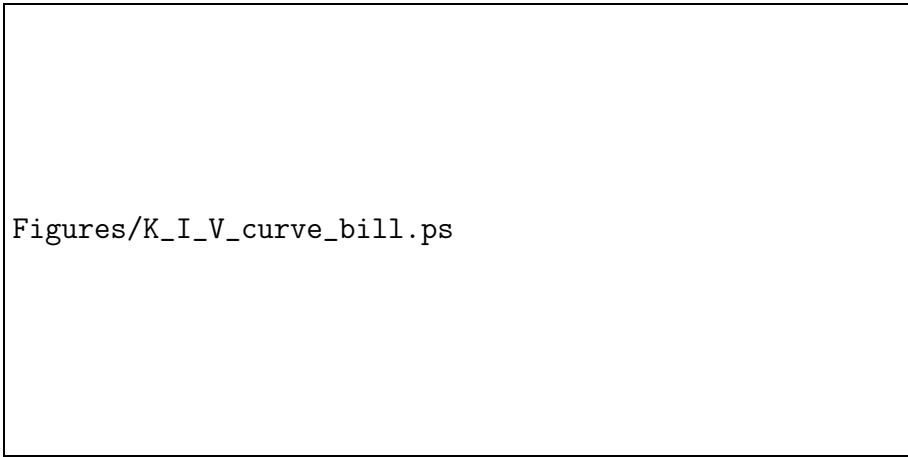
Figure 12: Extraction of Na^+-current by partial replacement of extracellular Na^+ by choline. Na^+-current is transient.

- measure conductances: $I(V)$-curves

  – procedure:
    * long depolarizing voltage step to V_1 to open the channel
    * then second step to V_2 to probe the conductance of the channel at that voltage V_2
    * measure current $I(V_2)$ immediately after second voltage step before the channel state changes

  – K^+ (Fig.13)
    * initial current $I(V_2)$:
      · linear $I(V_2)$-relationship: channels represent an Ohmic resistance (Fig.13)
      $$I_K = g_K (V - E_K)$$
      · current $I(V_2)$ vanishes at reversal potential E_K of K^+
      · slope of $I(V_2)$=conductance $g_K(V_2)$ depends on V_1 and on duration of first stimulus
    * asymptotic current $I(V_1)$ (reached after channels adjust to voltage V_1):
      · goes to 0 for strongly negative V_1: channels close
      · becomes linear for strongly positive V_1: once channels are maximally open the channel behaves like an Ohmic resistor
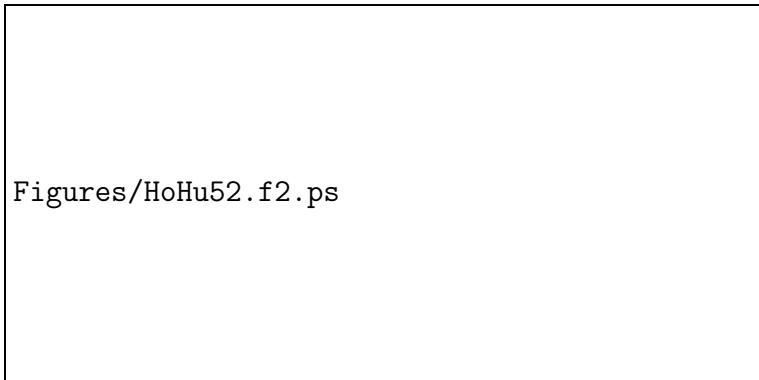
26

```
Figures/K_I_V_curve_bill.ps
```

Figure 13: Ohmic resistance of K^+-channel.

    ⚹ Na^+:

        ∗ also Ohmic resistance for given channel state

- Evolution of K^+-conductance (Fig.14)

  – after step in voltage the conductance g_K evolves smoothly to asymptotic value

```
Figures/HoHu52.f2.ps
```

Figure 14: Sigmoidal growth and exponential decay of g_k with voltage [28].

  – increase from $g_K = 0$: *sigmoidal* ('tanh'-like) increase
  – decrease from $g_K > 0$: exponential
  – no oscillations in the evolution
    $\Rightarrow$ first-order evolution equation may be sufficient
    simplest attempt: linear equation

$$\tau_n \frac{dn}{dt} = n_\infty(V) - n \tag{4}$$

27

$n_\infty(V)$ asymptotic value reached after a sufficiently long time ($t \gg \tau_n$)
evolution after step in V :

* decay after step from $n_\infty(V) > 0$ to $n_\infty = 0$ is exponential

$$n = n(0)e^{-t/\tau_n}$$

* growth after step from $n_\infty = 0$ to $n_\infty(V) > 0$ is initially **linear**

$$n(t) = n_\infty(V)\left(1 - e^{-t/\tau_n}\right) \sim n_\infty(V)\frac{t}{\tau_n}$$

not sigmoidal
* Hodgkin-Huxley proposed

$$g_K = \bar{g}_K\, n^4 \tag{5}$$

with the exponent 4 resulting from a fit to the data (Fig.14)
* $n_\infty(V)$ and $\tau_n(V)$ extracted from data by fitting

- Evolution of Na^+-conductance

  – main difference to K^+- current: the Na^+-current is transient
  – Hodgkin-Huxley proposed

  $$g_{Na}(V,t) = \bar{g}_{Na}m^3h$$

  exponent 3 again from fitting the data
  – activation variable m
  $$\tau_m\frac{dm}{dt} = m_\infty(V) - m$$
  – inactivation variable h
  $$\tau_h\frac{dh}{dt} = h_\infty(V) - h$$
  – difference between activation and inactivation variable:
  $m_\infty(V)$ *increases* with increasing voltage
  $h_\infty(V)$ *decreases* with increasing voltage

Complete Hodgkin-Huxley model for a single-compartment neuron

$$C_m\frac{dV}{dt} + \bar{g}_K n^4\left(V - E_K\right) + \bar{g}_{Na}m^3h\left(V - E_{Na}\right) + \bar{g}_L\left(V - E_L\right) = \frac{I}{A} \tag{6}$$

with

- injected current I defined positive if inward (opposite to the definition of the currents through the ion channels. A is area of cell membrane

- leak current $\bar{g}_L \left(V - E_L \right)$ contains ungated channels (e.g. for Cl^- and other ions)

Hodgkin and Huxley solved the coupled differential equations numerically with a *mechanical calculator*.

Using fits to the voltage dependencies of $m_\infty(V)$, $\tau_m(V)$ etc. that they measured experimentally for the squid giant axon they obtained very good agreement with the experimentally observed temporal evolution of the currents after applied voltage steps (Fig.16) (Nobel Prize in 1963, jointly with Eccles).

The fits obtained by Hodgkin and Huxley for the squid axon [28] are

$$\alpha_n = \frac{0.01 \, (V + 55)}{1 - e^{-0.1(V+55)}} \qquad \beta_n = 0.125 \, e^{-0.0125(V+65)}$$

$$\alpha_m = \frac{0.1 \, (V + 40)}{1 - e^{-0.1(V+40)}} \qquad \beta_m = 4e^{-0.0556(V+65)}$$

$$\alpha_h = 0.07e^{-0.05(V+65)} \qquad \beta_h = \frac{1}{1 + e^{-0.1(V+35)}}$$

where the evolution equation (4) for n is written as

$$\frac{dn}{dt} = \alpha_n(V) \, (1 - n) - \beta_n(V)n \tag{7}$$

with

$$\tau_n(V) = \frac{1}{\alpha_n(V) + \beta_n(V)} \qquad n_\infty(V) = \frac{\alpha_n(V)}{\alpha_n(V) + \beta_n(V)}$$

and analogously for m and h.

Here voltages are in mV and times are in ms.


```
Figures/DaAb01.f5.10.ps
```
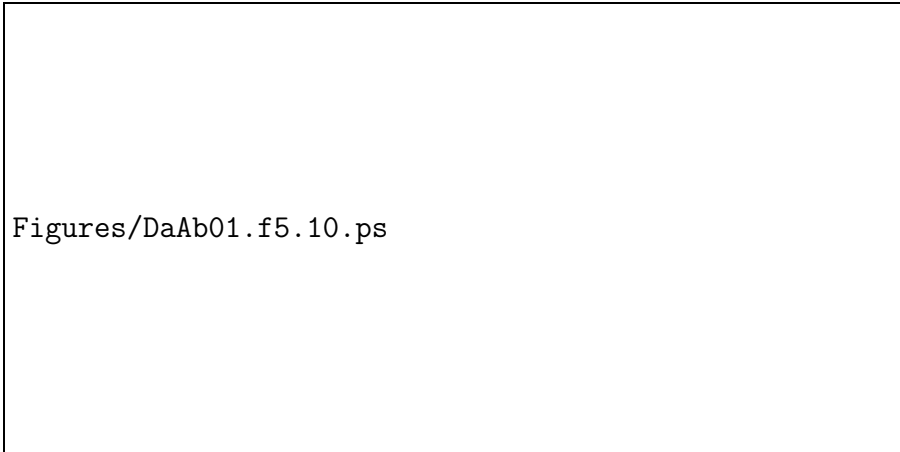
Figure 15: Steady-state levels m_∞, h_∞, n_∞ and the time scales $\tau_{m,h,n}$ for the activation and inactivation variables of the Na^+- and K^+-channels of the Hodgkin-Huxley model.

Figures/HoHu52.f11.ps
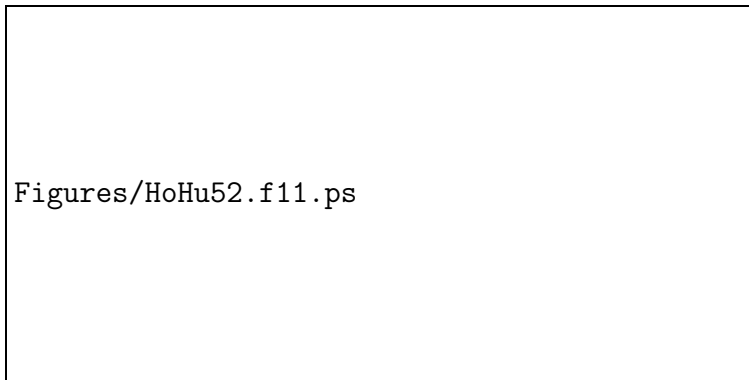
Figure 16: Comparison of current trace from numerical simulation of HH-model (left) with the experimental curves (right). [28].

Simulations (use, e.g., hhsim, cf. Fig.4)

- mechanism underlying the generation of the action potential:

  - depolarizing stimulation
  - activation variable m of Na^+ increases rapidly (cf. Fig.15)
    $\Rightarrow Na^+$-channels open $\Rightarrow Na^+$ rushes into the cell leading to further rapid depolarization (positive feed-back)
  - inactivation variable h of Na^+ and activation variable of K^+ evolve more slowly but speed up as cell becomes more depolarized: Na^+ channels close and K^+ channels open $\Rightarrow Na^+$-flux is stopped and K^+ flows out of the cell $\Rightarrow$ voltage decreases, cell repolarizes again
  - upon reaching V_r some K^+-channels are still open
    $\Rightarrow$ overshoot of V beyond V_r

- inhibition can also trigger action potential ('rebound')

  - hyperpolarization beyond V_r by injecting negative current increases inactivation variable h of Na^+ (Na^+-channels become deinactivated) and decreases activation n variable of K^+ (K^+-channels become more inactivated)
  - at off-set of negative current m increases rapidly to its equilibrium value while h decreases only slowly and n also increases only slowly $\Rightarrow$ increased Na^+-current that is not balanced by increased K^+-current $\Rightarrow$ depolarization of the cell that can lead to an action potential

- steady current injection $\Rightarrow$ periodic spike train (homework: does frequency change significantly when current is reduced below the value needed for stimulating action potential?)

- stimulus during action potential does not trigger second action potential: *refractory period* (see homework)

30

Notes:

- Hodgkin-Huxley modeled squid axon:
  the same Na^+- and K^+- currents arise across all types of species (evolutionarily conserved), with somewhat modified parameters $\Rightarrow$ HH-model forms basis for almost all other neuron models

- modeling of the currents:

  - in HH-model $I(V)$-dependence is assumed linear
  - GHK-current (2) depends nonlinearly on V
  - so far theory not good enough to be predictive from first principles: theory provides functional form of dependence. Parameters need to be determined by fitting to experiments.
    Usually no drastic difference, given the variability between cells. (Fig.17)
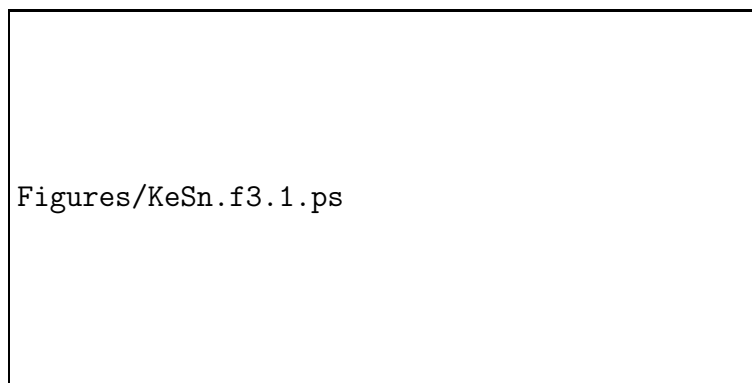
Figure 17: a) Comparison of the Ohmic resistance in the Hodgkin-Huxley model with the current given by the Goldman-Huxley-Katz model (2) [39].
b) Voltage at which no current flows when channels for Na$^+$ and K$^+$ are both open as a function of the K$^+$ concentration for GHK-model and for a combination of Ohmic resistances for the Na$^+$- and the K$^+$-conductance, with E_{Na^+} and E_{K^+} determined separately.

- other neurons can exhibit more complex behavior due to additional channel types

Interpretation of the activation/inactivation equations:

Write (4) again as

$$\frac{dn}{dt} = \alpha_n(V)\,(1-n) - \beta_n(V)n \tag{8}$$

with

$$\tau_n(V) = \frac{1}{\alpha_n(V) + \beta_n(V)} \qquad n_\infty(V) = \frac{\alpha_n(V)}{\alpha_n(V) + \beta_n(V)}$$

or equivalently

$$\alpha_n = \frac{n_\infty}{\tau_n} \qquad \beta_n = \frac{1 - n_\infty}{\tau_n}$$

Eq.(7) can be read as the evolution equation for the probability n of a gate to be open

$$
n(t + \Delta t) \quad = \quad \underbrace{n(t)}_{\text{probability for gate to be open}} \quad +
$$
$$
+ \quad \underbrace{\Delta t\, \alpha_n(V)}_{\text{probability for a closed gate to open}} \quad \times \quad \underbrace{(1 - n(t))}_{\text{probability of gate to be closed}}
$$
$$
- \quad \underbrace{\Delta t\, \beta_n(V)}_{\text{probability for an open gate to close}} \quad \times \quad \underbrace{n(t)}_{\text{probability for a gate to be open}}
$$

- alternatively n can also be read as the mean number of open gates.

If

- l gates are required to be open for the channel to be open and

- the gates open and close independently of each other

then the probability for the channel to be open (= fraction of open channels) is given by

$$\frac{g_K}{\bar{g}_K} = n^l$$

Thus, (5) suggests that the K^+-channel consists of 4 independently operating gates that all have to be open for the K^+-channel to allow ions to pass.

Microsopically, 4 equivalent gates have been identified only very recently by MacKinnon in the form of 4 proteins, which can switch between 2 different conformations (geometric arrangements) one of which blocks the channel (Nobel Prize in 2003).

Analogously, for the Na-channel one can think of m as the probability of one of three gates at the channel pore to be open and of h as the probability that an additional blocking particle is *not* sitting in the pore of the channel. The probability for the pore to let charge pass is then $m^3 h$. [Note: this picture is not to be taken too literally, although the blocking particle can be thought of as a tethered plug formed by parts of the α-unit protein that forms the core of the channel.]

3.4   Conductance-Based Models: Additional Currents[6]

In Hodgkin-Huxley model only two active currents are included

---

[6]DA Chap 6.2

- transient Na^+-current

- delayed rectifying K^+-current (kicks in more slowly than Na^+)

In the brain there is a zoo of neurons, which exhibit a variety of additional currents giving the neurons specific properties.

Very commonly they are modeled similar to the currents in the HH-model in terms of a

- reversal potential and a

- Ohmic resistance with a conductance that may be controled by

  – an activation variable
  – an inactivation variable

- activation and inactivation variables are modeled by first-order differential equations

3.4.1   A-Type Potassium-Current

The A-type K^+- current was introduced by Connor & Stevens [8, 9] to model repetitive firing in walking-leg neurons of crustaceans. They can fire repetitive spikes at a very *low frequency*. Not possible in HH-model.

In contrast to the delayed rectifying K^+-current, the A-type K^+-current I_A inactivates. The Connor-Stevens model includes both K^+-currents.

$$I_A = \bar{g}_A a^3 b \ (V - E_A)$$
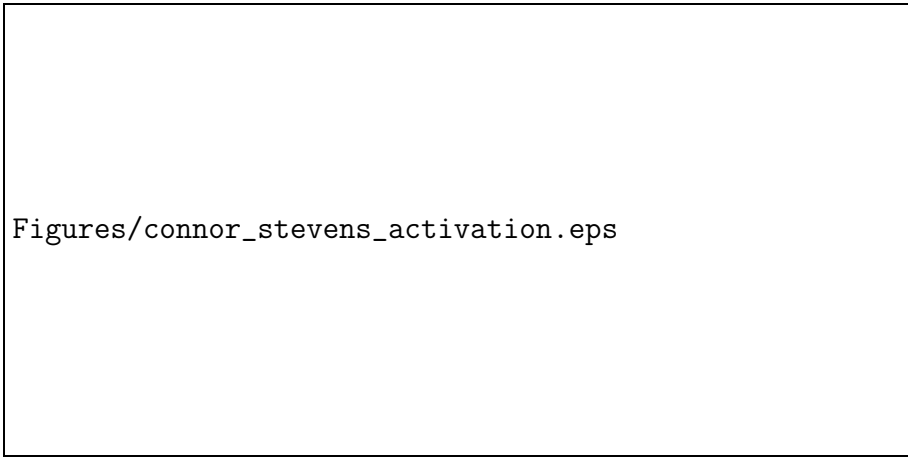
with

- activation variable a

$$\tau_a \frac{da}{dt} = a_\infty(V) - a$$

- inactivation variable b

$$\tau_b \frac{db}{dt} = b_\infty(V) - b$$

Figures/connor_stevens_activation.eps
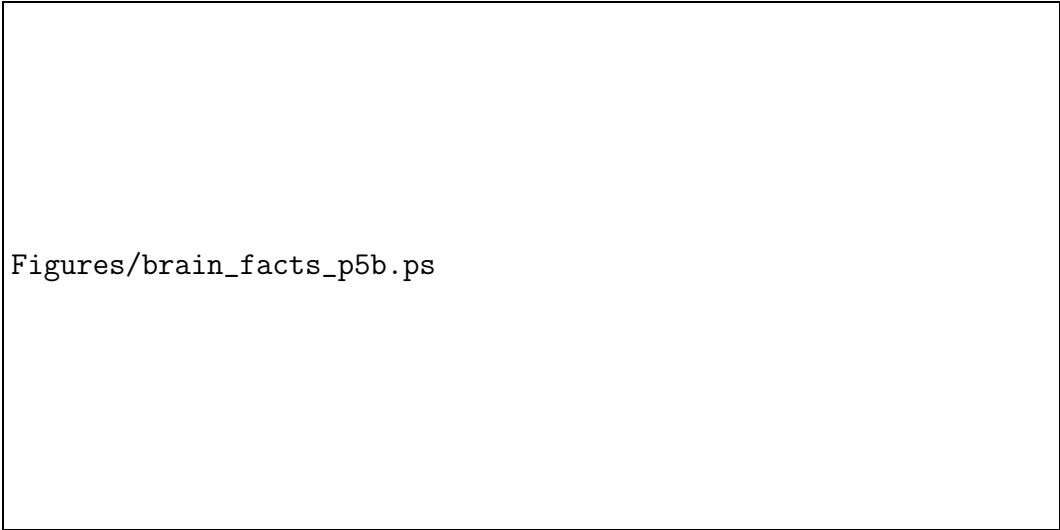
Figure 18: Voltage dependence of the parameters in the Connor-Stevens model. Note that the parameters for I_{Na} and I_K are also different than in the HH-model [9].

One finds (see homework)

- I_A delays spiking after depolarizing voltage step

- firing rate grows from 0 when spiking threshold is crossed, allows arbitrarily slow repetitive firing: Type-I neuron (HH-neuron is Type-II neuron)

3.4.2 T-Type Calcium Current

Thalamus functions as a relay from sensory organs to cortex and also between different cortical areas.

Figures/brain_facts_p5b.ps

Figure 19: Brain structures: thalamus (above spinal cord and hindbrain) functions as relay for sensory information.

- in awake states and during REM sleep the relay neurons fire single spikes: signal can be transmitted faithfully

- during slow-wave sleep (EEG shows slow waves) the thalamo-cortical relay neurons fire repetitive bursts

T-type Ca^{2+}-current is involved in the repetitive bursting [44, 33].

$$I_{CaT} = \bar{g}_{CaT} M^2 H \left(V - E_{Ca} \right)$$

with M and H satisfying

$$\tau_M \frac{dM}{dt} = M_\infty(V) - M \qquad \tau_H \frac{dH}{dt} = H_\infty(V) - H$$

Figures/HuMc92.f1.AB.ps

Figures/HuMc92.f1.D.ps
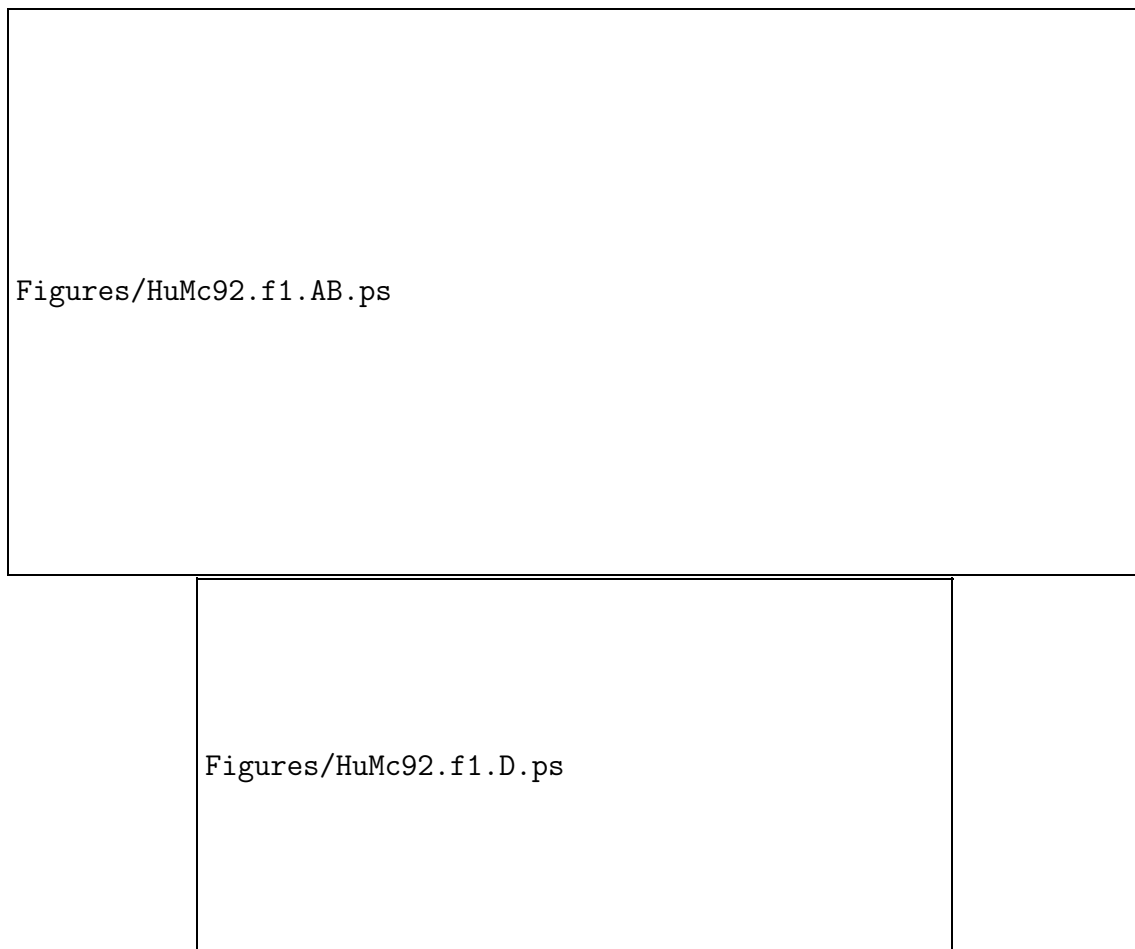
Figure 20: a) Steady-state activation and inactivation M_∞ and H_∞ for I_T, c) time constant τ_M of activation, d) time constant τ_H of inactivation. Note the very slow recovery from inactivation for $V < -70mV$ [33].

Notes:

- extracellular Ca^{2+}-concentration is much higher than the intracellular one
  $\Rightarrow E_{Ca} = +120mV$, I_{CaT} is *depolarizing* similar to the Na^+-current

- I_{CaT} is transient (like Na^+-current);
  almost no 'overlap' of activation and inactivation curves $\Rightarrow$ for no voltage significant *steady* current

- I_{CaT} is much slower than Na^+-current; deinactivation of I_{CaT} is very slow (Fig.20d)

- I_{CaT} can induce spiking even without I_{Na}: Ca-spikes (broader than Na^+-spikes)

```
Figures/DaAb01.f6.2.ps
```
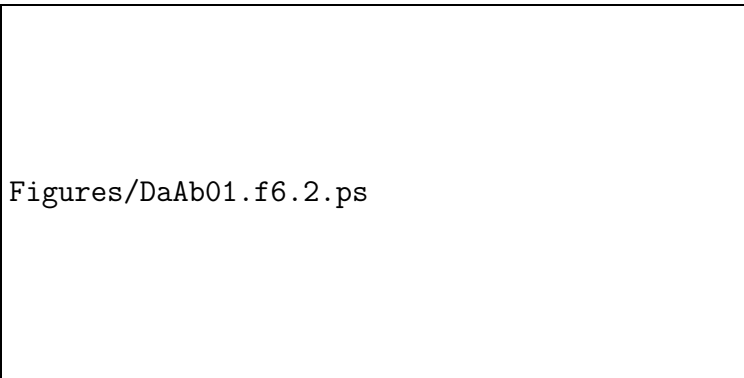
Figure 21: Burst due to I_{CaT}. Delay of the action potential due to I_A. Note decrease in frequency across burst [10].
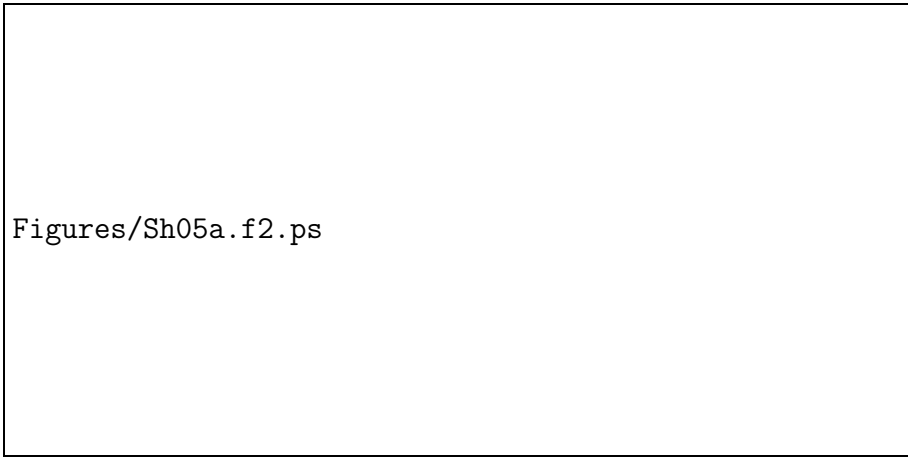
Burst after hyperpolarization:

- injection of hyperpolarizing current $\Rightarrow I_{CaT}$ deinactivates, i.e. inactivation is removed: $H \rightarrow 1$

- stop current injection $\Rightarrow$ increase in voltage activates $I_{CaT} \rightarrow$ further depolarization

- strong depolarization triggers multiple Na-spikes, which occur on a much faster time scale than the variation in I_{CaT} activation

- eventually I_{CaT} becomes inactivated ($H \rightarrow 0$) and bursting stops

Tonic *depolarizing* current injection does not deinactivate I_{CaT}: single Na-spikes, no bursting

What could be the function of these two modes?

- tonic spiking regime: single spikes, relay cells can transmit sensory input faithfully in a graded manner

- bursting regime: immediately above the threshold for spike output the spike frequency is high during the burst (could be like a wake-up call).

36
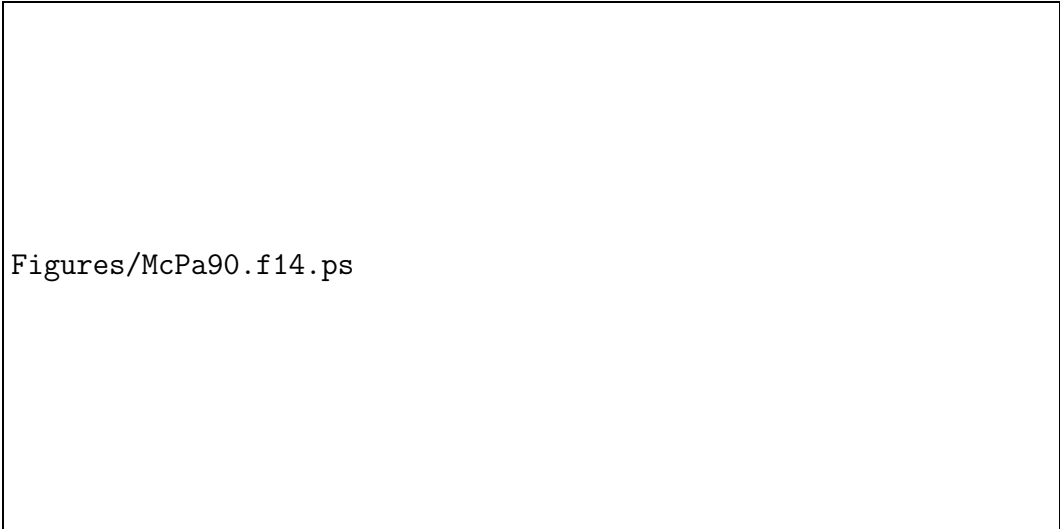
```
Figures/Sh05a.f2.ps
```

Figure 22: Response of a thalamic neuron (in LGN) in the tonic and the bursting regime. Same current injection induces tonic firing from a holding potential of $V = -59mV$ (a) but to a transient burst for $V = -70mV$ (b). Graded vs. discontinuous response of the neuron in the two regimes (c). In the tonic regime the firing rate encodes the sinusoidal input very well (d), in the bursting regime only the onset of each wave is encoded (e) [55]

Both modes arise in a given neuron in the awake and the sleeping animal. But the tonic mode increases in prevalence with increased alertness/wakefulness of the animal.

3.4.3 Sag Current I_h

In thalamic neurons I_{CaT} can exhibit not only single bursts but also rhythmic bursting (1-2Hz).

```
Figures/McPa90.f14.ps
```

Figure 23: Rhythmic bursting of thalamic relay neurons. [45]

This is mediated by a hyperpolarization-activated cation current, I_h, [45]

- permeable to Na^+ and K^+ $\Rightarrow$ reversible potential $E_h \approx -40mV$

- I_h is activated below $V \approx -70mV$

- activation and deactivation is slow $\mathcal{O}(100ms - 1,000ms)$

Figures/McPa90.f1.eps
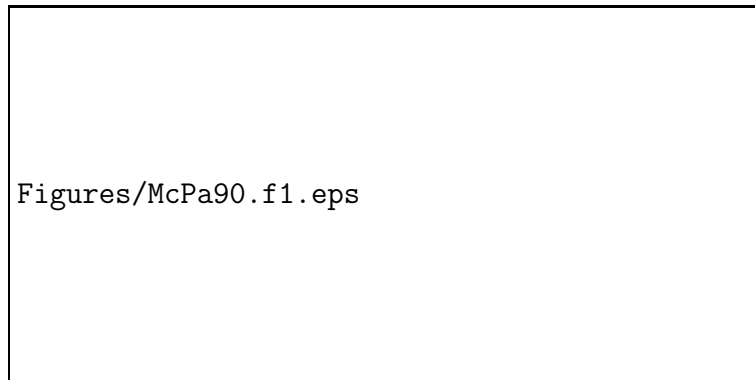
Figure 24: Sag current I_h. Current and voltage clamp results. The 'sag' refers to the slow decrease in hyperpolarization after strong hyperpolarizing current injection (arrows). [45]

Figures/McPa90.f2a.eps

Figures/McPa90.f2b.eps
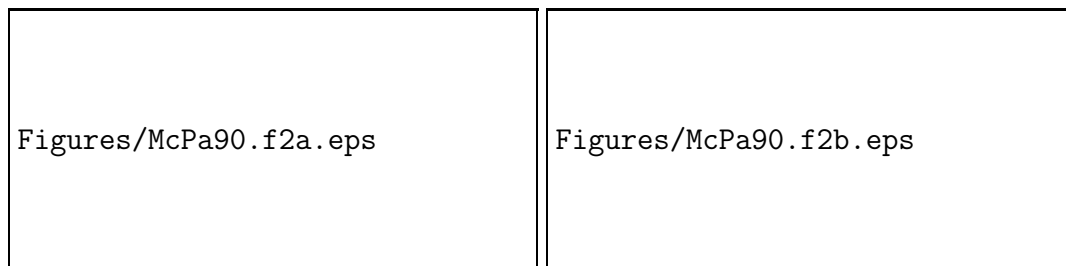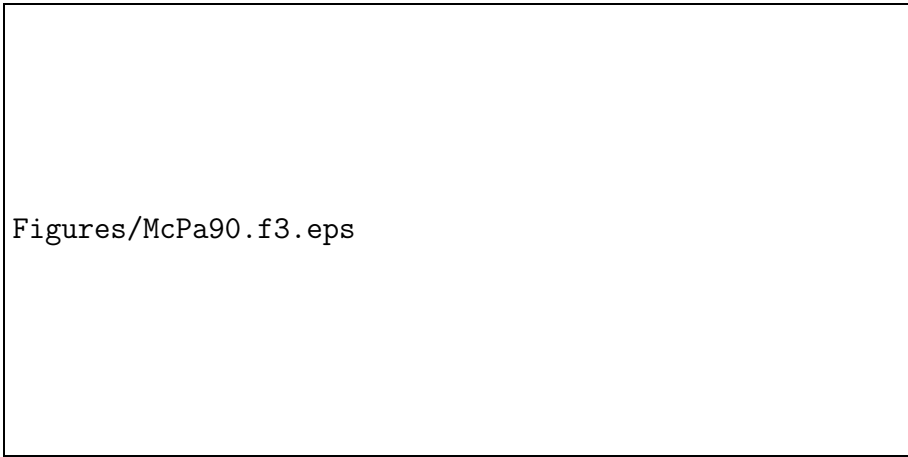
Figure 25: a) Activation curve of I_h (obtained from 7 different neurons, solid symbols 1 neuron). b) Time scales for activation and deactivation, c) enlargement of the tail current after repolarization to $V = -49mV$ (between arrows in b). [45]

Figures/McPa90.f3.eps

Figure 26: Voltage dependence of activation and deactivation times. Fits to transients using single exponentials are quite good. [45]

Rhythmic bursting when the cell receives input (or leak or other current) that tends to hyperpolarize it:

- the I_h-current can depolarize the cell from hyperpolarized states

- activates I_{CaT} inducing a (rebound) burst

- during the depolarized state I_h deactivates

- when I_{CaT} inactivates the cell becomes hyperpolarized again due to the inputs (or other conductances)

- I_h becomes activated again ....

3.4.4 Calcium-Dependent Potassium Current

Central pattern generators control locomotion (swimming of lamprey, walking, running) or chewing and digestive rhythms. Often the control is in the form of periodic bursting.

For instance, California spiny lobster (and other crustaceans) grinds its food in the stomach. Controlled by stomatogastric ganglion cells that fire repetitive *bursts* with low frequency in the *absence* of any input. The frequency depends mainly on a Ca^{2+}-dependent K^+-current I_{KCa}.

I_{KCa} is mainly activated by Ca^{2+}, although activation may also depend somewhat on voltage.

Model it as

$$I_{KCa} = \bar{g}_{KCa} c^4 \left(V - E_K \right)$$

with c satisfying

$$\tau_c \frac{dc}{dt} = c_\infty(V, [Ca^{2+}]) - c$$

Activation variable c depends on voltage V and the Ca^{2+}-concentration $[Ca^{2+}]$.
Evolution of $[Ca^{2+}]$:

$$\tau_{Ca} \frac{d[Ca^{2+}]}{dt} = -\tau_{Ca}\gamma I_{Ca} - [Ca^{2+}]$$

- Ca^{2+} influx I_{Ca} through Ca^{2+}-channels (I_{CaT}), note $I_{Ca} < 0$

- slow buffering by Ca^{2+}-buffers (remove Ca^{2+} from the solution) with time constant τ_{Ca}
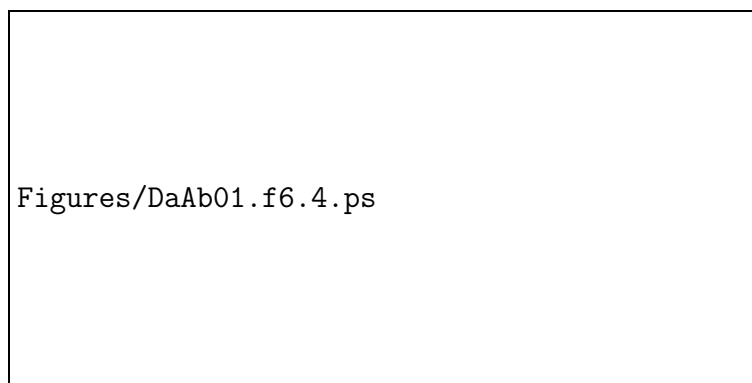
Figure 27: Periodic bursting in a model for a stomatogastric ganglion cell.

Burst Cycle:

- I_{CaT} induces Ca-spike with Na-spikes riding on top of it (burst)

- rise in $[Ca^{2+}]$ activates I_{KCa}

- burst turned off by inactivation of I_{CaT} and by activation of I_{KCa}

- after burst $[Ca^{2+}]$ decreases (slow buffering) and deactivates I_{KCa}

- when I_{CaT} is deinactivated (very slow process; Fig.20) and I_{KCa} is deactivated next burst can arise.

Note:

- over multiple spikes I_{KCa} builds up an *after-hyperpolarization conductance* (AHP)

- it increases time until next spike
  frequency of spikes decreases despite constant stimulation: *spike-frequency adaptation*

Thus:

- even individual, single-compartment (point) neurons can exhibit a wide range of behavior (see also Sec.3.7)

3.5   Two-Dimensional Reduction of Hodgkin-Huxley Model

Reconsider HH-neuron. Even standard HH-model with only fast Na-conductance I_{Na} and delayed rectifier I_K is a four-dimensional dynamical system: hard to visualize.
Can the equations be simplified to get at least a semi-quantitative intuitive understanding?

Observations:

- activation variable m of Na^+-current is very fast

- inactivation variable h of Na^+ and activation variable n of K^+ are strongly correlated
$$h \approx 0.89 - 1.1n$$

⇒ replace

  – $m(t) \to m_\infty(V)$
  – $h(t) \to 0.89 - 1.1n(t)$

Figures/hh_h-n_V-n.eps
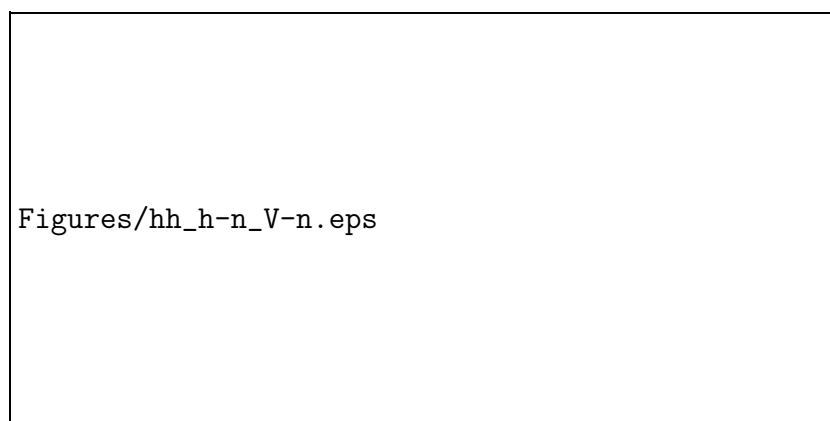
Figure 28: Strong correlation between n and h in standard Hodgkin-Huxley model.

```
Figures/hh_adiabatic_approx.eps
```
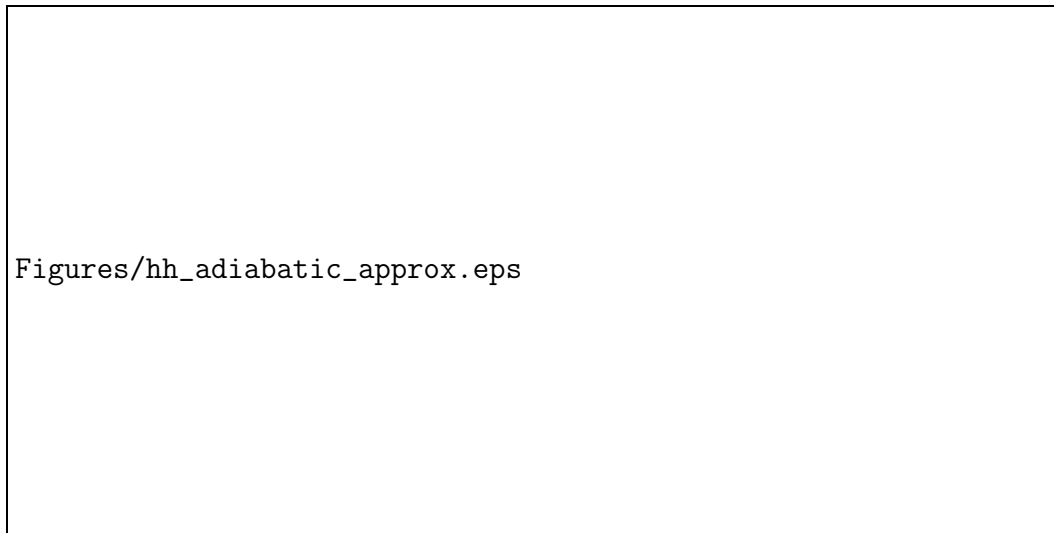
Figure 29: Deviations of the activation variables m, n, h from their steady-state values m_∞, n_∞, h_∞ during regular firing. The large values of m/m_∞ and h/h_∞ are due to m_∞ and h_∞ becoming very small during deactivation and inactivation, respectively.

These assumptions yield reduction of HH-model to a two-dimensional system

$$
\begin{aligned}
C\frac{dV}{dt} &= -g_K n^4 \left(v - E_K\right) - g_{Na} m_\infty^3(V) \left(0.89 - 1.1n\right) \left(V - E_{Na}\right) - \\
&\quad -g_L \left(V - E_L\right) + I_e \equiv F_V(V, n) \\
\tau_n(V)\frac{dn}{dt} &= n_\infty(V) - n \equiv F_n(V, n)
\end{aligned}
$$
(9)

(10)

Note:

- this type of reduction underlies also the FitzHugh-Nagumo model (cf. [39] [41])

3.5.1   Phase-Plane Analysis[7]

Many aspects of two-dimensional dynamical systems can be understood using a *phase-plane analysis*

---

[7]For introductions to nonlinear dynamics see, e.g., S.H. Strogatz *Nonlinear Dynamics and Chaos* or the lecture notes for *Interdisciplinary Nonlinear Dynamics 438* $http://people.esam.northwestern.edu/~riecke/new\_www/lectures.htm$ on the web

Figures/Iz05.f5.20.ps

Figure 30: a) stable fixed point, large perturbation can lead to excitation. b) unstable fixed point, periodic spiking.

To get V_{rest} need *fixed points* of (9,10). They are given by the intersections of the two *nullclines*

$$F_V(V, n) = 0 \tag{11}$$
$$F_n(V, n) = 0 \tag{12}$$

The nullcline F_V separates regions with $\frac{dV}{dt} > 0$ from those with $\frac{dV}{dt} < 0$, and analogously for F_n.

Any fixed point (V_0, n_0) satisfies (11,12) simultaneously.

What happens in the vicinity of the fixed point?

Consider small deviations $(\Delta V, \Delta n)$

$$V = V_0 + \Delta V \qquad n = n_0 + \Delta n$$

and linearize (9,10) around the fixed point (V_0, n_0)

$$\frac{d}{dt}(V_0 + \Delta V) = F_V(V_0 + \Delta V, n_0 + \Delta n_0) \approx \underbrace{F_V(V_0, n_0)}_{=0} + \left.\frac{\partial F_V}{\partial V}\right|_{(V_0 n_0)} \Delta V + \left.\frac{\partial F_V}{\partial n}\right|_{(V_0 n_0)} \Delta n$$

$$\frac{d}{dt}(n_0 + \Delta n) = F_n(V_0 + \Delta V, n_0 + \Delta n_0) \approx \underbrace{F_n(V_0, n_0)}_{=0} + \left.\frac{\partial F_n}{\partial V}\right|_{(V_0 n_0)} \Delta V + \left.\frac{\partial F_n}{\partial n}\right|_{(V_0 n_0)} \Delta n$$

$$\frac{d}{dt}\Delta V = \left.\frac{\partial F_V}{\partial V}\right|_{(V_0 n_0)} \Delta V + \left.\frac{\partial F_V}{\partial n}\right|_{(V_0 n_0)} \Delta n \tag{13}$$

$$\frac{d}{dt}\Delta n = \left.\frac{\partial F_n}{\partial V}\right|_{(V_0 n_0)} \Delta V + \left.\frac{\partial F_n}{\partial n}\right|_{(V_0 n_0)} \Delta n \tag{14}$$

43

We have a linear system of homogeneous differential equations with constant coefficients $\Rightarrow$ exponential ansatz

$$\Delta V = V_1 e^{\lambda t} \qquad \Delta n = n_1 e^{\lambda t}$$

$$\lambda \begin{pmatrix} v_1 \\ n_1 \end{pmatrix} e^{\lambda t} = \begin{pmatrix} \left.\frac{\partial F_V}{\partial V}\right|_{(V_0 n_0)} & \left.\frac{\partial F_V}{\partial n}\right|_{(V_0 n_0)} \\ \left.\frac{\partial F_n}{\partial V}\right|_{(V_0 n_0)} & \left.\frac{\partial F_n}{\partial n}\right|_{(V_0 n_0)} \end{pmatrix} \begin{pmatrix} v_1 \\ n_1 \end{pmatrix} e^{\lambda t} \equiv \mathbf{L} \begin{pmatrix} v_1 \\ n_1 \end{pmatrix} e^{\lambda t}$$

with $\mathbf{L}$ the Jacobian of (9,10) at the fixed point (V_0, n_0)

$\Rightarrow \lambda$ has to be an eigenvalue of $\mathbf{L}$ and $\begin{pmatrix} v_1 \\ n_1 \end{pmatrix}$ is the associated eigenvector[8]

The number of eigenvalues is equal to the number N of time-derivatives of the system.

The general solution of (13,14) is a *linear superposition* of the *eigenmodes* with N unknown constants to satisfy arbitrary initial conditions

$$\begin{pmatrix} \Delta V(t) \\ \Delta n(t) \end{pmatrix} = A_1 \begin{pmatrix} v_1^{(1)} \\ n_1^{(1)} \end{pmatrix} e^{\lambda_1 t} + A_2 \begin{pmatrix} v_1^{(2)} \\ n_1^{(2)} \end{pmatrix} e^{\lambda_2 t}$$

The eigenvalues determine the qualitative character of the 'flow' in the phase space near the fixed point:

- real λ:
  saddle ($\lambda_1 \lambda_2 < 0$), stable ($\lambda_{1,2} < 0$) or unstable ($\lambda_{1,2} > 0$) node

- complex z$\lambda_{1,2} \equiv \sigma \pm i\omega$:
  $\mathbf{L}$ is real $\Rightarrow \lambda_2 = \lambda_2^*$ and $\mathbf{v}^{(2)} = \mathbf{v}^{(1)*}$

$$\Delta V(t) = e^{\sigma t} \left(A_1 v_1 e^{i\omega t} + A_1^* v_1^* e^{-i\omega t} \right)$$

  stable ($\sigma < 0$) and unstable ($\sigma > 0$) spiral

- fixed point is *linearly stable* $\Leftrightarrow$ *all* eigenvalues have negative real parts

---

[8]To calculate the eigenvalues you determine in general for which values of λ the determinant of the matrix $\mathbf{L} - \lambda \mathbf{I}$ vanishes. Here $\mathbf{I}$ is the identity matrix. In the 2x2 case at hand here one can also solve the first row of the equation for n_1,

$$n_1 = \left\{ \lambda - \left.\frac{\partial F_V}{\partial V}\right|_{(V_0 n_0)} \right\} v_1 \frac{1}{\left.\frac{\partial F_V}{\partial n}\right|_{(V_0 n_0)}}. \tag{15}$$

Inserting this expression in the second row yields

$$\left\{ \lambda - \left.\frac{\partial F_n}{\partial n}\right|_{(V_0 n_0)} \right\} \left\{ \lambda - \left.\frac{\partial F_V}{\partial V}\right|_{(V_0 n_0)} \right\} v_1 \frac{1}{\left.\frac{\partial F_V}{\partial n}\right|_{(V_0 n_0)}} = \left.\frac{\partial F_n}{\partial V}\right|_{(V_0 n_0)} v_1.$$

For $v_1 \neq 0$ this results in a quadratic equation for the eigenvalues $\lambda^{(1,2)}$ and (15) yields an equation for the eigenvectors $\begin{pmatrix} v_1^{(1,2)} \\ n_1^{(1,2)} \end{pmatrix}$ associated with these eigenvalues.

Figure 31: Generic (typical) trajectories in the phase plane close to a fixed point. Eigenvectors need not be orthogonal.

Note:

- linear stability: stable with respect to *infinitesimal* perturbations

- even a linearly stable fixed point can be unstable to finite-size perturbations

Need to get insight into global properties of the phase plane

Often the two variables evolve on different time scales (time-scale separation): fast-slow analysis allows approximation to action potential, firing frequency, ...

If V is much faster than n: *fast-slow analysis*

- V reaches its nullcline $F_V(V, n) = 0$ quickly without n changing much

- most of the time the system follows the V-nullcline $F_V(V, n) = 0 \Rightarrow V = V_{nc}(n)$
  slow *one-dimensional* dynamics driven by $n(t)$

$$\frac{dn}{dt} = F_n(V_{nc}(n), n)$$

- at turning points (V_{TP}, n_{TP}) the system cannot follow the V-nullcline any more:
  $\Rightarrow$ fast *one-dimensional* evolution ('jump') to another branch of the V-nullcline
  without much change in n

$$\frac{dV}{dt} = F_V(V, n_{TP})$$

Can construct an approximation to the complete action potential from simpler pieces.

3.6 Integrate-and-Fire Model[9]

The Hodgkin-Huxley model is computationally slow

- 4 differential equations: V, m, n, h

- even in the two-dimensional reduction the equations are stiff:
  resolving the voltage spike requires very small time steps
  time between spikes can be long compared to the spike width

  - single neuron: adaptive time step to step quickly between spikes (implicit scheme for stability)

  - many coupled neurons: likely that some neuron spikes for any given time $\Rightarrow$ small time steps all the time or complex code that updates only neurons undergoing spike

Consider simplified models that capture essential *qualitative* features of the neuron

The shape of the voltage spike is often not important:

- do not model the dynamics of the spiking dynamics explicitly:
  do not resolve the dynamics of activation and inactivation/deactivation of the fast Na^+-current and the delayed K^+-rectifier.
  Assume the conductances of the Na^+- and K^-−currents do not depend on voltage: lump all reversal potentials and conductances together into

$$\tau_m \frac{dV}{dt} = E_L - V + R_m I_e \tag{16}$$

- the input current I_e (injection or from other neurons) can drive the voltage to the spiking threshold $V_{th} \Rightarrow$

  - the voltage is reset explicitly to a reset voltage V_{reset}

$$V(t_{spike}^-) = V_{th} \qquad \Rightarrow \qquad V(t_{spike}^+) = V_{reset} \tag{17}$$

  - spike-like output, which serves as input to other neurons, is generated 'by hand' :

$$V_{out}(t) = V_{sp}\delta(t - t_{spike})$$

  or

$$V_{out}(t) = V_{sp}\left\{ e^{-\frac{t}{\tau_1}} - e^{-\frac{t}{\tau_2}} \right\} \qquad \text{with} \qquad \tau_2 < \tau_1$$

This leaky Integrate-and-Fire model was proposed by Lapicque already in 1907 by Lapicque [42] http://www.springerlink.com/content/x03533370x281257/.

Note:

---

[9]DA 5.4

- for small fluctuations of V around resting potential the assumption of constant Na^+- and K^+- conductance is reasonable; further away from V_{rest} it is not a good assumption

Firing Rate:

IF-model allows simple analytical solution for $I_e = const.$

$$\tau_m \frac{d}{dt}\left(e^{t/\tau_m} V\right) = e^{t/\tau_m}\left(E_L + R_m I_e\right)$$

$$V(t) = \left(E_L + R_m I_e\right)\left(1 - e^{-t/\tau_m}\right) + V_0 e^{-t/\tau_m}$$

with $V_0 \equiv V(t=0)$. Rewrite using

$$V_\infty \equiv E_L + R_m I_e$$

as

$$V(t) = V_\infty - \left(V_\infty - V_0\right)e^{-t/\tau_m}$$

Without the spike triggering mechanism one would have for $t \to \infty$

$$V(t) \to V_\infty$$

For small I_e, more precisely for $V_\infty < V_{th}$, no spike is triggered.

For

$$V_\infty > V_{th} \qquad \text{i.e.} \qquad I_e > \frac{1}{R_m}(V_{th} - E_L)$$

a spike is triggered at time t_{spike}, which is obtained by solving $V(t_{spike}) = V_{th}$ for t_{spike}

$$t_{spike}(V_0) = -\tau_m \ln\left(\frac{V_\infty - V_{th}}{V_\infty - V_0}\right)$$

The spike time $t_{spike}(V_0)$ depends on the initial condition V_0.

For fixed I_e the neuron fires periodically:

- the initial condition for the voltage after the nth-spike is given by $V(t_{spike}^{(n)+}) = V_{reset}$

- the inter-spike interval (ISI) $T_{ISI} \equiv t_{spike}^{(n+1)-} - t_{spike}^{(n)+}$ is given by

$$T_{ISI} = \tau_m \ln\left(\frac{V_\infty - V_{reset}}{V_\infty - V_{th}}\right) = \tau_m \ln\left(\frac{1 - \frac{V_{reset}}{V_\infty}}{1 - \frac{V_{th}}{V_\infty}}\right) \qquad \text{for} \quad V_\infty \geq V_{th} > V_{reset}$$

and the firing rate by

$$r_{ISI} = \left(\tau_m \ln\left(\frac{V_\infty - V_{reset}}{V_\infty - V_{th}}\right)\right)^{-1}$$

47

Notes:

- as I_e is increased the spiking sets in first with vanishing firing rate:
  in that respect the Type-I neuron is like the neuron of the Connor-Stevens model
  (cf. the standard HH-neuron sets in with a fixed finite frequency: Type-II neuron)

- for large I_e and large V_∞ one has

$$
\begin{aligned}
T_{ISI} \quad &\sim \quad \tau_m \ln\left((1 - \frac{V_{reset}}{V_\infty})(1 + \frac{V_{th}}{V_\infty}) \right) \\
&\sim \quad \tau_m \frac{V_{th} - V_{reset}}{V_\infty}
\end{aligned}
$$

Thus, for large I_e the firing rate grows linearly with I_e,

$$
r_{ISI} \sim \frac{1}{\tau_m} \frac{R_m}{V_{th} - V_{reset}} I_e
$$

- in the IF-model (16,17) sufficiently large inputs I_e trigger spikes with arbitrarily small ISI (no absolute refractory period, see below)

- time-dependence of the voltage in the IF-model does not show the up-swing that is characteristic of the regenerative action potential; instead the voltage has a negative second derivative (concave downward) before the spike

Refractory Period

In the Hodgkin-Huxley model the Na^+-current is still inactivated shortly after an action potential: generating another action potential is more difficult

To get an action potential the depolarizing Na^+-current must overcome the hyperpolarizing K^+-current. This requires

$$
\bar{g}_K n^4 \left(V - E_K \right) < -\bar{g}_{Na} m^3 h \left(V - E_{Na} \right)
$$

$$
V < V_{bal} \equiv \frac{\bar{g}_K n^4 E_K + \bar{g}_{Na} m^3 h E_{Na}}{\bar{g}_K n^4 + \bar{g}_{Na} m^3 h}
$$

V_{bal} determined by reversal potentials that are weighted by the degree that the respective channels are open.

For action potential we need roughly $V_{bal} \geq V_{peak}$

When Na^+-current is inactivated, $h \ll 1$, $V_{bal} \approx E_K$

m reaches quickly $m_\infty(V) \leq 1$, while n and h vary only slowly.

Shortly after action potential:

- h very small

- $V_{bal} \approx E_k < V_{peak}$ even for $m = 1$
  $\Rightarrow$ even arbitrarily strong inputs cannot trigger action potential, i.e. no regenerative event that is driven by the activation of Na is possible: *absolute* refractory period

Later after an action potential

- larger h

- if $V_{bal} > V_{peak}$ for $m > m_\infty(V_{min})$
  $\Rightarrow$ for inputs that drive the cell to $V = V_{min}$ the activation variable can quickly grow to $m_\infty(V_{min})$ and push V_{bal} above V_{peak}
  $\Rightarrow$ action potential triggered by super-threshold inputs

- as long as h has not recovered, triggering an action potential requires larger inputs than the inputs to trigger an action potential from the resting state: *relative* refractory period

- firing threshold decreases with time

Modeling in IF-model:

- absolute refractory period: explicitly disallow firing for a duration after any spike

- relative refractory period:

  - $V_{reset} < V_{rest}$: effective firing threshold decreases as V relaxes from V_{reset} to V_{rest}
  - introduce a decaying hyper-polarizing conductance (cf. I_{KCa}) or time-dependent (relaxing) threshold V_{th} (cf. [10]) or some generalized recovery variable (cf. Sec.3.7)

3.7 Izhikevich's Simple Model[10]

Aim: model a wide spectrum of types of neurons phenomenologically with a single, computationally efficient model

Extend the IF-model to include additional variable that may capture effects of I_A, I_{KCa}, I_{CaT}, ...

If the spike-shape is not essential: focus on *subthreshold* behavior

- in reduced HH-model we the dynamics of V and n

---

[10][39, 35, 36]

- extensions of HH (I_A, I_{CaT}, I_{KCa}, ...) would introduce additional conductances with dynamics that are slow compared to the spike generating Na
  replace n by a generalized *recovery* variable u

Approximate the nullclines of V and u near the minimum of the V-nullcline

$$\begin{aligned} V\text{-nullcline:} \quad u &= u_{min} + P\left(V - V_{min}\right)^2 \\ u\text{-nullcline:} \quad u &= s\left(V - V_0\right) \end{aligned}$$

thus

$$\begin{aligned} \tau_V \frac{dV}{dt} &= P\left(V - V_{min}\right)^2 - \left(u - u_{min}\right) \\ \tau_u \frac{du}{dt} &= s\left(V - V_0\right) - u \end{aligned}$$

Adding the injected I current, Izhikevich writes the model in the form [35]

$$\frac{dv}{dt} = 0.04v^2 + 5v + 140 - u + I \tag{18}$$

$$\frac{du}{dt} = a\left(bv - u\right) \tag{19}$$

Note:

- numbers chosen such that time is measured in ms, v in mV

- v can diverge in finite time

$$\frac{dv}{dt} = \gamma v^2$$

$$\int_{v_0}^{v} \frac{dv}{v^2} = \gamma \int_0^t dt$$

$$-\left(\frac{1}{v} - \frac{1}{v_0}\right) = \gamma t$$

$$v = \frac{v_0}{1 - \gamma v_0 t} \to \infty \quad \text{for} \quad t \to \frac{1}{\gamma v_0} > 0$$

$\Rightarrow$ 'escape' from the region near the left branch of the V-nullcline: action potential

- the nonlinearity gives an up-swing before the action potential

Supplement (18,19) with a reset condition like in the integrate-and-fire model

$$v(t_{sp}^-) = 30mV \quad \Rightarrow \quad \begin{cases} v(t_{sp}^+) = c \\ u(t_{sp}^+) = u + d \end{cases} \tag{20}$$

Notes:

- a is the relaxation time of u

- b characterizes the dependence of the steady-state value of the recovery variable u on v, e.g. deinactivation of I_{CaT} by hyperpolarization

- c is a reset voltage, in general not the resting potential; it could, for instance, include an after-hyperpolarization (for $V_{reset} < V_{rest}$)

- d characterizes the change in the recovery variable during the spike 'excursion' to the other branch of the nullcline, e.g. Ca^{2+}-influx controling I_{KCa} or the inactivation of I_{CaT} due to the high voltage during the spike.
  size of d provides a second time scale to the slow evolution of u
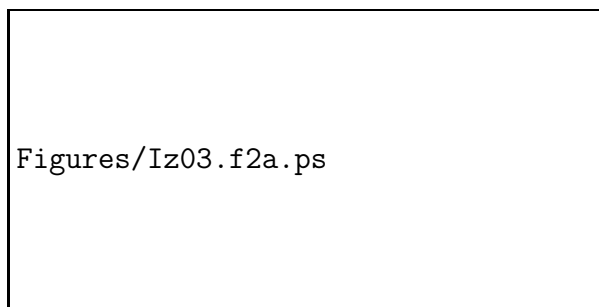
Figure 32: Parameters of Izhikevich's simple model.

Note:
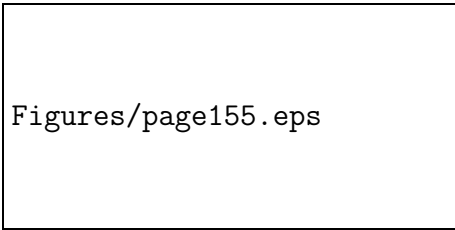
- the simple model is computationally efficient and captures qualitative aspects of many neuronal types (Fig.34)

- the model can be thought of as an extension of the quadratic integrate-and-fire model (QIF)

$$\frac{dv}{dt} \;=\; b + v^2 \qquad \text{with} \tag{21}$$

$$v(t_{sp}^-) = v_{peak} \Rightarrow v(t_{sp}^+) = v_{reset} \tag{22}$$

(21) is the normal form for a saddle-node bifurcation

- the saddle-node bifurcation leads to a periodic orbit due to the reset, which implements - by hand - the existence of an attracting invariant circle in phase space.

51

Figure 33: Sketch of a pair of fixed points on an invariant circle (parametrized by the phase θ of the oscillation during regular firing). The mutual annihilation of the fixed points in a saddle-node bifurcation generates an infinite-period limit cycle (SNIC-bifurcation leading to Type-I oscillation).

- the normal form for the transition to spiking in a saddle-node bifurcation on an invariant circle (SNIC) is the θ-neuron by Ermentrout-Kopell [14]

$$\frac{d\theta}{dt} = (1 - \cos\theta) + (1 + \cos\theta)\,g \qquad (23)$$

where θ describes the phase of the neuron (oscillator) and $\theta = \pm\pi$ corresponds to a spike, and g represents input to the neuron. The rest state is near $\theta = 0$. For small θ and weak forcing it reduces to (21),

$$\frac{d\theta}{dt} = \theta^2 + g + \mathcal{O}(\theta^4, g\theta^2)$$

For parameters close to the saddle-node bifurcation at $g = 0$ the neuron spends almost all of the time near the 'ghost' of the fixed point $\Rightarrow$ the period T can be approximated by the time it takes the neuron to go from $\theta = -\infty$ to $\theta = +\infty$

$$\int_{-\infty}^{+\infty} \frac{d\theta}{\theta^2 + g} = \int_{-\frac{T}{2}}^{\frac{T}{2}} dt$$

i.e.

$$T \approx \frac{1}{g}\sqrt{g}\,\arctan\frac{\theta}{\sqrt{g}}\Big|_{-\infty}^{+\infty} = \frac{1}{\sqrt{g}}\pi$$

thus the firing rate goes to zero like $r \propto \sqrt{g}$, with g measuring the distance from the saddle-node bifurcation.

```
Figures/Iz03.f2b.ps
```
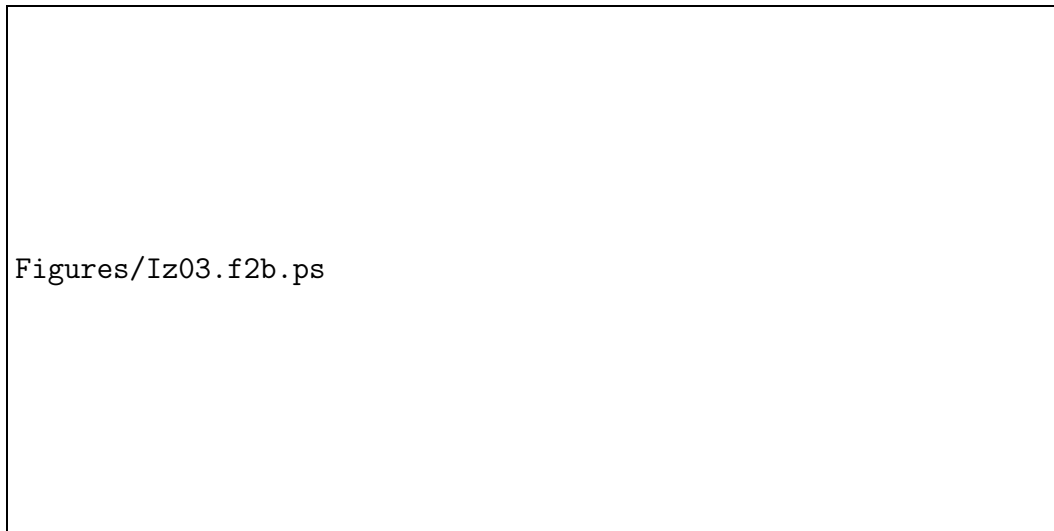
Figure 34: Some of the neuronal types captured by Izhikevich's simple model [35]. Compare behavior labeled thalamo-cortical with that discussed for I_{CaT}-current in Sec.3.4.2.

4   Cable Equation[11]

So far we assumed that the neuron is characterized by a single value of the voltage: point neuron.

Many neurons are, however, very long and branched.

- what determines how good the single-compartment model is?

- how to describe spatial structure of neurons

---

[11]DA 6.3

Figures/neuron_morph_kath.ps
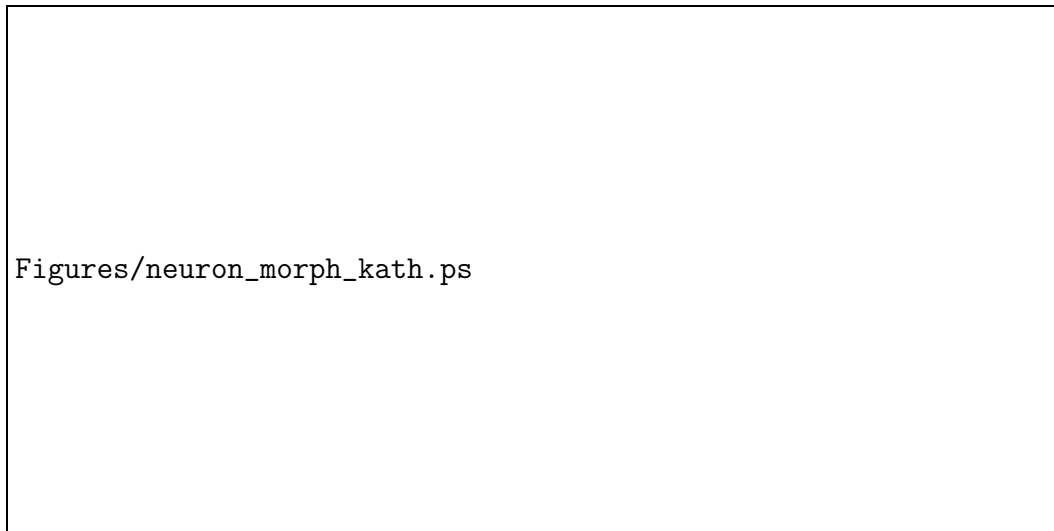
Figure 35: Neurons are not pointlike. Their morphology varies widely.

Figures/DaAb01.f6.5.ps

Figure 36: Voltage attenuation along a dendrite. A) current injection in soma triggers large action potential there but delayed and reduced action potential in dendrite. B) converse arrangement with stimulation (via synapses) of dendrite [10].

Voltage can be strongly attenuated further away from the stimulation site

Most parts of a neuron are long and thin: cable of radius a

- assume voltage depends only on the axial position, but not on the transverse coordinate: one-dimensional theory, radius may depend on position as well: $a = a(x)$

- two types of currents:

- **–** longitudinal current I_L
- **–** transverse current across membrane I_m

• Kirchhoff's law for charge conservation
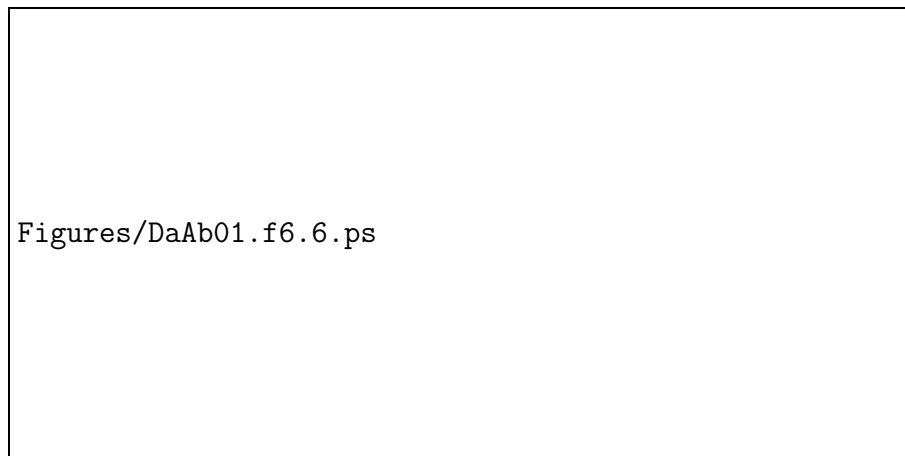
Figure 37: Sketch of currents in an axon [10]

Longitudinal current I_L:

Consider Ohm's law for a section of length Δx of the cable

$$I_L = -\frac{V(x + \Delta x) - V(x)}{R_L} = -\frac{\Delta V}{R_L}$$

• current driven by the voltage drop ΔV across the section

• consider I_L positive if it flows in the positive x-direction

• the current (positive charges) flows from the more positive potential (voltage) to the more negative potential

• in terms of the intra-cellular resistivity r_L

$$R_L = \frac{\Delta x}{\pi a^2} r_L$$

For small Δx

$$I_L = -\frac{\pi a^2}{r_L} \frac{\Delta V}{\Delta x} \quad \text{becomes} \quad I_L = -\frac{\pi a^2}{r_L} \frac{\partial V}{\partial x} \qquad \text{for } \Delta x \to 0$$

- **–** similar to Fick's law of diffusion: current driven by gradient in voltage

Transverse current I_m:

In terms of the membrane current density i_m

$$I_m = 2\pi a \Delta x \, i_m$$

Similarly, write the current injected by an electrode in terms of the density i_e

$$I_e = 2\pi a \Delta x \, i_e$$

Kirchhoff's law for charge conservation for a cable segment of length Δx

$$\underbrace{2\pi a(x)\Delta x c_m \frac{\partial V}{\partial t}}_{\text{capacitive current}} = \underbrace{-\left.\left(\frac{\pi a(x)^2}{r_L}\frac{\partial V}{\partial x}\right)\right|_{\text{left}}}_{I_L \text{ into the segment}} \underbrace{+\left.\left(\frac{\pi a(x)^2}{r_L}\frac{\partial V}{\partial x}\right)\right|_{\text{right}}}_{I_L \text{ out of the segment}}$$

$$\underbrace{-2\pi a(x)\Delta x \, i_m}_{i_m \text{ out of the segment}} \qquad \underbrace{+2\pi a(x)\Delta x \, i_e}_{i_e \text{ into the segment}}$$

Dividing by Δx and using

$$\frac{1}{\Delta x}\left(\left.\left(\frac{\partial V}{\partial x}\right)\right|_{\text{right}} - \left.\left(\frac{\partial V}{\partial x}\right)\right|_{\text{left}}\right) \rightarrow \frac{\partial}{\partial x}\left(\frac{\partial V}{\partial x}\right) \qquad \text{for } \Delta x \rightarrow 0$$

one obtains

$$c_m \frac{\partial V}{\partial t} = \frac{1}{2ar_L}\frac{\partial}{\partial x}\left(a(x)^2 \frac{\partial V}{\partial x}\right) - i_m + i_e \tag{24}$$

- diffusive partial differential equation for the voltage

- in general i_m contains all the ion conductances discussed for the point neuron (single compartment neuron): in a Hodgkin-Huxley framework the PDE is coupled to ODEs for the activation and inactivation variables (they do not contain any spatial derivatives)

4.1   Linear Cable Theory: Passive Cable

To make analytical progress consider passive cable with only leak current

$$i_m = g_L \left(V - E_L\right)$$

For passive neuron

$$g_L = \frac{1}{r_m} \qquad E_L = V_{rest}$$

Rewrite in terms of deviation v from V_{rest}: $v = V - V_{rest}$

For simplicity assume constant radius $a = const.$

$$c_m \frac{\partial v}{\partial t} = \frac{a}{2r_L} \frac{\partial^2 v}{\partial x^2} - \frac{1}{r_m} v + i_e$$

Using $\tau_m = r_m c_m$ the linear cable equation can be written as

$$\tau_m \frac{\partial v}{\partial t} = \lambda^2 \frac{\partial^2 v}{\partial x^2} - v + r_m i_e \tag{25}$$

with

$$\lambda = \sqrt{\frac{a r_m}{2 r_L}}$$

- λ has the dimension of a length: this *electrotonic length* λ characterizes the length scale on which the voltage varies in the cable

- with increasing length Δx of a segment

  - the membrane resistance goes down

    $$R_m(\Delta x) = \frac{1}{2\pi a \Delta x} r_m$$

  - the longitudinal resistance of the intracellular medium goes up

    $$R_L(\Delta x) = \frac{\Delta x}{\pi a^2} r_L$$

- at what length is the two resistances equal?

  $$R_m(\ell) = \frac{r_m}{2\pi a \ell} = R_L(\ell) = \frac{\ell r_L}{\pi a^2}$$

  $$\ell^2 = \frac{a r_m}{2 r_L} = \lambda^2$$

  Thus: the electrotonic length λ is that length for which the membrane resistance and the longitudinal resistance are equal

  $$R_\lambda = \frac{r_m}{2\pi a \lambda} = \frac{r_L \lambda}{\pi a^2}$$

Consider injecting current at a point. Flowing away from the injection site the current flows

- along the cable

- across the membrane

The situation is somewhat similar to the flow of water in a soaker house (i.e. a leaky pipe).

How the current is distributed between these two paths depends on the relative resistances:

- if $R_L < R_m$ the current predominantly flows into the cable and spreads away from the injection site

- if $R_L > R_m$ the current predominantly flows across the membrane and does not spread away from the injection site

- the current spreads to a length ℓ at which $R_L(\ell) = R_m(\ell)$, i.e. $\ell = \lambda$.

Explicit solution for the steady state $v = v(x)$ for a point injection current

$$i_e(x) = \frac{I_e}{2\pi a}\delta(x)$$

with $\delta(x)$ being the Dirac δ-function[12]

$$\lambda^2 \frac{d^2v}{dx^2} = v - r_m \frac{I_e}{2\pi a}\delta(x) \tag{26}$$

Consider the two domains separately

- $x > 0$: the general solution is given by

$$v^+(x) = A^+ e^{+x/\lambda} + B^+ e^{-x/\lambda}$$

- $x < 0$: the general solution is given by

$$v^-(x) = A^- e^{+x/\lambda} + B^- e^{-x/\lambda}$$

- boundary conditions:
  for $x \to \pm\infty$ the voltage must remain finite:

$$v(x) = \begin{cases} B^+ e^{-x/\lambda} & \text{for } x > 0 \\ A^- e^{x/\lambda} & \text{for } x < 0 \end{cases}$$

At $x = 0$ we need to match the two solutions:

- $\frac{d^2v}{dx^2}$ must be infinite to balance $\delta(x)$, i.e. the first derivative $\frac{dv}{dx}$ makes a jump

$$\frac{d^2v}{dx^2} = \lim_{\Delta x \to 0} \frac{\left.\frac{dv}{dx}\right|_{x+\frac{1}{2}\Delta x} - \left.\frac{dv}{dx}\right|_{x-\frac{1}{2}\Delta x}}{\Delta x}$$

[12]Definition of the Dirac-δ-function: $\delta(x) = 0$ for $x \neq 0$ and $\int_{-\infty}^{+\infty} \delta(x)\,dx = 1$. The δ-function has dimension $1/\text{length}$.

- $\frac{dv}{dx}$ is well-defined on both sides of $x = 0$

- $v(x)$ is continuous[13]

$$A^- = B^+ \equiv v_0$$

- Integrate (26) across $x = 0$

$$\lambda^2 \int_{-\epsilon}^{+\epsilon} \frac{d^2 v}{dx^2}\, dx = \int_{-\epsilon}^{+\epsilon} v(x) - r_m \frac{I_e}{2\pi a} \delta(x)\, dx$$

In the limit $\epsilon \to 0$ the integral $\int_{-\epsilon}^{+\epsilon} v(x)\, dx$ goes to 0 since the integrand is finite

$$\lambda^2 \left(\frac{dv}{dx}\bigg|_{+\epsilon} - \frac{dv}{dx}\bigg|_{-\epsilon} \right) = -r_m \frac{I_e}{2\pi a}$$

$$\lambda^2 \frac{2}{-\lambda} v_o = -r_m \frac{I_e}{2\pi a} \qquad v_0 = \frac{r_m I_e}{4\pi \lambda a} = \frac{1}{2} R_\lambda I_e$$

Thus

$$v(x) = \frac{1}{2} R_\lambda I_e e^{-|x|/\lambda}$$

As expected, the injected current spreads into the cable to a distance λ.

Notes:

- the point-neuron model is a good approximation as long as the spatial extend of the neuron is smaller than λ

- $\lambda \propto \sqrt{a} \Rightarrow$ for thin axons or thin dendrites, which have relatively more surface area than cross section, λ is small and the space-dependence of the voltage has to be taken into account to capture, e.g., the propagation of the action potential along the axon to the next neuron.

The cable equation (25) is a diffusive equation: a pulse-like current injection diffuses away from the source like heat (cf. Fig.38).

---

[13]can be derived by taking antiderivative twice of (26). Alternatively, if $v(x)$ was not continuous, its first derivative would be a δ-function and its second derivative would be the derivative of the δ-function; but the equation contains only a δ-function to balance.

```
Figures/DaAb01.f6.7.ps
```
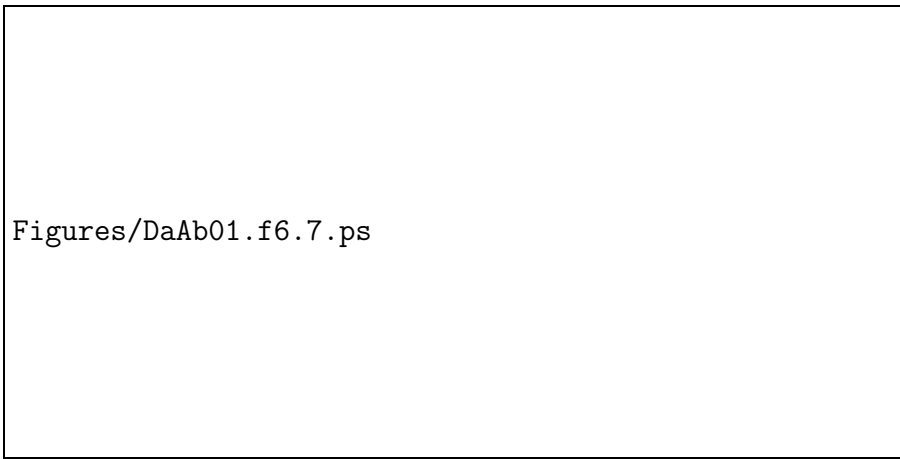
Figure 38: Voltage $v(x)$ for steady current injection (A) and for short current pulse (B) [10].

4.2 Axons and Active Dendrites

For almost all neurons the linear cable theory is insufficient

- all axons support action potentials

- most dendrites have voltage-gated channels or Ca^{2+}-dependent channels, some even support action potentials

$\Rightarrow i_m$ in (24) includes currents like I_{Na}, I_K, I_{CaT}, I_{KCa}, ...
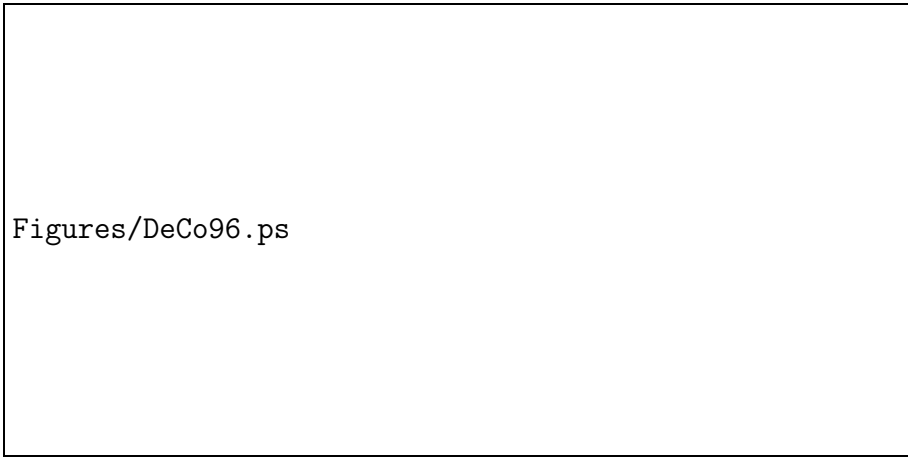
$\Rightarrow$ coupled, nonlinear PDE on a complex geometry: cannot expect to solve it analytically

Numerical solution:

- discretize dendrite and/or axon in space $\Rightarrow$ compartments (small cylinders)

- ODEs in each compartment for V and activation/inactivation variables

- coupling between the compartments via the current flowing into and out of the compartments
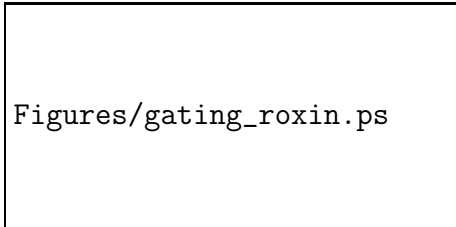
Numerical simulation package/language:
NEURON developed by M. Hines, J.W. Moore, and T. Carnevale: NEURON web site `http://www.neuron.yale.edu` has free downloads for any relevant operating system, documentation, tutorials. In addition, it has a large **database** called ModelDB, which contains NEURON codes (models) that have been developed and used for neuroscience publications. (For example see Fig. 39)

```
Figures/DeCo96.ps
```

Figure 39: Burst in thalamic reticular neuron driven by low-threshold $T-$type Ca^{2+}-current which is slower than the T-current in thalamocortical relay cells (cf. Sec.3.4.2) [12]. For movies see
Thalamic reticular neurons `http://cns.iaf.cnrs-gif.fr/alain_movies.html`

```
Figures/gating_roxin.ps
```

Figure 40: Gating of dendritic inputs by other dendritic inputs in pyramidal cells in CA1 in hippocampus [37]. Movie at `http://people.esam.northwestern.edu/~kath/gating.html`.
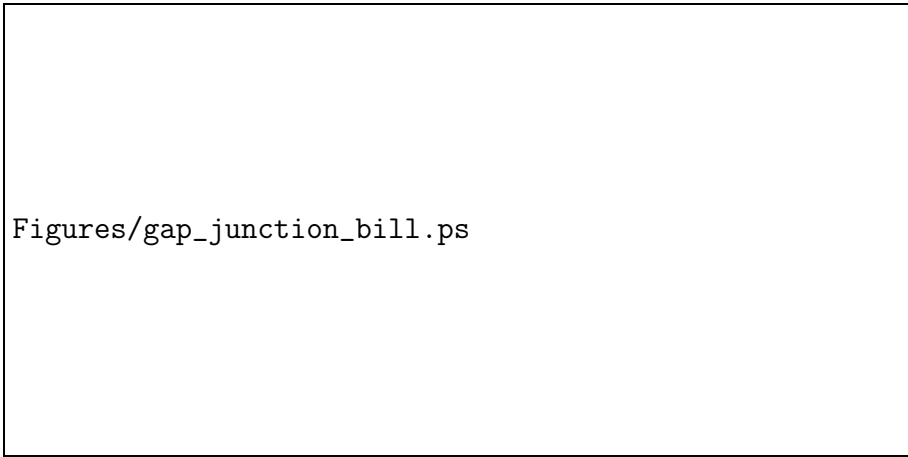
5 Synapses

Connections between neurons are provided by synapses

- electrical synapses: gap junctions

- chemical synapses

5.1 Gap Junctions

Gap junctions provide a direct electrical connection between neurons

```
Figures/gap_junction_bill.ps
```

Figure 41: Sketch of gap junctions.

- channel ('hole') formed by the protein connexin, of which there exist different types

- hemi-channels ('connexons') in the two cell membranes connect to each other and form the gap junction

- gap junction channels are permeable for any ion (unspecific)

- permeability can be modulated by neuromodulators

Ohmic resistance

$$I_{gap} = g_{gap} (V_1 - V_2) \qquad \text{with} \qquad V_i \text{ voltage of cell } i$$
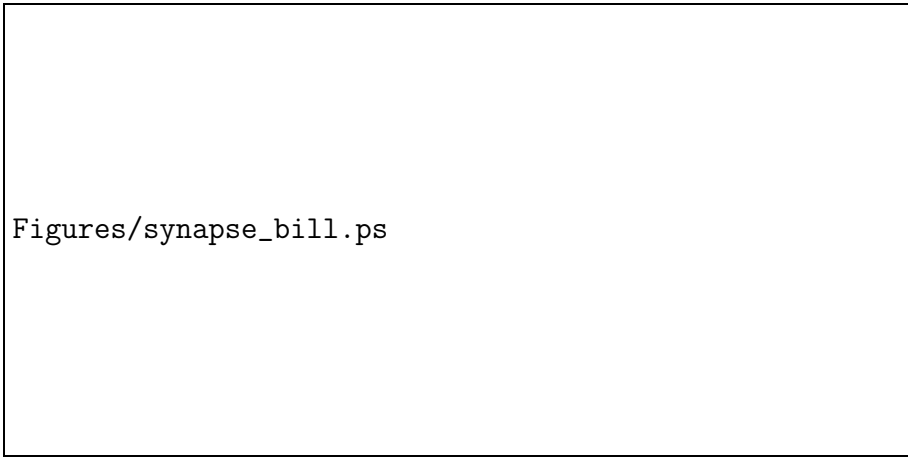
Notes:

- direct electrical coupling tends to make coupled neurons to behave similarly, e.g. synchronizes them

- gap junctions are *bi-directional*, coupled cells affect each other reciprocally

5.2 Chemical Synapses

Chemical synapses do not provide a direct electrical coupling between cells.

The information is transmitted by a *neurotransmitter*

```
Figures/synapse_bill.ps
```

Figure 42: Electromicrograph of synapse displaying many vesicles and the active zone (darker area at synaptic cleft).

Mechanism of synaptic transmission

- neurotransmitter is stored in vesicles (small 'bags' made of a lipid bilayer) in the pre-synaptic terminal

- depolarization of the pre-synaptic neuron by an incoming action potential induces Ca^{2+}-influx into the pre-synaptic cell

- increased $[Ca^{2+}]$ cause vesicles to dock at the cell membrane and merge with it. This releases the neurotransmitter into the synaptic cleft (narrow space) between the pre-synaptic terminal and the post-synaptic cell

- the neurotransmitter diffuses across the cleft ($\sim 20 - 40nm$)

- binding of neurotransmitter to the receptors activates them

    - ionotropic receptor
        * binding opens ion channel directly
        * ion flux through channel creates
            · excitatory postsynaptic current (EPSC) (Na^+ and K^+, also Ca^{2+} for NMDA) induces excitatory postsynaptic potential (EPSP)
            · inhbitory postsynaptic current (IPSC) (Cl^-) induces a IPSP
        * response is fast and decays quickly (in millisecond range)
    - metabotropic receptor
        * binding activates a G-protein in the membrane, which triggers a signaling pathway
            · eventually opens channels
            · can induce other changes (e.g. protein synthesis)

∗ response is slow and can last very long (up to hours)

- neurotransmitter is removed from the cleft through re-uptake by the pre-synaptic cell

- new vesicles are formed in pre-synaptic terminal by budding

```
Figures/synapse_mousedb_erlangen.ps
```
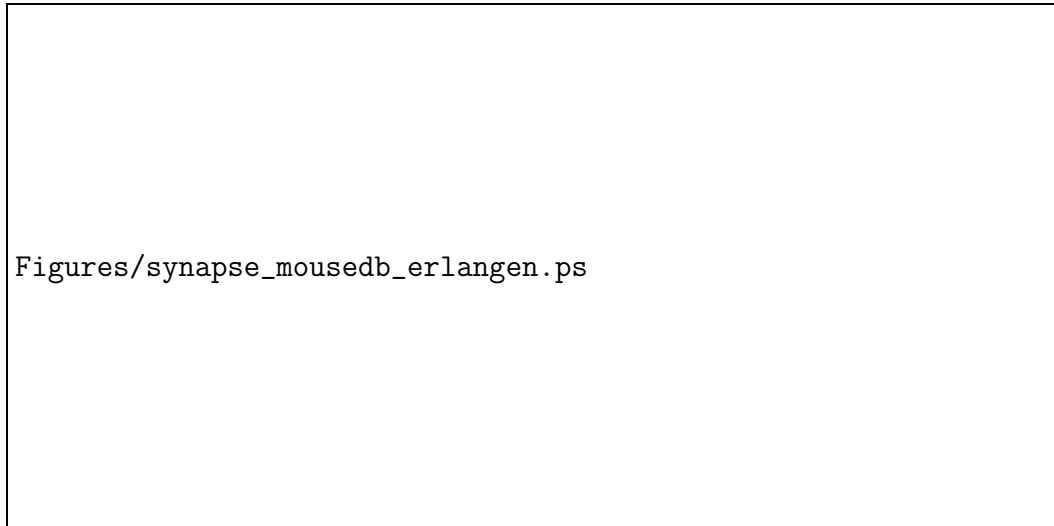
Figure 43: Sketch of chemical synapse(www.biochem.uni-erlangen.de/MouseDB)

Notes:

- transmission is *uni-directional* from the pre-synaptic to the post-synaptic cell

    – pre-synaptic cell is not affected at all by post-synaptic cell

- different neurotransmitters bind to different receptors, which open different channels

    – the post-synaptic cell can become *excited* or *inhibited* by the pre-synaptic cell

- synapses can amplify signals: *single* vesicle release can open thousands of ion channels

- Dale's principle:
  essentially all neurons express only a single neurotransmitter type $\Rightarrow$ a neuron can generate *either* excitatory *or* inhibitory output:
  it is *either* an excitatory neuron *or* an inhibitory neuron

- neurons can express excitatory *and* inhibitory receptors:
  they can receive excitatory and inhibitory inputs simultaneously

Excitatory synapses

- neurotransmitters: mostly glutamate and also kainate

- two major types of glutamate receptors:

  - AMPA (responds also to AMPA[14]):
    * activates very fast and deactivates quickly ($\sim$ 5ms)
      · permeable to Na^+ and K^+ (mixed kation channel)
      · reversal potential $E_{AMPA} \sim 0mV$
      · Ohmic $I(V)$-dependence

  - NMDA (responds also to NMDA[15]):
    * activates more slowly ($\sim$ 2ms) and deactivates much more slowly ($\sim$ 150ms) than AMPA
      · permeable to Na^+, K^+, and to Ca^{2+}
      · reversal potential $E_{NMDA} \sim 0mV$
      · nonlinear $I(V)$-dependence:
        extra-cellular Mg^{2+} binds to the pore in the open channel and blocks it, depolarization of the postsynaptic cell expells the Mg^{2+}

Inhibitory synapses

- neurotransmitters: mostly GABA and glycine

- two types of GABA receptors:

  - GABA$_A$
    * ionotropic receptor
    * permeable to Cl^- with reversal potential $E_{Cl} \sim -80mV$
    * Ohmic $I(V)$-dependence

  - GABA$_B$
    * metabotropic receptor
      · slower response
      · can induce long-lasting change inside the post-synaptic neuron
    * permeable to K^+
    * Ohmic $I(V)$-dependence

Synapses respond probabilistically

---

[14]AMPA=alpha-amino-3-hydroxy-5-methyl-4-isoxazolepropionic acid
[15]NMDA=N-methyl-D-aspartic acid

- pre-synaptic neuron: docking of vesicles at the membrane is a random process

  - **–** docking energy is comparable to thermal energy
  - **–** process characterized by probability of release
  - **–** vesicles have a typical size: quantal release consisting of 1, 2, ... vesicles
    $\Rightarrow$ EPSCs and IPSCs are roughly quantized (multiples of a minimal unit)

- post-synaptic neuron: binding with post-synaptic receptor is also a random process

Thus:

- not each action potential needs to lead to synaptic transmission

- even without an action potential one can have spontaneous release of neurotransmitter

- different types of synapses have different levels of *reliability*

- if many synapses connect the same neurons the random fluctuations average out

Note:

- by contrast, gap junctions are not probabilistic.

5.2.1 Modeling Chemical Synapses[16]

Ionotropic receptors are like other ion channels

$$I_s = g_s \left(V - E_{syn} \right)$$

with E_{syn} the reversal potential of the synapse, which determines whether it is excitatory or inhibitory.

The conductance is determined by the number of open synaptic channels:

$$g_s = \bar{g}_s P(t)$$

where

$$
\begin{aligned}
P &= \text{Prob(postsynaptic channel open)} \\
&= \underbrace{\text{Prob(release occurs)}}_{\text{pre-synaptic}} \times \underbrace{\text{Prob(channel open} \mid \text{transmitter released)}}_{\text{post-synaptic}} \\
&= P_{rel} \times P_s \quad\quad\quad\quad\quad\quad\quad\quad\quad\quad\quad\quad (27)
\end{aligned}
$$

---

[16]DA 5.8

Evolution of P_s:

Model the probability $P_s(t)$ of a channel to be open

$$\frac{dP_s}{dt} = \alpha_s \left(1 - P_s\right) - \beta_s P_s \tag{28}$$

- opening rate α_s depends on the concentration of the neurotransmitter:
  for larger concentration the probability that a neurotransmitter molecule is close
  to the receptor and therefore can bind to the receptor is larger

- closing rate β_s is typically assumed to be independent of the concentration
  channel closes when the neurotransmitter molecule unbinds from the receptor

Need to model the transmitter concentration in the cleft.

Very simple 'square-wave' model

- triggered by the pre-synaptic action potential at $t = 0$ the concentration jumps to
  a positive value and remains constant for a duration T

$$\alpha_s \gg \beta_s \qquad 0 < t \leq T$$

- after the duration T the concentration jumps to 0 again

$$\alpha_s = 0 \qquad T < t$$

Evolution of P_s

$$P_s(t) = \begin{cases} 1 + \left(P_s(0) - 1\right) e^{-\alpha_s t} & 0 < t \leq T \\ P_s(T) e^{-\beta_s(t-T)} & T < t \end{cases} \tag{29}$$

Figures/DaAb01.f5.14.ps
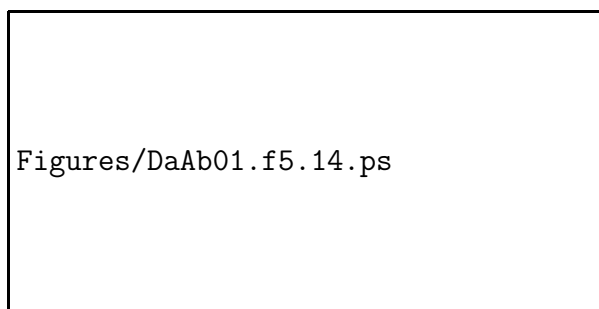
Figure 44: Fit of (29) to experimentally obtained EPSC (averaged over many stimuli)
[13].

Note:

- release of multiple vesicles will not change the concentration significantly compared to teh release of single vesicles

  - if the synaptic cleft is much narrower than the distance between release sites, since then concentration at receptor right across from release site will be much larger than at neighboring receptors
  - if re-uptake is very quick, since then the neurotransmitter will be removed before the next vesicle is released.

  then one has essentially independent release sites and times, each of which contributes $\propto P_{rel}P_s$ to the overall current.

Fast Synapses

For fast synapses with large α_s one need not resolve $P_s(t)$ during the short rise time: replace the evolution by a jump.

For $P_s(0) = 0$ the jump is given by $\Delta P_s = 1 - e^{-\alpha_s T}$.

For general $P_s(0)$ one can rewrite $P_s(T)$ as given by (29) as

$$P_s(T) = P_s(0) + \Delta P_s\left(1 - P_s(0)\right)$$

with

$$\Delta P_s = 1 - e^{-\alpha_s T}.$$

Model the synapse then by

$$\begin{cases} P_s \to P_s + \Delta P_s\left(1 - P_s\right) & \text{when synaptic event occurs} \\ \frac{dP_s}{dt} = -\beta_s P_s & \text{between synaptic events} \end{cases}$$

Note:

- Since $\Delta P_s \leq 1$ one has $P_s \leq 1$ after the spike

- due to the slow decay of P_s subsequent synaptic currents can overlap

Slow Synapses

Need to resolve also the rising phase of the synaptic current. The rise time introduces a *delay* in the information transmission. This can have significant effects on the dynamics of the neuronal network.

Could use (28) with solution (29). The switching from one solution to the other at $t = T$ is awkward: one would need to keep track of the spike *and* the time switching time T later.

For simplicity, often two other approaches are taken (keeping in mind that the square-wave model is not really realistic either)

1. Difference of two exponentials
   For $P_s(0) = 0$

   $$P_s(t) = \Delta P_s \, N \left(e^{-t/\tau_1} - e^{-t/\tau_2} \right) \tag{30}$$

   with $\tau_1 > \tau_2$

   - Decay time:
     for large t

     $$P_s(t) = \Delta P_s \, N \, e^{-t/\tau_1}$$

     $$\tau_{decay} = \tau_1$$

   - Maximal conductance is reached at

     $$t_{max} = \ln \left(\frac{\tau_1}{\tau_2} \right) \frac{\tau_1 \tau_2}{\tau_1 - \tau_2} \equiv \ln \left(\frac{\tau_1}{\tau_2} \right) \tau_{rise}$$

     N normalizes $P_s(t)$ such that $P_s(t_{max}) = \Delta P_s$,

     $$N = \left(\left(\frac{\tau_2}{\tau_1} \right)^{\frac{\tau_2}{\tau_1 - \tau_2}} - \left(\frac{\tau_2}{\tau_1} \right)^{\frac{\tau_1}{\tau_1 - \tau_2}} \right)^{-1}$$

   - For general $P_s(0)$ implement the evolution of $P_s(t)$ as

     $$P_s(t) = N \, (A(t) - B(t)) \tag{31}$$

     where between spikes

     $$\tau_1 \frac{dA}{dt} = -A$$
     $$\tau_2 \frac{dB}{dt} = -B$$

     and at spike the amplitudes are reinitiated (somewhat analogous to treatment of fast synapse)

     $$A(t^+) \rightarrow A(t^-) + \Delta P_s \left(1 - P_s(t^-) \right) \tag{32}$$
     $$B(t^+) \rightarrow B(t^-) + \Delta P_s \left(1 - P_s(t^-) \right) \tag{33}$$

     such that $P_s(t)$ is continuous at spike:

     $$A(t^+) - B(t^+) = A(t^-) - B(t^-)$$

2. α-function
   for $P_s(0) = 0$

   $$P_s(t) = \Delta P_s \frac{t}{\tau_s} e^{-t/\tau_s}$$

   has decay time τ_s and reaches maximal conductance at

   $$t_{max} = \tau_s$$

   69

Example:

Consider 2 IF-neurons with neuron 1 giving excitatory synaptic input to neuron 2 and vice versa

$$\tau \frac{dV_1}{dt} = -V_1 + I_e(t) - g_1 P_2(t)(V_1 - E_{syn}) \tag{34}$$

$$\tau \frac{dV_2}{dt} = -V_2 + I_e(t) - g_2 P_1(t)(V_2 - E_{syn}) \tag{35}$$

with $V_{threshold} = 30$ and $V_{reset} = -55$. $P_i(t)$ is given by $P_s(t)$ triggered by spike in neuron i (assuming $P_{rel} = 1$).

a)
```
Figures/2cells_IF_membrane_nosummation.eps
```
b)
```
Figures/2cells_IF_membrane_summation.eps
```
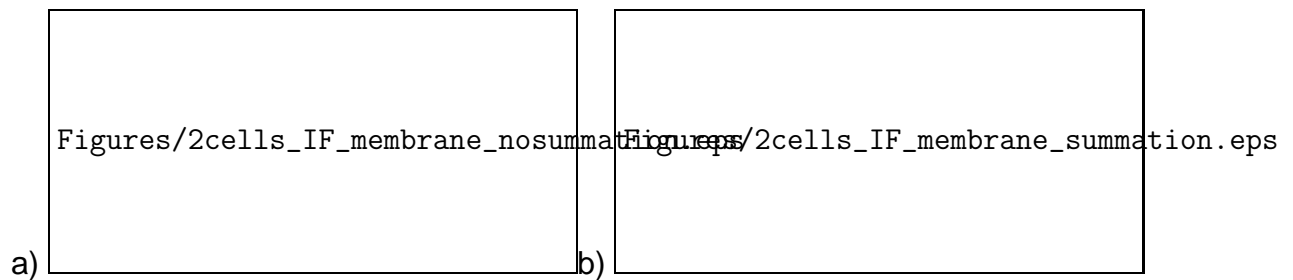
Figure 45: Integration of multiple inputs by slow membrane. IF-modell (34,35) with $\tau = 1$, $\tau_1 = 0.05$, $g_1 = 0$, $\tau_2 = 0.025$, $g_2 = 50$, $E_{syn} = 50$ a) $I_e = 50$ b) $I_e = 250$.

Fig.45a:

- weak synaptic coupling: single spike of neuron 1 does not trigger a spike in neuron 2

- inter-spike interval (ISI) large enough for most channels to close between synaptic events

- slow membrane dynamics (large τ_m):
  some temporal summation of post-synaptic currents by the membrane

Fig.45b:

- higher firing frequency (smaller ISI): more spikes during membrane relaxation $\Rightarrow$ stronger integration in time $\Rightarrow$ second neuron spikes.

- multiple synaptic inputs needed to trigger spike in neuron 2

a)
```
Figures/2cells_IF_synapse_nosummation.eps
```

b)
```
Figures/2cells_IF_synapse_summation.eps
```
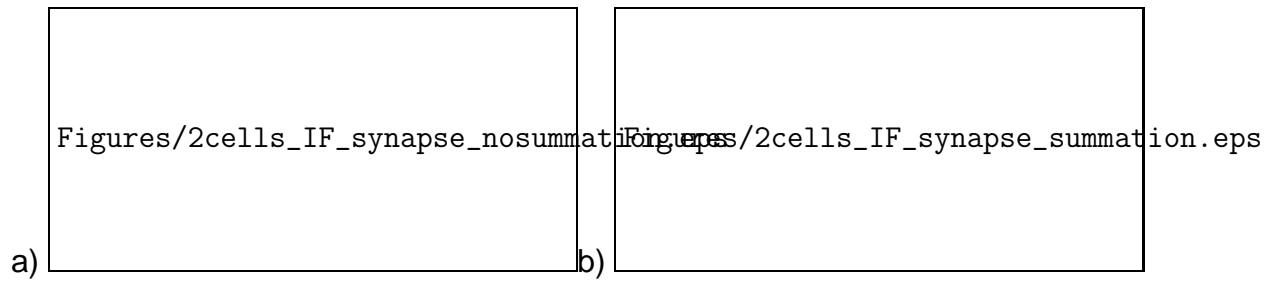
Figure 46: Integration of multiple inputs by slow synapse. IF-modell (34,35) with $\tau = 0.1$, $\tau_1 = 0.5$, $g_1 = 0$, $\tau_2 = 0.25$, $g_2 = 10$, $E_{syn} = 50$, a) $I_e = 302$, b) $I_e = 400$.

Fig.46:

- synapses slower than membrane:
  channels do not close during ISI $\Rightarrow$ temporal summation of open synaptic channels

- large fraction of channels are open persistently

Synaptic Conductance g_s**:**

For AMPA and GABA receptors $\bar{g}_s$ is independent of voltage.

For NMDA receptors the conductance depends on the voltage of the *post-synaptic* neuron

$$\bar{g}_s = \bar{g}_s(V_{post})$$

- near the resting potential the NMDA receptors are blocked by Mg^{2+} ions

- the Mg^{2+}-block is reduced/removed as voltage is increased

$$\bar{g}_{NMDA} = \bar{\bar{g}}_{NMDA} \frac{1}{1 + a\,[Mg^{2+}]\,e^{-V_{post}/V_{block}}}$$

```
Figures/StEd92.f10.eps
```
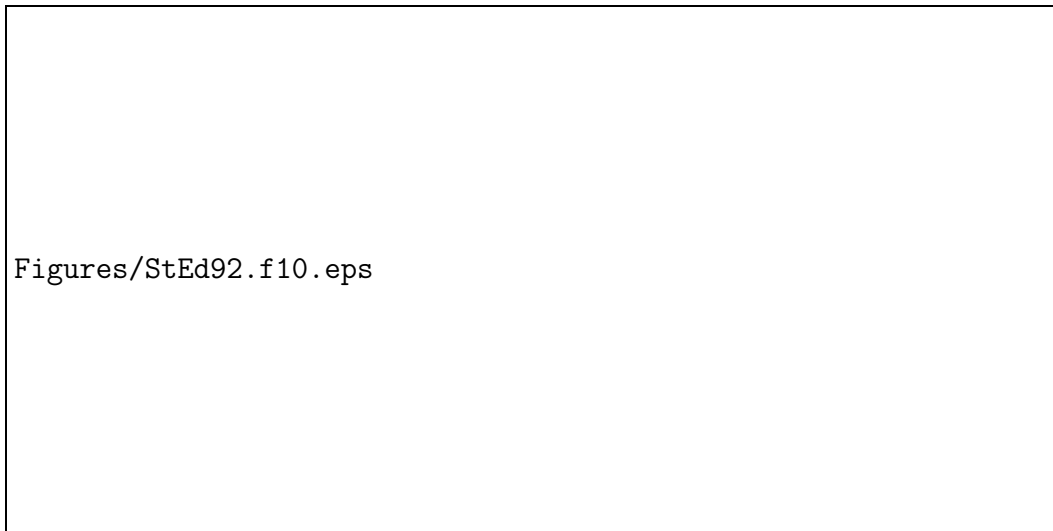
Figure 47: Different time scales and different voltage dependence of synaptic currents evoked by AMPA and by NMDA receptors. CNQX blocks AMPA receptors, APV blocks NMDA receptors. [57]

```
Figures/DaAb01.f5.16.ps
```
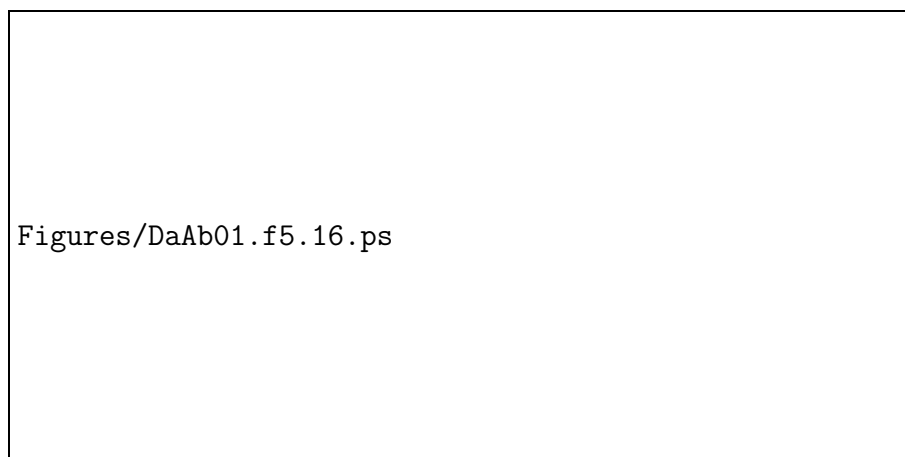
Figure 48: Dependence of NMDA-conductance on $[Mg^{2+}]$ and voltage [10].

Notes:

- NMDA-mediated excitatory currents require

  - pre-synaptic action potential
  - post-synaptic depolarization

- NMDA-receptors can function as *coincidence detectors*

- NMDA-receptors are permeable to Ca^{2+}

- Ca^{2+} plays important role in modifying the strength of synapses (synaptic plasticity) and learning

- NMDA-receptors are likely a neural substrate for 'Hebbian learning' : 'neurons that fire together are wired together' (see Sec.7.3.5)

5.2.2 Short-Term Plasticity

The magnitude and probability of synaptically evoked currents can depend on the history of the activity at the synapes

- short-term plasticity: modifications that last from milliseconds to seconds

- long-term plasticity: modifications that last much longer, possibly as long as the animal lives

Many mechanisms can contribute to plasticity. They can be pre-synaptic and post-synaptic.

We focus here on the short-term plasticity through changes in the probability of release P_{rel} (cf. (27)).

- depression: P_{rel} is reduced by action potential
  e.g. the pool of releasable vesicles can become depleted if it does not become replenished sufficiently fast after the release

- facilitation: P_{rel} is increased by action potential
  e.g. the presynaptic $[Ca^{2+}]$ and with it the release probability can rise through multiple action potentials

Simple phenomenological model:

- Between action potentials P_{rel} relaxes to its 'usual' value P_∞

$$\tau_{rel}\frac{dP_{rel}}{dt} = P_\infty - P_{rel} \tag{36}$$

relaxation to the steady-state value could be that of the number of releasable vesicles (vesicle fusion, transmitter re-uptake) or of $[Ca^{2+}]$ (action of Ca^{2+}pumps).

- Depression:

$$P_{rel} \to f_D P_{rel}, \qquad f_D < 1 \qquad \text{at } t^+_{spike} \quad \text{immediately after spike}$$

- Facilitation:

$$P_{rel} \to P_{rel} + f_F\left(1 - P_{rel}\right) \quad \text{at } t^+_{spike} \quad \text{immediately after spike}$$

Consider the steady state that is reached when transmitting a regular train of action potentials with period T

- relaxation between spikes must be balanced by increments/decrements at spikes

Facilitation:

After a spike at $t = 0^+$ P_{rel} gets incremented

$$P_{rel}(0^+) = P_{rel}(0^-) + f_F \left(1 - P_{rel}(0^-)\right) \tag{37}$$

Then P_{rel} relaxes according to (36)

$$P_{rel}(T^-) = P_\infty + \left(P_{rel}(0^+) - P_\infty\right) e^{-T/\tau_{rel}}$$

For periodic solution we need

$$P_{rel}(T^-) = P_{rel}(0^-)$$

Inserting $P_{rel}(0^+)$ into $P_{rel}(T^-)$ yields

$$P_\infty + \left(P_{rel}(0^-) + f_F \left(1 - P_{rel}(0^-)\right) - P_\infty\right) e^{-T/\tau_{rel}} = P_{rel}(0^-)$$

Thus

$$P_{rel}(0^-) = P_\infty \frac{1 - \left(1 - \frac{f_F}{P_\infty}\right) e^{-T/\tau_{rel}}}{1 - (1 - f_F) e^{-T/\tau_{rel}}} \geq P_\infty$$

For low firing rate ($T \gg \tau_{rel}$) the exponential is small and the denominator can be expanded

$$P_{rel}(0^-) = P_\infty + f_F \left(1 - P_\infty\right) e^{-T/\tau_{rel}} + \mathcal{O}(e^{-2T/\tau_{rel}})$$

Facilitation decays between spikes, P_{rel} only slightly increased

For high firing rate ($T \ll \tau_{rel}$)

$$P_{rel}(0^-) \approx \frac{f_F + (P_\infty - f_F) \frac{T}{\tau_{rel}}}{f_F + (1 - f_F) \frac{T}{\tau_{rel}}} = 1 - \frac{1 - P_\infty}{f_F} \frac{T}{\tau_{rel}} + \mathcal{O}\left(\left(\frac{T}{\tau_{rel}}\right)^2\right)$$

Facilitation raises P_{rel} to values close 1

Depression:

(37) is replaced by

$$P_{rel}(0^+) = f_D P_{rel}(0^-)$$

yielding for the periodicity condition

$$P_\infty + \left(f_D P_{rel}(0^-) - P_\infty\right) e^{-T/\tau_{rel}} = P_{rel}(0^-)$$

$$P_{rel}(0^-) = P_\infty \frac{1 - e^{-T/\tau_{rel}}}{1 - f_D e^{-T/\tau_{rel}}} \leq P_\infty$$

For low firing rate ($T \gg \tau_{rel}$)

$$P_{rel}(0^-) = P_\infty \left(1 - (1 + f_D)e^{-T/\tau_{rel}}\right) + \mathcal{O}\left(e^{-2T/\tau_{rel}}\right)$$

For high firing rate ($T \ll \tau_{rel}$)

$$P_{rel}(0^-) = P_\infty \frac{1}{1 - f_D} \frac{T}{\tau_{rel}} + \mathcal{O}\left(\left(\frac{T}{\tau_{rel}}\right)^2\right)$$

depression severely suppresses release.

How many spikes are actually transmitted by the synapse?
Per period of the presynaptic train of action potentials $1 \cdot P_{rel}$ spikes are transmitted $\Rightarrow$ the transmission rate of spikes is given by

$$R = P_{rel} \cdot \frac{1}{T}$$

For high firing rates the transmission rate of the depressing synapse saturates

$$R = \frac{P_\infty}{1 - f_D} \frac{1}{\tau_{rel}} + \dots$$

Note:

- For high firing rates this depressing synapse does not transmit any information about the value of the input firing rate $1/T$.

- R is the output firing rate of an array of parallel synapses

For high firing rates consider step change in input firing rate $r \equiv \frac{1}{T}$

$$r \to r + \Delta r$$

Before the step

$$P_{rel}^- = \frac{P_\infty}{(1 - f_D)\,\tau_{rel}} \cdot \frac{1}{r} \qquad R^- = \frac{P_\infty}{(1 - f_D)\,\tau_{rel}}$$

Immediately after the step P_{rel} is unchanged

$$R^+ = P_{rel}^- \,(r + \Delta r) = R^- \frac{r + \Delta r}{r}$$

and

$$\frac{R^+ - R^-}{R^-} = \frac{\Delta r}{r}$$

where for long plateaus R^- is close to the asymptotic value $R = \frac{P_\infty}{1 - f_D} \frac{1}{\tau_{rel}}$.
Thus

- For high firing rates this depressing synapse responds only to *changes* in input firing rate

- The change in output firing rate is given by the *relative change* of the input firing rate, independent of its absolute value (scale-invariant)

- synapse performs a 'computation' on the input

```
Figures/DaAb01.f5.19.ps
```

Figure 49: Response of depressing synapse to varying input firing rates [10]

Note:

- for natural conditions *irregular* input spiking is a better approximation
  for randomly distributed spike times (Poisson train) the analogous computation
  yields an equivalent result (cf. Dayan & Abbott Ch.5.8)

- depression and facilitation can occur at the same synapse on different time scales.

For a more detailed model of short-term plasticity see [59, 43].

6   Firing Rates[17]

Purpose of neurons is to transmit information

- from sensory organs

---

[17]DA 1.2,1.4

- to cortex (merging of sensory information, storage in memory, comparison with memory, decisions)

- to motor control

- to muscles

In most parts of the brain the information is transmitted via action potentials. How do they transmit the information?

- the shape of the action potential is stereo-typical

    - presumably it contains little information
    - can replace it by an elementary 'event'

- timing of the spike

- rate at which spikes are fired

- correlations between spikes of pairs of neurons

    - synchrony
    - given time difference between spikes
    - ...

- correlations between spikes of neuron triplets

- firing sequences

- ...

```
Figures/visual_receptive_fields_HW.ps
```
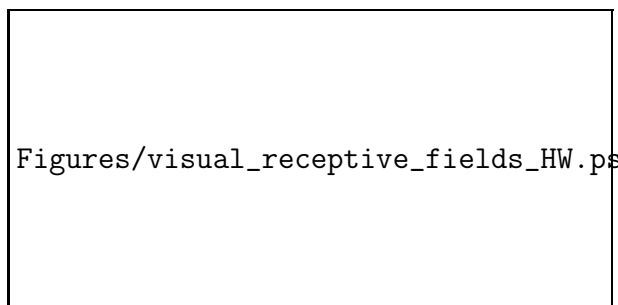
Figure 50: Receptive fields of neurons in primary visual cortex. Hubel & Wiesel video. Long movie `http://people.esam.northwestern.edu/riecke/Vorlesungen/Comp_Neuro/Notes/Movies/VisualCortex.mov`
There are a number of short movies on www.youtube.com.

Figures/BaBu08.f2A.ps
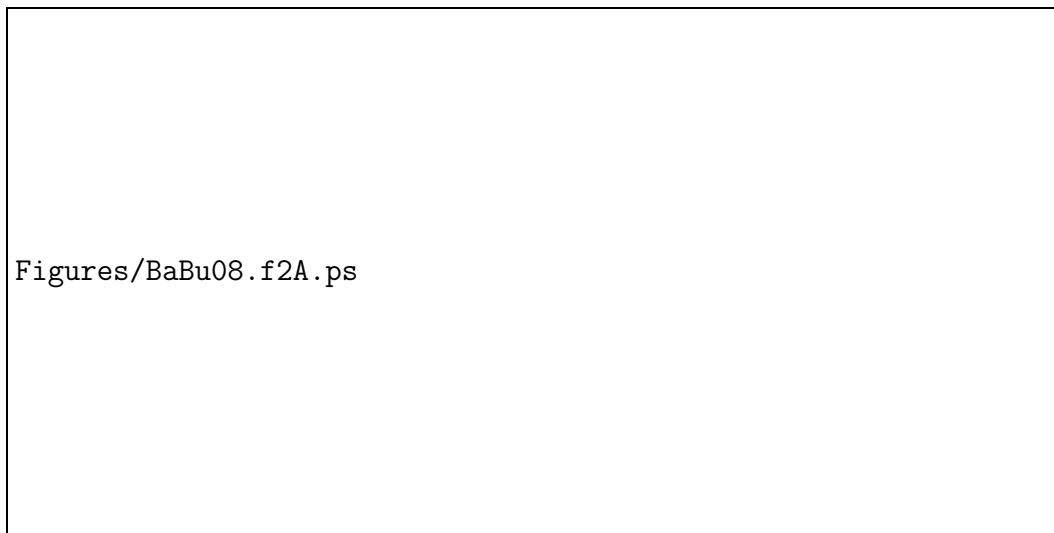
Figure 51: Spike responses to odor inhalation of a mouse. Bars in horizontal lines denote spikes in different trials under the same conditions [1].

Figures/DaAb01.f1.6.ps
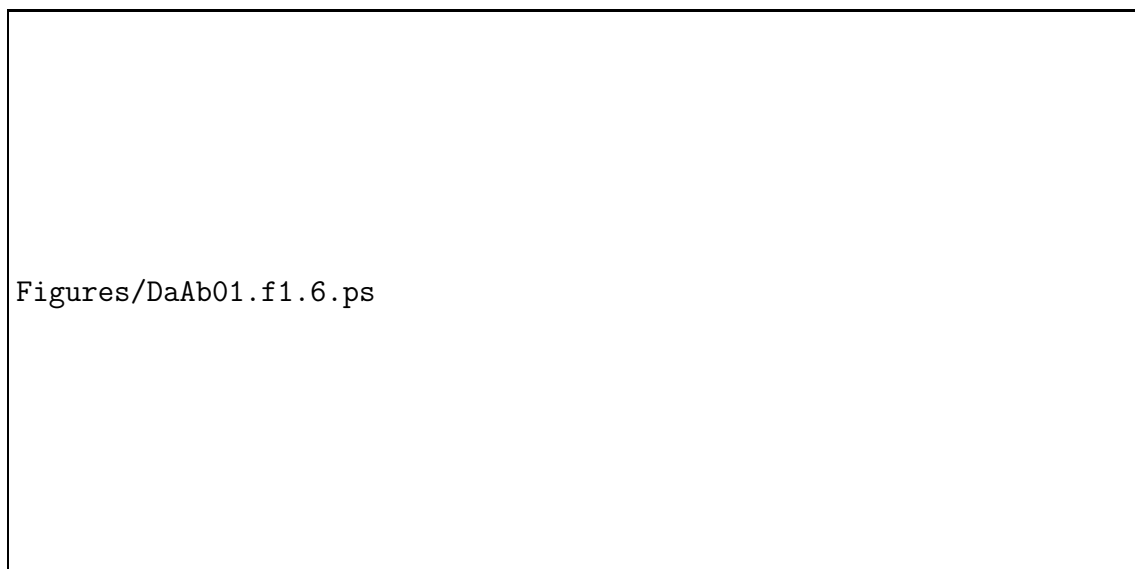
Figure 52: Neuron in primary motor cortex. a) raster plots during reaching movements in different directions. b) average firing rate as a function of the reaching direction [10].

Notes:

- The rate at which spikes are fired seems to contain significant information.

- There is a significant variation in the individual spike times across repeated trials.

- To assess the significance of correlations between spikes of different neurons one needs to measure multiple/many neurons simultaneously

- barn owl: in echo-location the coincidence of spikes from neurons from the left and the right ear provides the information about the location of the object

- in general, role of spike synchrony and correlations is still being debated very actively.
  oscillations and rhythms are observed in coarse measures (e.g. local field potential, EEG) of many large ensembles of neurons: function?
  difficulties:

  * data acquisition
    · voltage-sensitive dies and Ca^{2+}-imaging are slow
    · multi-electrode arrays require spike sorting (neuron identification)
    · ...
  * data analysis: binomial explosion of correlations (which neurons are read?)

Firing Rate

There are different ways to define a firing rate of a neuron.

Consider the neural reponse function

$$\rho(t) = \sum_{i=1}^{n} \delta(t - t_i)$$

where t_i, $i = 1 \ldots n$, are the spike times and $\delta(t)$ is the Dirac δ-function.

- Spike-count rate
$$r = \frac{n}{T} = \frac{1}{T} \int_0^T \rho(t) dt$$

  - counts the total number of spikes over the whole duration T of the trial

  - does not give any temporal resolution

  - for uncorrelated spikes the variability in r depends on the total number of spikes in the interval:
    variability becomes small for $rT \gg 1$

- Time-dependent firing rate

  - to get temporal resolution need an integration window Δt that is short compared to the time scale τ over which the firing rate changes

    * fluctuations in firing rate are small if
      · if the firing rate is high and
      · if it varies only on a slow time scale τ allowing $\Delta t = \mathcal{O}(\tau)$:
        the number of spikes during τ must be large: $r\tau \gg 1$.

- **–** if Δt is very short it will contain very few spikes
  to get a reliable measure average over multiple trials of the same experiment

$$r(t) = \left\langle \frac{1}{\Delta t} \int_t^{t+\Delta t} \rho(t')dt' \right\rangle_{trials} = \frac{1}{\Delta t} \int_t^{t+\Delta t} \langle \rho(t') \rangle \ dt'$$

  where $\langle \ldots \rangle_{trials}$ denotes the average over trials

  - $*$ the size of Δt limits the temporal resolution
  - $*$ Δt can be chosen small if many trials are available

- **–** in the limit $\Delta t \to 0$ at most 1 spike occurs during Δt

  - $*$ $r(t)\Delta t$ is the fraction of trials during which a spike occurred in the interval $[t, t + \Delta t]$
  - $*$ thus, $r(t)\Delta t$ is the probability of firing a spike during that interval

Figures/DaAb01.f1.4.ps
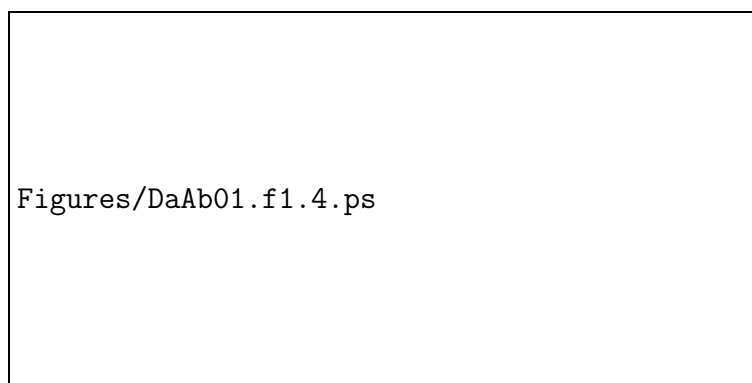
Figure 53: Spike train and firing rates obtained by binning in fixed windows (b), in sliding rectangular window (c), in sliding Gaussian window (d), causal window (e). [10].

- Population firing rate

  - **–** in many situations an animal does not have the privilege to average over many trials
  - **–** if multiple, statistically independent neurons convey the same information the animal can use a population average $\langle \ldots \rangle_{pop}$ summing up the spikes of those neurons during an interval Δt

$$r_{pop}(t) = \frac{1}{\Delta t} \int_t^{t+\Delta t} \langle \rho(t') \rangle_{pop} dt'$$

6.1 Poisson Spike Trains

Averaging over trials relies on the variability of the spiking response across trials (cf.Fig.51). If the spikes always occurred at precisely the same times averaging would not make ρ any smoother.

Consider random spike trains

The trains are thought of as being generated by a stochastic process. We are interested in

$$P[t_1, t_2, \ldots, t_n] = \text{Probability of spikes occuring at the specified times}$$

Spikes are events: a stochastic process that generates a sequence of discrete events is called a *point process*.

Events could depend on all previous events. Simpler processes are

- renewal process: spiking probability depends only on the previous spike time

- Poisson process: spiking probability is completely independent of all previous spike times

Note:

- if only the firing rate is relevant a suitable model for the spike train is a Poisson process

    - constant firing rate r: homogeneous Poisson process
    - time-varying firing rate $r(t)$: inhomogeneous Poisson process

Homogeneous Poisson process:

Determine the probability that during interval T exactly n spikes are fired (at *arbitrary* times): $P_T[n]$

Divide T into $M = T/\Delta t$ bins with $M \to \infty$ eventually

$$P_T[n] = \lim_{\Delta t \to 0} \underbrace{(r\Delta t)^n}_{\text{spike in } n \text{ bins}} \times \underbrace{(1 - r\Delta t)^{M-n}}_{\text{no spikes in } M-n \text{ bins}} \underbrace{\frac{M!}{(M - n!)\, n!}}_{\text{choose } n \text{ from } M}$$

Rewrite second factor using $\epsilon = -r\Delta t$

$$\lim_{\epsilon \to 0} (1 + \epsilon)^{\frac{T}{\Delta t} - n} = \lim_{\epsilon \to 0} (1 + \epsilon)^{-\frac{Tr}{\epsilon} - n} = \lim_{\epsilon \to 0} \left(\left((1 + \epsilon)^{\frac{1}{\epsilon}} \right)^{-rT} (1 + \epsilon)^{-n} \right) = e^{-rT}$$

Using Stirling formula for $\ln N$ for large N

$$\ln N! = N \ln N - N + \mathcal{O}(\ln N)$$

for large M at fixed n we get then

$$
\begin{aligned}
\ln \frac{M!}{(M - n)!} &\approx M \ln M - M - \left((M - n) \ln \left(M \left(1 - \frac{n}{M}\right) \right) \right) + M - n \\
&= M \ln M - (M - n) \ln M + \mathcal{O}(n) \\
&\approx n \ln M
\end{aligned}
$$

yields the limit

$$\frac{M!}{(M-n)!} \to M^n \qquad \text{for } M \to \infty$$

Thus

$$P_T[n] = \lim_{\Delta t \to 0} (r\Delta t)^n \, e^{-rT} \frac{1}{n!} \left(\frac{T}{\Delta t}\right)^n$$

Thus, the Poisson process is described by the Poisson distribution

$$P_T[n] = \frac{1}{n!} (rT)^n \, e^{-rT}$$

Figures/DaAb01.f1.11.ps
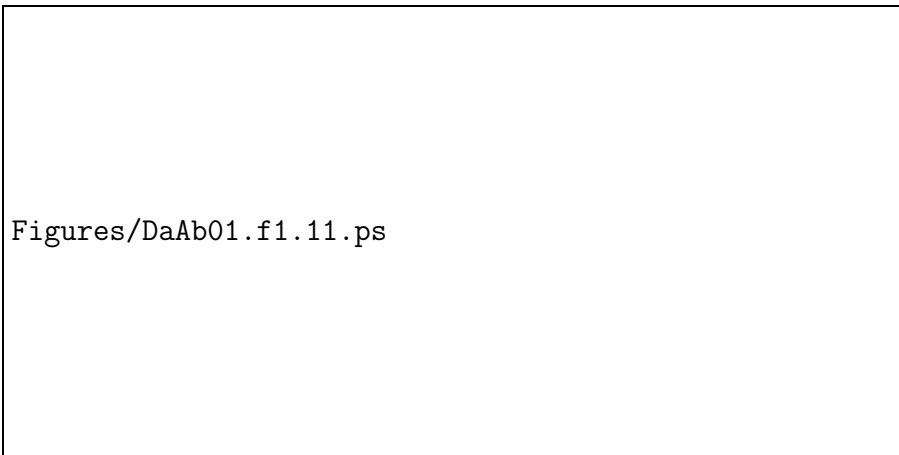
Figure 54: a) Probability of having exactly n spikes as a function of rescaled firing rate rT. b) For not too small rT the Poisson distribution is well approximated by a Gaussian distribution with a variance that is equal to its mean [10].

Compute mean and variance

$$\langle n \rangle = \sum_{n=0}^{\infty} n \, P_T[n] \qquad \sigma_n^2 \equiv \langle n^2 \rangle - \langle n \rangle^2 = \sum_{n=0}^{\infty} (n - \langle n \rangle)^2 \, P_T[n]$$

To compute these it is useful to introduce what is called the moment-generating function

$$g(\alpha) = \sum_{n=0}^{\infty} e^{\alpha n} P_T[n]$$

It allows to calculate the moments $\langle n^k \rangle$ very easily,

$$\langle n^k \rangle = \left. \frac{d^k}{d\alpha^k} g(\alpha) \right|_{\alpha=0}$$

Now

$$g(\alpha) = \sum_{n=0}^{\infty} e^{\alpha n} \frac{1}{n!} (rT)^n \, e^{-rT} = e^{-rT} \sum_{n=0}^{\infty} \frac{1}{n!} (e^\alpha rT)^n = e^{-rT} e^{e^\alpha rT}$$

using the Taylor series of the exponential

$$e^x = \sum_{n=0}^{\infty} \frac{1}{n!} x^n$$

$$\left.\frac{dg}{d\alpha}\right|_{\alpha=0} = e^{-rT} e^{rTe^\alpha} rTe^\alpha \big|_{\alpha=0} = rT$$

$$\left.\frac{d^2g}{d\alpha^2}\right|_{\alpha=0} = e^{-rT} e^{rTe^\alpha} (rTe^\alpha)^2 + e^{-rT} e^{rTe^\alpha} rTe^\alpha \big|_{\alpha=0} = (rT)^2 + rT$$

Thus:

$$\langle n \rangle = rT \qquad \sigma_n^2 = rT$$

Note:

- the Fano factor is defined as

$$F = \frac{\sigma_n^2}{\langle n \rangle}$$

- for the Poisson distribution the mean and the variance are equal, independent of T

$$F = 1$$
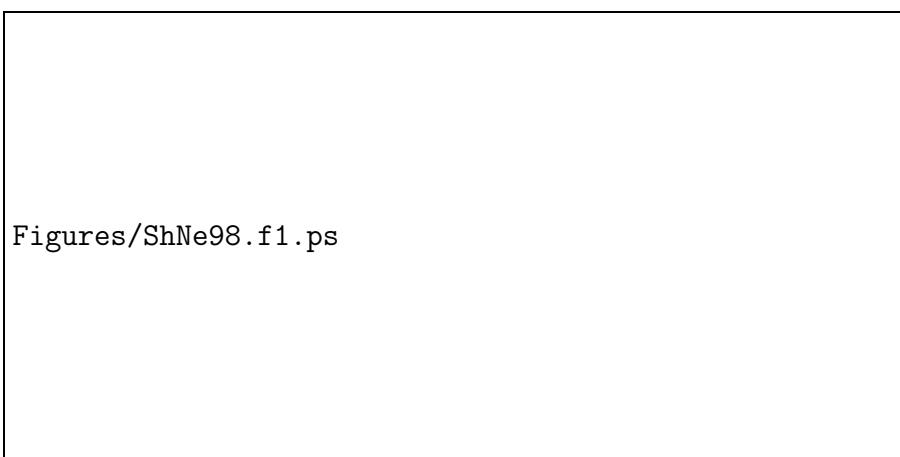
Figure 55: High firing variability of cortical neurons (area MT of an alert monkey) reflecting balanced excitatory and inhibitory input from a large number of neurons. Variance grows (super-linearly) with mean firing rate [53].

```
Figures/FiCh07.f4_top.ps
```
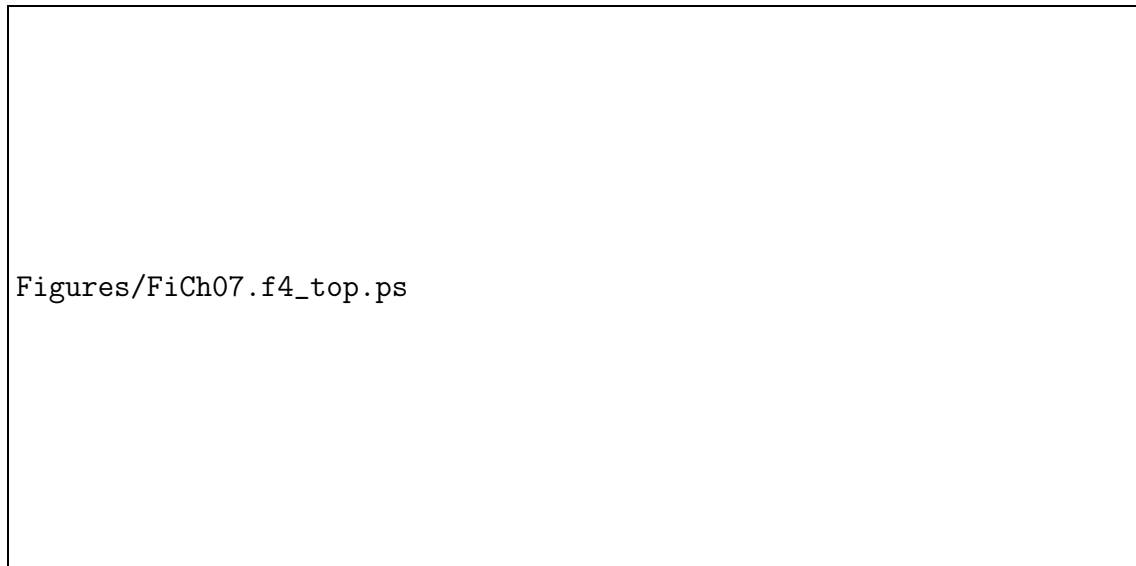
Figure 56: Low firing variability of retinal ganglion cells (sub-Poisson). [17]

```
Figures/SrYo06.f11.ps
```
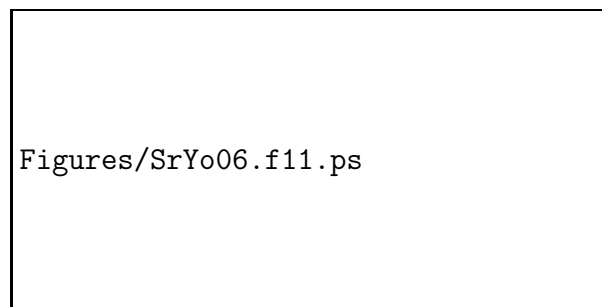
Figure 57: Mean firing rate and variability of firing rate of peripheral (SA1 and RA) and cortical neurons (3b and 1) in response to tactile stimulation of macaque monkey [56].

6.2 What Makes a Neuron Fire?[18]
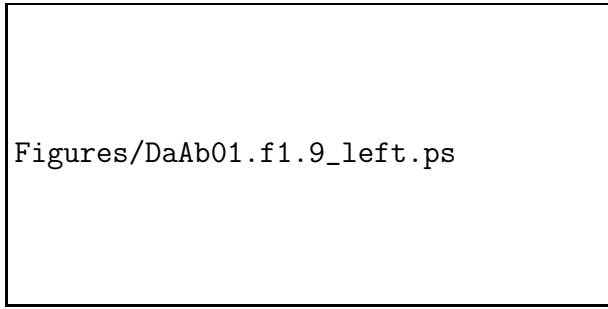
Tuning curves like Fig.52 show how a neuron responds for a range of selected stimuli, e.g. different orientations of a given grating pattern.
Can one assess what kind of stimulus would elicit maximal response from the neuron without restricting the stimulus to a specific type (e.g. grating pattern with a given wavelength)?

6.2.1 Spike-Triggered Average

Consider a neuron responding to a stimulus $s(t)$ with a spike train $\{t_i, i = 1 \ldots n\}$

---

[18]DA 1.3 +2.2

```
Figures/DaAb01.f1.9_left.ps
```
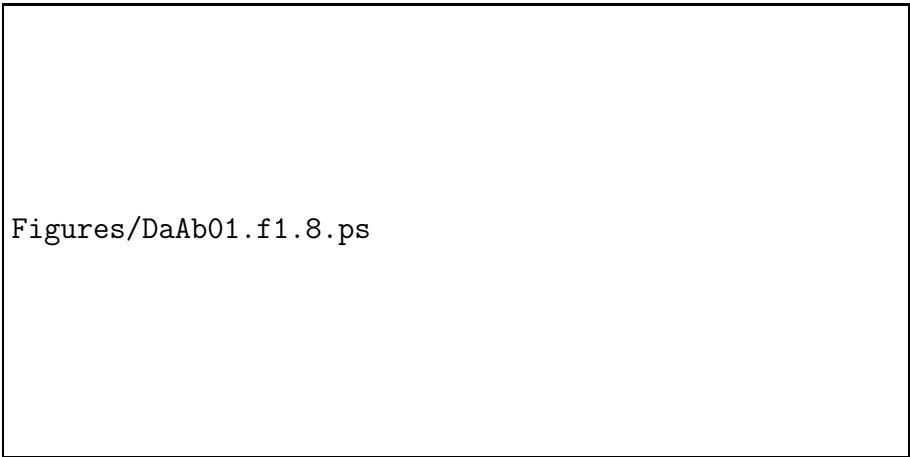
Figure 58: Time-dependent stimulus and resulting spiking activity of electrosensory neuron in weakly electric fish [10].

- The stimulus provides a time-varying input current to the neuron.

- The neuron accumulates the input and spikes when the threshold voltage is surpassed (cf. Fig.45).

- what is the average stimulus history that leads to a spike?

For each spike at time t_i in the experimental interval $[0, T]$ measure the stimulus at a time $t_i - \tau$ contributing to the spike
To get spike-triggered average stimulus average the spike trains for many presentations ('trials') of the *same* stimulus $s(t)$

$$C(\tau) = \left\langle \frac{1}{n} \sum_{i=1}^{n} s(t_i - \tau) \right\rangle$$

```
Figures/DaAb01.f1.8.ps
```

Figure 59: Procedure to compute the spike-triggered average stimulus [10].

Assuming small fluctuations in the number of spikes across the trials ($\sim 1/\langle n \rangle^{1/2}$) to pull the factor $\frac{1}{n}$ out of the average over trials and using the neural response function $\rho = \sum_{i=1}^{n} \delta(t - t_i)$

$$C(\tau) \approx \frac{1}{\langle n \rangle} \left\langle \sum_{i=1}^{n} \underbrace{s(t_i - \tau)}_{\int_0^T \delta(t'-t_i)\, s(t'-\tau)\, dt'} \right\rangle =$$

$$= \frac{1}{\langle n \rangle} \left\langle \int_0^T \rho(t')\, s(t' - \tau)\, dt' \right\rangle$$

$$= \frac{1}{\langle n \rangle} \int_0^T \langle \rho(t') \rangle \; s(t' - \tau)\, dt'$$

$$= \frac{1}{\langle n \rangle} \int_0^T r(t')\, s(t' - \tau)\, dt'$$

Consider the correlation function between stimulus and firing rate

$$Q_{rs}(\tau) = \frac{1}{T} \int_0^T r(t')\, s(t' + \tau)\, dt'$$

Using $\langle n \rangle = rT$ we get

$$C(\tau) = \frac{Q_{rs}(-\tau)}{r}$$

Note:

- the spike-triggered average stimulus is proportional to the reverse correlation (because of the minus-sign)

- $C(\tau)$ depends on the stimulus set used:

    - to cover all possible inputs: use random stimulus ensemble (e.g. white noise)
    - statistically *stationary* stimulus
        * the response properties of a neuron could depend on its mean firing rate (e.g. by facilitation or depression); statistically nonstationary stimuli would average over different 'states' of the neuron.
    - $\langle \ldots \rangle$ is the average over many realizations from that ensemble

To characterize stimulus ensemble: auto-correlation function of $s(t)$

$$Q_{ss}(\tau) = \frac{1}{T} \int_0^T s(t')s(t' + \tau)dt'$$

Use white noise without any correlations between different times

$$Q_{ss}(\tau) = \sigma_s^2 \delta(\tau)$$

```
Figures/DaAb01.f1.9.ps
```
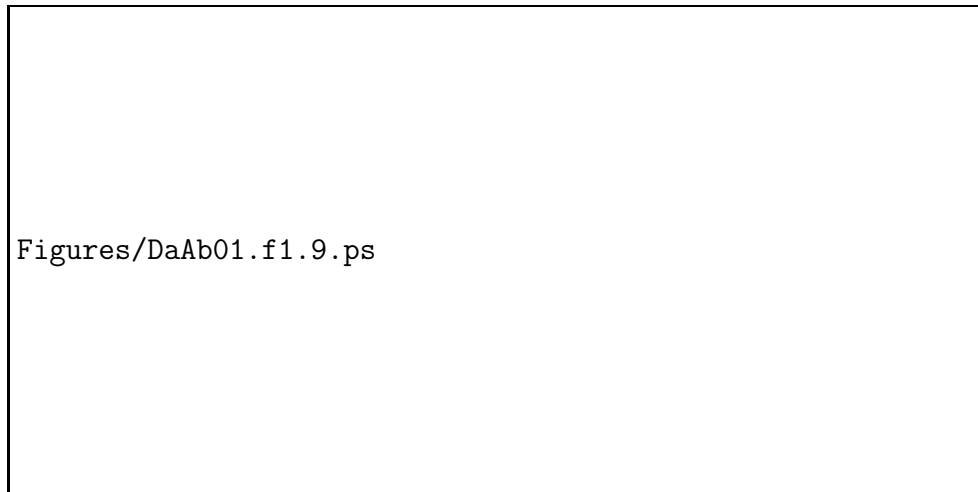
Figure 60: Spike-triggered average stimulus for a pyramidal neuron in the electrosensory lateral line-lobe, which is the first central nucleus of the electrosensory pathway in weakly electric fish [20] (in [10]).

6.2.2 Linear Response Kernel and Optimal Stimulus

The spike-triggered average gives information about the stimulus that contributed to triggering a spike, i.e. to information about the stimulus given a spike.

Can one conversely estimate/predict how a neuron will respond to a given stimulus?

Assume a linear response of the neuron

$$r_{est}(t) = r_0 + \int_0^\infty D(\tau)s(t-\tau)d\tau \tag{38}$$

- r_0 is the spontaneous firing rate for $s = 0$

- effect of mean stimulus $s_0 \equiv \int_0^T s(t')dt' = 0$ can be absorbed in r_0:
  assume $s_0 = 0$

- the kernel $D(\tau)$ measures the degree to which the stimulus at the earlier time
  $t - \tau$ contributes to the firing rate at time t

Notes:

- neurons are nonlinear

  - assumption of linear response is non-trivial
  - approximation expected to be good if the spontaneous firing rate r_0 is only slightly modulated by the stimulus

– one can go beyond the linear response using a Volterra expansion (or a Wiener expansion), which is an analog of a Taylor expansion)

- firing-rate framework requires that firing rate and stimulus vary sufficiently slowly

Determine $D(\tau)$ by minimizing the error in estimating the firing rate r_{est} compared to the measured firing rate r

$$E = \frac{1}{T} \int_0^T (r_{est}(t') - r(t'))^2 \, dt'$$

Using the linear response assumption

$$E\{D(\tau)\} = \frac{1}{T} \int_0^T \left(r_0 + \int_0^\infty D(\tau)s(t' - \tau)d\tau - r(t') \right)^2 dt'$$

Goal:
find $D(\tau)$ such that E is minimal, i.e. *arbitrary* small changes $\epsilon\Delta(\tau)$ of $D(\tau)$ do not change E (cf. $\frac{df}{dx} = 0$ at the minimum of the function $f(x)$), i.e. require

$$\delta E \equiv E\{D(\tau) + \epsilon\Delta(\tau)\} - E\{D(\tau)\} = 0 + \mathcal{O}(\epsilon^2)$$

$$
\begin{aligned}
\delta E &= \frac{1}{T} \int_0^T \left(r_0 - r(t') + \int_0^\infty D(\tau)s(t' - \tau)d\tau + \epsilon \int_0^\infty \Delta(\tau')s(t' - \tau')d\tau' \right)^2 dt' - \\
&\quad - \frac{1}{T} \int_0^T \left(r_0 - r(t') + \int_0^\infty D(\tau)s(t' - \tau)d\tau \right)^2 dt' \\
&= 2\epsilon\frac{1}{T} \int_0^T \left[\left(r_0 - r(t') + \int_0^\infty D(\tau)s(t' - \tau)d\tau \right) \int_0^\infty \Delta(\tau')s(t' - \tau')d\tau' \right] dt' + \mathcal{O}(\epsilon^2) \\
&= \frac{2\epsilon}{T} \int_0^\infty \Delta(\tau') \left\{ \int_0^T s(t' - \tau') \left(r_0 - r(t') + \int_0^\infty D(\tau) \int_0^\infty s(t' - \tau)d\tau \right) dt' \right\} d\tau' + \mathcal{O}(\epsilon^2)
\end{aligned}
$$

For $D(\tau)$ to be optimal the term proportional to ϵ must vanish for *arbitrary* $\Delta(\tau')$. This requires the term inside $\{\}$ to vanish [19]

$$\int_0^T (r_0 - r(t')) \, s(t' - \tau') \, dt' + \int_0^\infty D(\tau) \left\{ \int_0^T s(t' - \tau)s(t' - \tau')dt' \right\} d\tau = 0$$

Thus

$$\int_0^\infty D(\tau) \left(\frac{1}{T} \int_0^T s(t' - \tau)s(t' - \tau') \, dt' \right) d\tau = \frac{1}{T} \int_0^T (r(t') - r_0) \, s(t' - \tau') \, dt'$$

---

[19]In Appendix B this is derived using functional derivatives.

Shifting integration variable $t'' = t' - \tau'$

$$\frac{1}{T} \int_0^T s(t' - \tau)s(t' - \tau') \, dt' = \frac{1}{T} \int_{-\tau'}^{T-\tau'} s(t'' + \tau' - \tau)s(t'') \, dt'' = Q_{ss}(\tau' - \tau)$$

Using $\int_0^T s(t')dt' = 0$ and interchanging τ and τ' we get

$$\int_0^\infty D(\tau')Q_{ss}(\tau - \tau')d\tau' = Q_{rs}(-\tau)$$

For a white-noise stimulus $Q_{ss}(\tau - \tau') = \sigma_s^2 \delta(\tau - \tau')$

$$D(\tau) = \frac{Q_{rs}(-\tau)}{\sigma_s^2} = \frac{\langle r \rangle}{\sigma_s^2} C(\tau) \tag{39}$$

Notes:

- for white-noise stimuli the spike-triggered average gives the optimal kernel to predict the firing rate

- r_{est} is obtained by projecting the stimulus onto D (see (38))
  $\Rightarrow$ via (39) the maximal response[20] is obtained by a stimulus with the shape of the spike-triggered average stimulus
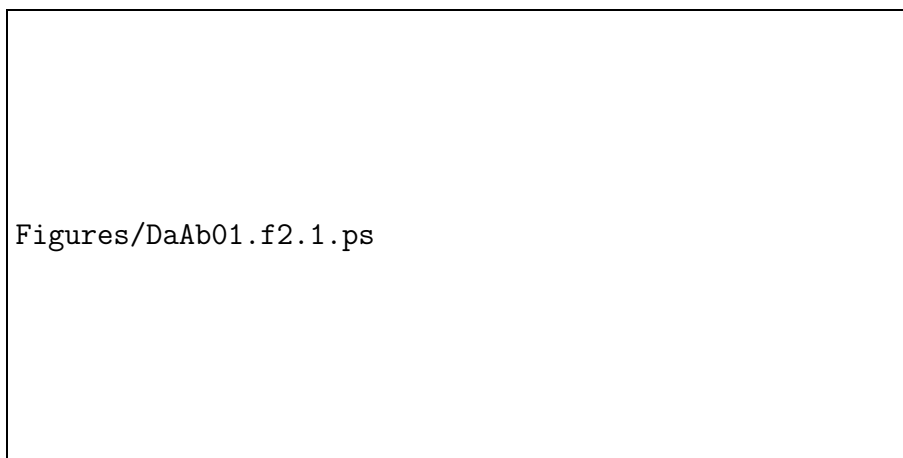
Figure 61: Response prediction using the optimal kernel (39) for the H1 neuron in the visual system of the fly. The H1 is sensitive to horizontal motion of large portions of the visual field.
a) image velocity used as input. b) two spike sequences obtained in response to that input. c) measured (dashed) and predicted (solid) firing rate [10].

---

[20] at fixed energy. See DA Appendix 2.9B

6.2.3   Receptive Fields: Visual System

Neurons may respond not only to a single stimulus, but to many different stimuli. The response depends then not only on the temporal characteristics of the stimulus but on the combination of the various stimuli.

Example: spatial information in the visual system

Sketch of initial stages:

- retina:
  rods and cones, temporal processing by bipolar cells, lateral connections via horizontal cells

- optical chiasm: left and right fields of vision combined for both eyes

- lateral geniculate nucleus in the thalamus: some integration with other information

- primary visual cortex V1

- ...

a)
```
Figures/DaAb01.f2.4a.ps
```
b)
```
Figures/KaSc00.f26-6.ps
```
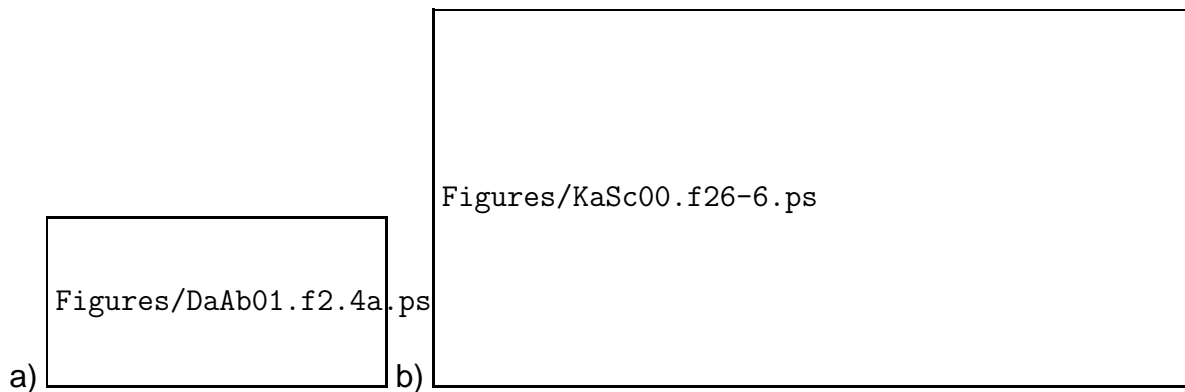
Figure 62: Structure of the retina. a) Drawing by Cajal (1911). b) Sketch of cone and rod pathway in the retina [38].

```
Figures/DaAb01.f2.5.ps
```
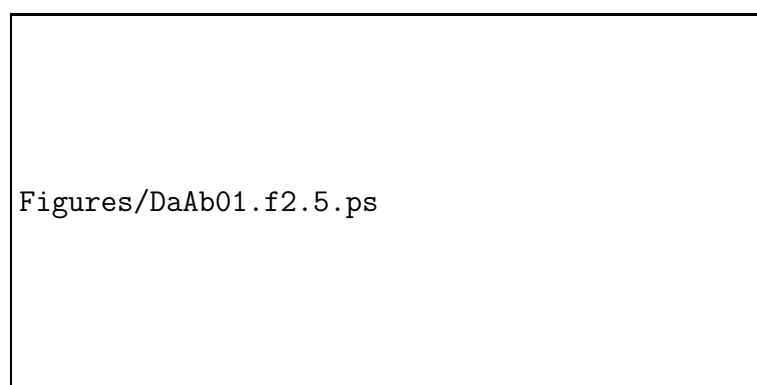
Figure 63: Visual pathway from the retina to primary visual cortex [10].

Each stage - even the retina - involves extensive neural computation.

Notes:

- The mapping between the stages is *retinotopic*: neighboring neurons respond to neighboring 'pixels' in the retina.

- In each stage there are different types of neurons with different response properties

The neural response is characterized by the *receptive field* $D(x, y, t)$, i.e. the spatio-temporal stimulus that elicits optimal response.

Focus here on neuron types for which the linear response theory appears to be adequate.

In analogy to (39) one then has

$$D(x, y, t) = \frac{\langle r \rangle}{\sigma_s^2} C(x, y, t)$$

with the spatio-temporal spike-triggered averaged stimulus $C(x, y, t)$.

Retinal ganglion cells/LGN cells:

The receptive field of many cells has a center-surround structure in space

$$D(x, y) = \frac{A_{center}}{2\pi\sigma_{center}^2} e^{-\frac{x^2+y^2}{2\sigma_{center}^2}} - \frac{A_{surround}}{2\pi\sigma_{surround}^2} e^{-\frac{x^2+y^2}{2\sigma_{surround}^2}}$$

- on-center cell: $A_{center} > 0$, $A_{surround} > 0$

- off-center cell: $A_{center} < 0$, $A_{surround} < 0$

a)

Figures/DeOh95.f1.ps

b)

Figures/DeOh95.f3.ps
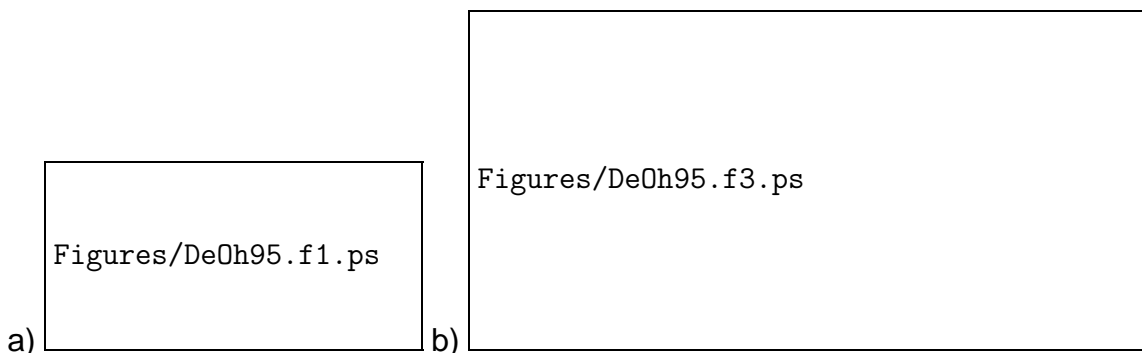
Figure 64: a) Center-surround receptive field of an on-center LGN-neuron in cat. b) Temporal structure of receptive field of LGN-neurons in cat. Horizontal axis: x, vertical axis: t, green: excitatory, red: inhibitory. A) Excitatory response at light onset. B) Excitatory response delayed, but stronger than immediate inhibitory response. [11]

Typically the receptive fields have also a temporal structure,

$$A_{center,surround} = A_{center,surround}(t),$$

as shown in Fig.64b.

6.3   LNP Cascade Models[21]

So far:

- To characterize response properties of neuronswe used spike-triggered average and the linear response.

- Linear response only expected to be successful if the firing rate varies by small amounts about a non-zero mean rate.

- Linear response does not capture

    - spiking threshold
    - saturation of firing rate

- Rate model does not include individual spikes, which can occur probabilistically (Poisson spiking)

Beyond linear response:

Volterra series: fit the input-ouput relation with higher-order polynomial in the stimulus s

$$r_{est}(t) = r_0 + \int_0^\infty D_1(\tau)s(t-\tau)d\tau + \int_0^\infty \int_0^\infty D_2(\tau,\tau')s(t-\tau)s(t-\tau')d\tau d\tau' + \dots$$

The kernels $D_i(\tau,\tau',\dots)$ are to be determined to give a good approximation for a wide range of stimuli: use white-noise stimulus with

$$Q_{ss}(\tau,\tau') = \sigma_s^2 \delta(\tau-\tau')$$

Then we had

$$D_1(\tau) = \frac{\langle r \rangle}{\sigma_s^2} C(\tau)$$

with $C(\tau)$ the spike-triggered average

$$C(\tau) = \left\langle \sum_{i=1}^n s(t_i - \tau) \right\rangle_{trials}$$

The higher-order kernels can be determined via higher powers of the stimulus with the output (spiking).

Notes:

---

[21]cf. [6]

- as in fitting data points with polynomials the coefficients of the polynomials change when the order of the polynomial changes (the fit is not a Taylor expansion)

The interdependence between the various kernels can be removed by switching to a Wiener series[50]

$$r_{est}(t) = g_0 + \int_0^\infty g_1(\tau)s(t-\tau)d\tau + \left\{ \int_0^\infty \int_0^\infty g_2(\tau,\tau')s(t-\tau)s(t-\tau')d\tau d\tau' - \sigma_s^2 \int_0^\infty g_2(\tau,\tau)d\tau \right\} + \dots$$

with the filters given by

$$
\begin{aligned}
g_0 &= \langle r(t) \rangle \\
g_1(\tau) &= \frac{1}{\sigma_s^2} \langle r(t)s(t-\tau) \rangle = D_1(\tau) \\
g_2(\tau,\tau') &= \frac{1}{\sigma_s^4} \langle r(t)s(t-\tau)s(t-\tau') \rangle \\
&\dots
\end{aligned}
$$

But:

- Sigmoidal dependence of the firing rate on the input is poorly approximated by polynomials

  - Volterra and Wiener series require high orders to give good results $\Rightarrow$ impracticable, would require huge amounts of data

Can one make use of the preferred stimulus (spike-triggered average) to construct a simpler *nonlinear* model?

Cascade Model:

- spike-triggered average generates from the input history a scalar quantity $r_{lin}(t)$

- $r_{lin}(t)$ is the input to a static nonlinearity F which gives a spiking probability

- spikes are generated from a Poisson distribution based on the time-dependent spiking probability $F(r_{lin}(t))$

$$r_{est}(t) = F\left(\int_0^\infty g(\tau)s(t-\tau)d\tau \right)$$

How to determine F and g?

This model has only a single filter, $g(\tau)$

Require:

93

- the first Wiener filter of the true data should agree with the first Wiener filter of the estimated data

$$\langle r(t)\, s(t-\tau)\rangle = \langle r(t)_{est}\, s(t-\tau)\rangle$$

Note:

- since the Wiener filters are independent of each other this condition does not require any knowledge of higher Wiener or Volterra filters

Slightly easier to consider discrete time series (binned data) s_i, $i = 1\ldots N$, for the N past values of the stimulus, which result in the current value of the output r and its estimate r_{est}. The model then reads

$$r_{est} = F\left(\mathbf{g}\cdot\mathbf{s}\right)$$

with the discrete filter $\mathbf{g}$.

Consider first spherically symmetric probability distributions for the stimuli

$$P(\mathbf{s}) = P(|\mathbf{s}|)$$

$$
\begin{aligned}
\langle r_{est}\mathbf{s}\rangle &= \int r_{est}\,\mathbf{s}P(\mathbf{s})ds_1\ldots ds_N \\
&= \int' \underbrace{P(|\mathbf{s}|)}_{\text{spherical}}\left[F\left(\mathbf{g}\cdot\mathbf{s}\right)\mathbf{s} + F\left(\mathbf{g}\cdot\mathbf{s}^+\right)\mathbf{s}^+\right]ds_1\ldots ds_N
\end{aligned}
$$

where $\mathbf{s}^+$ is chosen such that $\mathbf{g}\cdot\mathbf{s} = \mathbf{g}\cdot\mathbf{s}^+$, i.e.

$$\mathbf{s}^+ = 2\frac{\mathbf{s}\cdot\mathbf{g}}{|\mathbf{g}|^2}\mathbf{g} - \mathbf{s}$$

and the sum $\int'$ is adjusted to avoid double counting.

Then

$$\langle r_{est}\mathbf{s}\rangle = \left\{\int' \underbrace{P(|\mathbf{s}|)}_{\text{spherical}}\ F\left(\mathbf{g}\cdot\mathbf{s}\right)\right\}\underbrace{\left(\mathbf{s}+\mathbf{s}^+\right)}_{\propto\mathbf{g}}ds_1\ldots ds_N \propto \mathbf{g}$$

Since we require $\langle r_{est}\mathbf{s}\rangle = \langle r\,\mathbf{s}\rangle$ the filter $\mathbf{g}$ satisfies

$$\mathbf{g} = \alpha\,\langle r\,\mathbf{s}\rangle$$

The nonlinearity is then obtained by plotting r vs the linear filter output $\mathbf{g}\cdot\mathbf{s}$.

For Gaussian, not necessarily spherical, distributions one can show the equivalent result (Bussgang theorem[4, 10])

$$
\begin{aligned}
\langle r_{est}\mathbf{s}\rangle \quad &= \quad \int r_{est}(\mathbf{s})\,\mathbf{s}e^{-\frac{1}{2}\mathbf{s}^{t}\mathbf{C}^{-1}\mathbf{s}}ds_1\ldots ds_N \\[2mm]
&= \quad -\int r_{est}(\mathbf{s})\,\mathbf{C}\nabla_{\mathbf{s}}\left(e^{-\frac{1}{2}\mathbf{s}^{t}\mathbf{C}^{-1}\mathbf{s}}\right)ds_1\ldots ds_N \\[2mm]
\underbrace{=}_{\text{integration by parts}} \quad & \qquad \mathbf{C}\int e^{-\frac{1}{2}\mathbf{s}^{t}\mathbf{C}^{-1}\mathbf{s}}\nabla_{\mathbf{s}}r_{est}(\mathbf{s})ds_1\ldots ds_N \\[2mm]
&= \quad \mathbf{C}\left\langle \nabla_{\mathbf{s}}r_{est}(\mathbf{s})\right\rangle \\[2mm]
&= \quad \mathbf{C}\left\langle \nabla_{\mathbf{s}}F\left(\mathbf{g}\cdot\mathbf{s}\right)\right\rangle \\[2mm]
&= \quad \mathbf{C}\mathbf{g}\left\langle F'\left(\mathbf{g}\cdot\mathbf{s}\right)\right\rangle
\end{aligned}
$$

Thus, we have

$$
\mathbf{g}\propto \mathbf{C}^{-1}\left\langle r_{est}\,\mathbf{s}\right\rangle = \mathbf{C}^{-1}\left\langle r\,\mathbf{s}\right\rangle
$$

Notes:

- for Gaussian white noise: the filter $\mathbf{g}$ is proportional to the spike-triggered average

- for correlated Gaussian noise: the spike-triggered average needs in principle to be decorrelated.
  however: when the data sets are not large enough the average $\langle r\,\mathbf{s}\rangle$ often contains still noise. The decorrelation also amplifies this noise and may not improve the filter.

- the LN-model approach can also be used to characterize the membrane voltage response of neuron in response to a stimulus

a) b)
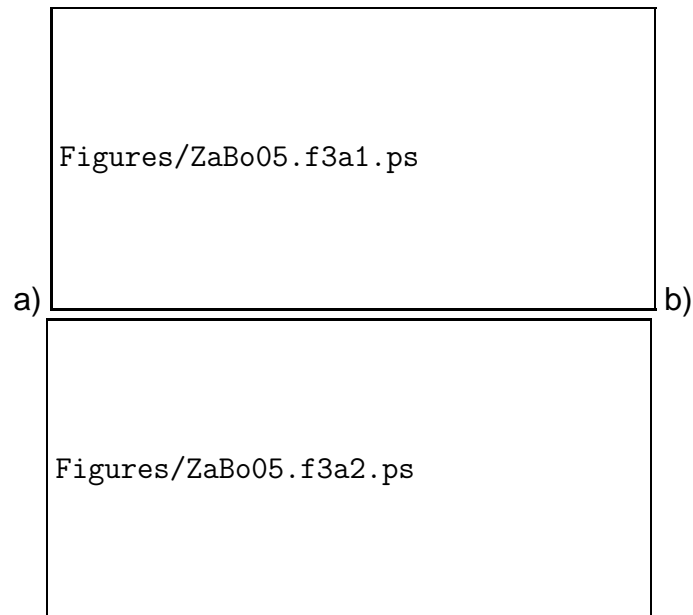
Figure 65: LN-model for OFF Y-type retinal ganglion cell for low and high contrast of the stimulus. a) Membrane voltage response. b) Spike rate response. [62]
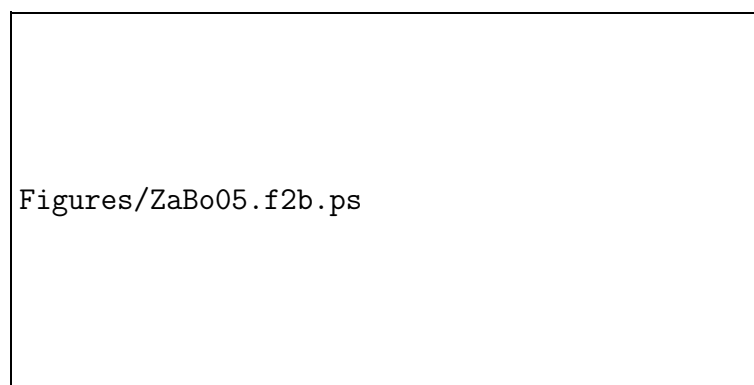
Figure 66: Comparison of the voltage prediction of LN-model for the OFF Y-type retinal ganglion cell shown in Fig.65 for low and high contrast of the stimulus (stimulus in top row) [62]..

LN-models can also be used to characterize quantitatively certain aspects of the neuronal response, like the gain.

Typically the gain depends on the contrast of the stimulus.

For the cell shown in Fig.65 the amplitude of the linear filter can be rescaled such that the nonlinearity is the same for both contrast conditions

$$r_{est} = F\left(\gamma_{low,high}\, \mathbf{g} \cdot \mathbf{s}\right) \qquad \text{with } \gamma_{high} < \gamma_{low}$$

Note:

- The gain is reduced for high contrast. This helps avoiding saturation of the response.

```
Figures/ZaBo05.f3b1.ps
```

a)   b)

```
Figures/ZaBo05.f3b2.ps
```
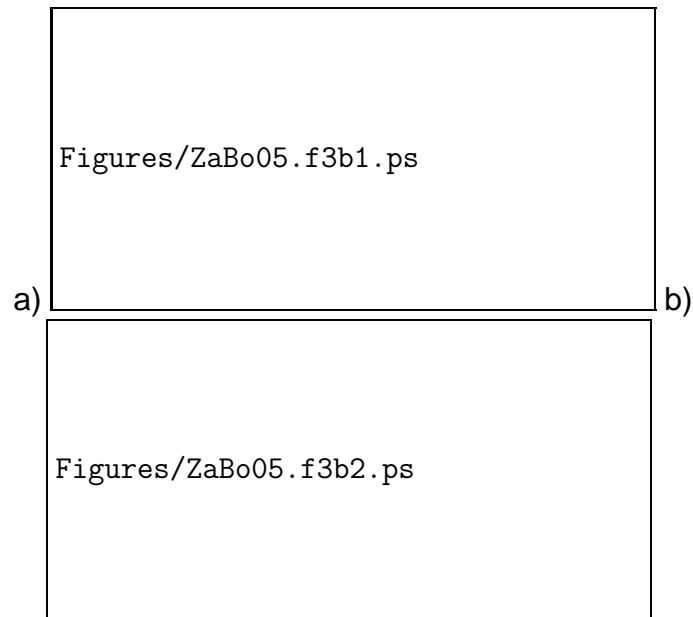
Figure 67: LN-model for the same OFF Y-type retinal ganglion cell as in Fig.65. After rescaling of the filter the nonlinearities become the same for low and high contrast of the stimulus (grey=low contrast, black=high contrast). a) Membrane voltage response. For high contrast gain is reduced to 0.83 of the gain for low contrast. b) Spike rate response. Gain reduced to 0.64 [62]

a)

```
Figures/ZaBo05.f3c1.ps
```

b)

```
Figures/ZaBo05.f3c2.ps
```
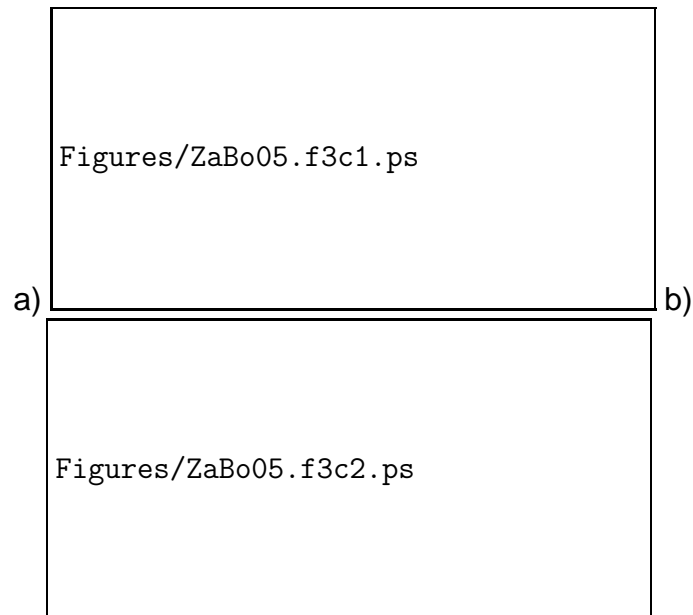
Figure 68: LN-model for ON Y-type retinal ganglion cell. After rescaling of the filter the nonlinearities become the same for low and high contrast of the stimulus (grey=low contrast, black=high contrast). a) Membrane voltage response. Gain redcued to 0.74. b) Spike rate response. Gain reduced to 0.54. [62]

The description of some cells require multiple filters and nonlinearities.

Shifting backgrounds in visual scenes can modify the response of ganglion cells to inputs in their receptive field. This could be relevant during saccades.

Figures/GeDe07.f1a.eps

a)   b)

Figures/GeDe07.f2.eps
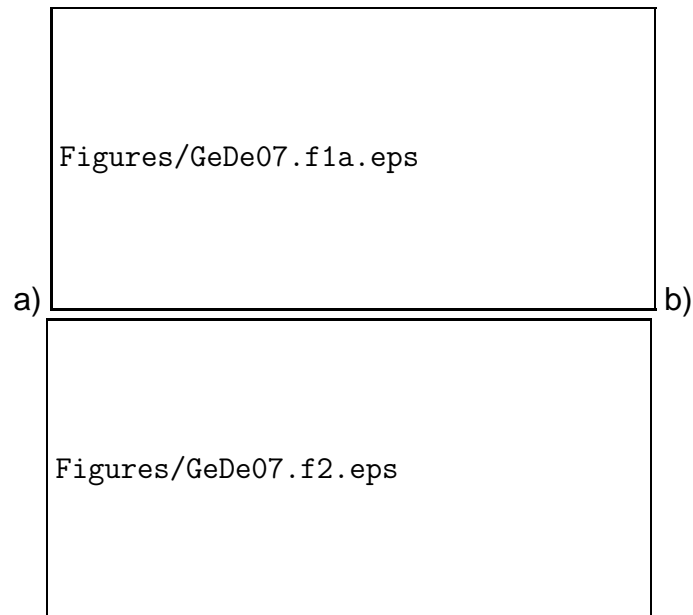
Figure 69: Input outside the classical receptive field can modify a ganglion cells response. a) grating exciting the periphery is shifted every 9s. b) The response of this ganglion cell is transiently changed from OFF-center to ON-center briefly after a peripheral shift. [21]

Figures/GeDe07.f4.eps
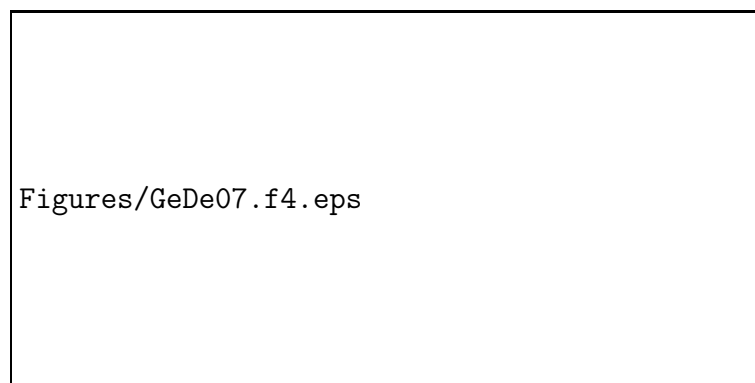
Figure 70: Extraction of two temporal filters using a principal component analysis (PCA) of the spike-triggered covariance matrix [21]

7 Neural Networks: Rate Models

The power of the brain stems to a large extent from the interaction between different neurons that communicate with each other.

Characteristics of most functional networks in the brain

- comprised of many neurons

- each neuron receives many inputs

- neurons are connected only to a fraction of the other neurons:
  'sparse connectivity'

Modeling with detailed spiking neurons very challenging

- time scales:

  - channel opening/closing: $< 1ms$
  - action potential: $\sim 2ms$
  - ...
  - period of θ-rhythm $\sim 100ms$
  - persistent activity in working memory $> 1s$
  - ...

- multiple variables V, m, n, h,...

- many compartments for branching dendrites, axons

- complex nonlinearities

- many parameters, of which many are poorly known

For large networks *firing-rate models* are useful

- do not resolve short time scales of action potential

- fewer variables

- simpler nonlinearities

- few parameters

- *cannot* capture aspects of spike synchrony

Note:

- In the Blue Brain Project a single neocortical column consisting of 10,000 neurons is being simulated with morphological details of neurons retained. It uses a 8192-processor Blue Gene computer.
  `http://bluebrain.epfl.ch/page18699.html`

100

7.1   Firing-Rate Models[22]

In a spiking model the activity of the network is characterized by the neural response function $\rho_j(t) = \sum_i \delta(t - t_i)$ of each neuron j.

In a firing-rate model $\rho_j(t)$ is replaced by its trial-average, the firing rate $r(t) = \langle \rho(t) \rangle$.

Necessary for firing-rate approximation:

- network behavior does not depend on specific timing of the spikes

The dynamics of a neuron depend on its total input.

The response of a neuron is insensitive to individual spike times of its inputs if

- large number N of *uncorrelated* spikes contribute to the response

    - many synapses

    - slow synapses

    - slow membrane properties ($\tau_m = RC$ large)
      (cf. Fig.45b)

    $\Rightarrow$ input fluctuations due to individual spikes $\propto \sqrt{N}$, mean input $\propto N$.

We need

- synaptic input current I_s to neuron (measured at soma) due to the changes in all the synaptic conductances as a function of pre-synaptic firing rate u

- output firing rate v as a function of I_s

Synaptic Current I_s

Consider a neuron with N_u synaptic inputs

$$I_s(t) = \sum_{i=1}^{N_u} w_i \sum_{t_j < t} K_s(t - t_j^{(i)}) = \sum_{i=1}^{N_u} w_i \int_{-\infty}^{t} K_s(t - \tau)\rho_i(\tau)d\tau$$

with

- synaptic kernel K_s

    - effect at the soma of the synaptic input (spike times given by $\rho_i(t)$)
      includes synaptic dynamics and propagation along dendritic cable

---

[22]DA 7.1

- – assume K_s equal for all synapse on the neuron
     need not be the case: the impact of a synapse may well depend on its distance from the soma
  - – normalized: $\int_{-\infty}^{t} K_s(t-\tau)d\tau = \int_0^{\infty} K_s(t')dt' = 1$

- • w_i strength of synapse i

  - – assume no short-term plasticity, w_i does not change from spike to spike, does not depend on inter-spike interval
  - – $w_i > 0$: excitatory synapse
     $w_i < 0$: inhibitory synapse

- • assume synaptic inputs sum up linearly
   however, active dendrites can sum up their input sub-linearly or super-linearly

Firing-rate assumption

- • the synaptic current I_s can be approximated by its trial average

$$I_s \approx \langle I_s(t)\rangle = \sum_{i=1}^{N_u} w_i \int_{-\infty}^{t} K_s(t-\tau) \underbrace{\langle \rho_i(\tau)\rangle}_{u_i(\tau)} d\tau \tag{40}$$

Assume a single-exponential kernel (fast rise time)

$$K_s(t) = \frac{1}{\tau_s} e^{-t/\tau_s} H(t)$$

with the Heaviside function

$$H(t) = \begin{cases} 1 & \text{for} \quad t > 0 \\ 0 & \text{for} \quad t < 0 \end{cases}$$

$H(t) = 1$ for $t > 0$ and $H(t) = 0$ for $t < 0$.

Then one can express (40) in terms of a differential equation

Using the derivative of (40)

$$\frac{dI_s}{dt} = \sum_{i=1}^{N_u} w_i \left(\frac{1}{\tau_s} u_i(t) - \int_{-\infty}^{t} e^{-(t-\tau)/\tau_s} u_i(\tau) d\tau \right)$$

yields

$$\tau_s \frac{dI_s}{dt} = -I_s + \sum_{i=1}^{N_u} w_i u_i \equiv -I_s + \mathbf{w} \cdot \mathbf{u} \tag{41}$$

Firing Rate

For steady input current I_s the output firing rate of the neuron is given by

$$v_\infty = F(I_s)$$

Typical choices

- threshold linear function

$$F(I_s) = [I_s - I_{threshold}]_+ \equiv \begin{cases} I_s - I_{threshold} & \text{for} \quad I_s - I_{threshold} > 0 \\ 0 & \text{for} \quad I_s - I_{threshold} \leq 0 \end{cases}$$

- sigmoid function for smoothness and for saturation

For time-dependent $I_s(t)$ a simple assumption is that v relaxes exponentially to v_∞ on a time scale τ_r.

This yields the coupled system

$$\tau_r \frac{dv}{dt} = -v + F\left(I_s(t)\right) \tag{42}$$

$$\tau_s \frac{dI_s}{dt} = -I_s + \mathbf{w} \cdot \mathbf{u} \tag{43}$$

i) $\tau_r \ll \tau_s$: v relaxes very quickly to v_∞

$$v = F(I_s) \qquad \tau_s \frac{dI_s}{dt} = -I_s + \mathbf{w} \cdot \mathbf{u} \tag{44}$$

ii) $\tau_r \gg \tau_s$: $I_s(t)$ relaxes quickly

$$\tau_r \frac{dv}{dt} = -v + F(\mathbf{w} \cdot \mathbf{u}) \tag{45}$$

Note:

- if the neurons providing the input are in turn described by a firing-rate model one gets for (44)

$$\tau_s \frac{dI_s}{dt} = -I_s + \sum_{i=1}^{N_u} w_i F\left(I_{si}(t)\right) \tag{46}$$

  with I_{si} the input current of the input neurons.

- comparing (46) with (45) shows:
  the two models differ then in the position of the nonlinearity F.

- the position of the nonlinearity, which is non-negative, is also related to the fact that I_s can be negative but v cannot.

7.2 Feed-Forward Networks

The brain can roughly be thought of as a modularly structured network

- feed-forward connections from one module to the next (e.g. sensory → thalamus → initial processing in cortex → ... higher level processing .... → motor control → motor output)

- recurrent connections within modules

- top-down (feed-back) input: most regions that receive feed-forward input from lower levels also project back to those levels

General form within the frame-work of firing-rate models:

- Feed-forward

$$\tau \frac{d\mathbf{v}}{dt} = -\mathbf{v} + \mathbf{F}(\mathbf{Wu}) \tag{47}$$

  with $\mathbf{W}$ the matrix of synaptic weights of the inputs.
  In components

$$\tau \frac{dv_i}{dt} = -v_i + F\left(\sum_j W_{ij} u_j\right)$$

- Recurrent

$$\tau \frac{d\mathbf{v}}{dt} = -\mathbf{v} + \mathbf{F}(\mathbf{Wu} + \mathbf{Mv}) \tag{48}$$

  with $\mathbf{M}$ the matrix of synaptic weights of the recurrent connections.

Consider first feed-forward networks. Although simpler to treat than recurrent ones, they can still perform very powerful computations.

Note:

- without input $\mathbf{u}$ feedforward networks are silent, $\mathbf{v} = 0$
  (unless the individual, uncoupled neuron fire spontaneously, $F(0) \neq 0$.)

7.2.1   Hubel-Wiesel Model for Visual Orientation Tuning

Observations of visual receptive fields:

- retinal ganglion cells and cells in lateral geniculate nucleus (LGN) in thalamus have center-surround receptive fields (cf.Sec.6.2.3)

- cells in the input layer (layer IV) of visual cortex V1 have more complex receptive fields:

  - for many cells the receptive field is based on an oriented stripe pattern
    * different orientations
    * different wavelengths

∗ stationary or moving at a certain speed

Figures/HuWi62.f2.ps
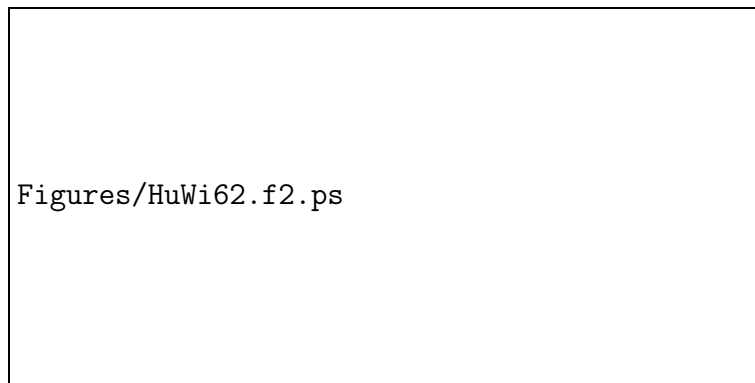
Figure 71: Receptive fields: A) ON-center in LGN, B) OFF-center in LGN, C)-G) simple-cell receptive fields in V1 [32]

How can orientation tuning in V1 arise from center-surround tuning of the ganglion cells in the retina?

Figures/HuWi62.f19.ps
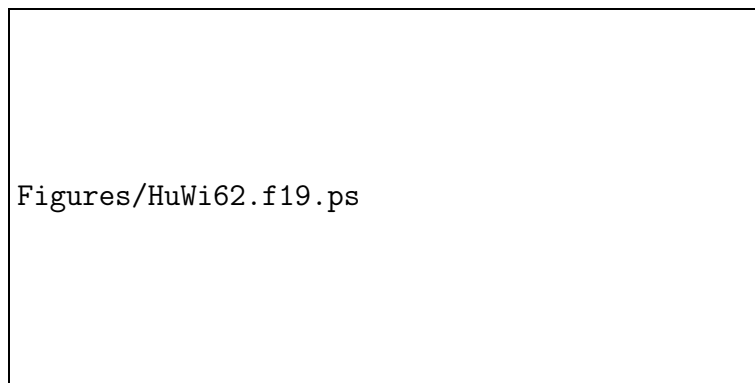
Figure 72: Feed-forward network for simple cell [32].

Simple cell responds most strongly to

- bright (dark) stripe in the center

- dark (bright) stripes next to the bright stripe

⇒ selective for orientation, wavelength *and* position.

Complex cells are not selective for position (phase) of the stripes, only for their orientation

Figures/HuWi62.f4.ps
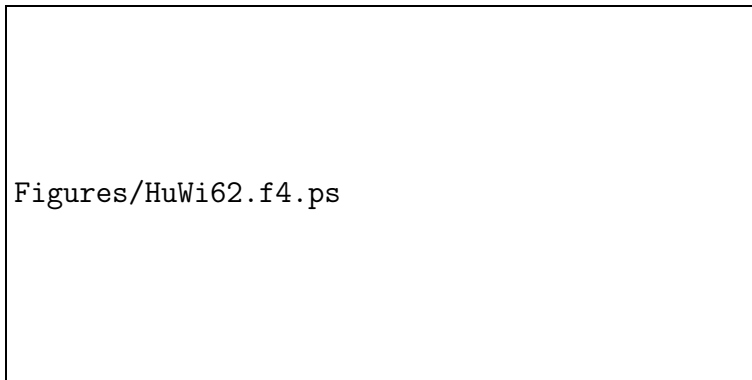
Figure 73: Receptive field of a complex cell. A)-D) same orientation but different location of the bar within the receptive field. E)-G) different orientations. H) bar with orientation as in A)-D) moved rapidly across the receptive field. The horizontal bars above the record indicate when the stimulus is on [32].

Figures/HuWi62.f20.ps
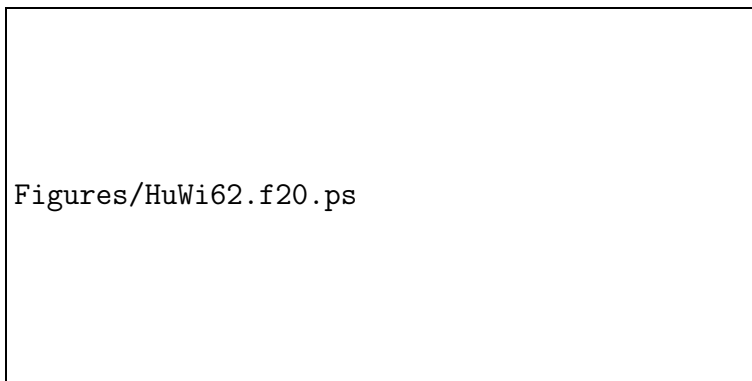
Figure 74: Possible connectivity of a complex cell: input from multiple simple cells with different preferred locations of the bar [32].

For any phase (position) of the grating some simple cell in the receptive field of the complex cell responds, while the others are quiet: no cancellation of the input from the active cells

Thus:

- the complex cell is not sensitive to the position of the stripe:

- it encodes the generalized information 'some stripe with this orientation'

Note:

- for linearly responding cells with high spontaneous firing rate the reduced input from the simple cells that are responding only weakly would compensate the enhanced input from the strongly responding simple cells.

Notes:

- it has been argued that the feed-forward architecture is insufficient to explain

    - sharpness of selectivity
    - contrast invariance of the selectivity
      selectivity is as sharp for high-contrast pattern as for low-contrast pattern (cf. ice-berg effect)

  recurrent network architectures have been proposed [2]
  it seems, however, that if data and models are analyzed in more detail the feed-forward network may well be sufficient [18]

7.2.2 Neural Coordinate Transformations[23]

Receptive fields of LGN cells and of cells in V1 are in terms of positions on the retina (retinotopic map), which depends on eye and head direction (gaze).

To manipulate an object its position needs to be known in a body-centered coordinate system.

$\Rightarrow$ brain needs to transform from the retinal to the body coordinate system

One-dimensional example:

s = angle in retina coordinates g = angle of the gaze $\Rightarrow s + g$ = body-centered angle

Figures/DaAb01.f7.4.ps
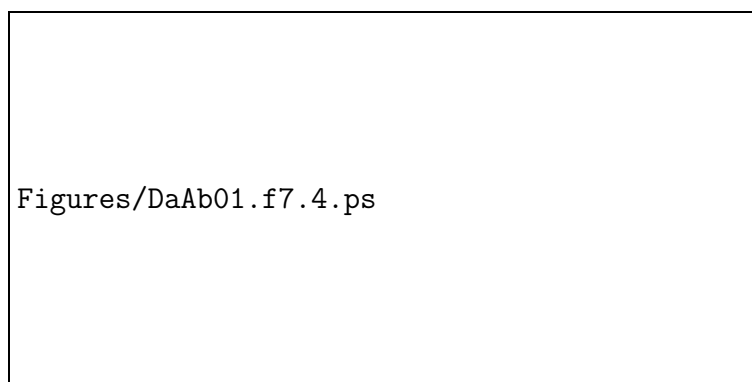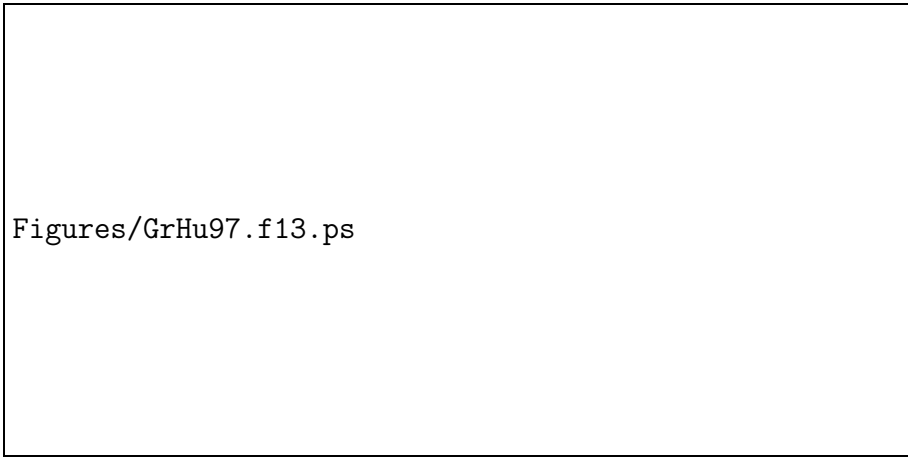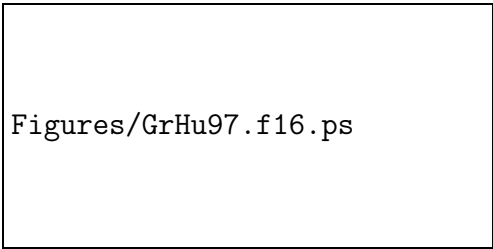
Figure 75: Coordinate transformation between body-centered coordinates and retina-centered coordinates.

---

[23]DA 7.3
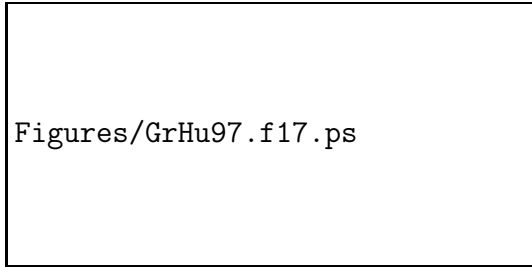
Figures/GrHu97.f13.ps

Figure 76: Response of a bimodal (visual-tactile) neuron in the ventral pre-motor cortex of a macaque monkey. Its tactile receptive field is near the left cheek. The visual response to an object approaching along paths marked I-V does not depend on the eye position (A1, B1, C1) (or the arm position (B2)), but it does depend on the head position (B3), i.e. it depends on the position of the object relative to its tactile receptive field (similar data for tactile field on the arm) [24].

Figures/GrHu97.f16.ps

Figures/GrHu97.f17.ps

a)   b)

Figure 77: Tuning curves of face+visual bimodal neurons in ventral pre-motor cortex are in head-centered coordinates. a) The receptive field is shifted when the head is turned. b) The receptive field is not shifted if the gaze, but not the head is rotated [24].

Figures/DaAb01.f7.6a.ps

Figure 78: Tuning curve of neurons in the posterior parietal cortex. The preferred location is given in retinal coordinates, but the magnitude of the response, i.e. the height of the tuning curve, is modulated by the gaze direction [3].

Consider two model networks at the interface between sensory function and motor control [51]

i) Sensory Network (posterior parietal cortex PP):

The response of bimodal neurons in PP depends on the retinal coordinate s and the gaze coordinate g. Different neurons have different preferred retinal angles ξ and different characeristic gaze angle γ.

The neurons have tuning curves in retina coordinates, but the gaze enters via the gain,

$$u_{\xi\gamma}(s,g) = f_u^{\pm}(s-\xi, g-\gamma) = A e^{-\frac{(s-\xi)^2}{2\sigma_s^2}} \cdot [M \pm (g-\gamma)]_+^M$$

Experimentally it is found that the gain varies rougly linearly with the gaze, here modeled with a threshold and saturation.

Depending on the neuron the gain can increase or decrease with the gaze angle. Assuming that the second network reads both types of neurons one can lump them together into an 'effective' population described by

$$f_u(s-\xi, g-\gamma) = A e^{-\frac{(s-\xi)^2}{2\sigma_s^2}} \cdot [M - |g-\gamma|]_+^M$$

which effectively has a preferred gaze angle.

For simplicity assume a continuum of neurons characterized by ξ and γ.

ii) Motor Control Network (ventral pre-motor cortex PMv):

Neurons in PMv receive input from the neurons of the sensory network

Can the input weights be chosen such that the neurons in the motor control network have tuning curves in body-coordinates?

Steady-state firing rate for one such neuron

$$v_\infty(s,g) = F\left(\mathbf{w} \cdot \mathbf{u}\right)$$

Assuming a continuum for the preferred angles ξ and γ the sum can be replaced by integrals and one obtains

$$v_\infty(s,g) = F\left(\int_\infty^{+\infty} \int_\infty^{+\infty} \underbrace{w(\xi,\gamma)}_{\text{connection from neuron labeled } (\xi,\gamma)} f_u(s-\xi, g-\gamma)\, \rho_\xi \rho_\gamma \, d\xi d\gamma\right)$$

where $\rho_\xi d\xi$ and $\rho_\gamma d\gamma$ are the numbers of neurons with preferred location and gaze in the ranges $[\xi, \xi+d\xi]$ and $[\gamma, \gamma+d\gamma]$, respectively. They are assumed to be independent of ξ and γ and can then be pulled out of the integral.

The tuning curve for this neuron should depend only on the angle in body coordinates

$$v_\infty = v_\infty(s+g)$$

To bring s and g together shift the variables

$$s - \xi = s + g - \xi' \qquad g - \gamma = -\gamma'$$

i.e.

$$\xi = \xi' - g \qquad \gamma = \gamma' + g$$

then

$$v_\infty(s, g) = F\left(\rho_\xi \rho_\gamma \int_{-\infty}^{+\infty} \int_{-\infty}^{+\infty} w(\xi' - g, \gamma' + g)\, f_u(s + g - \xi', -\gamma')\, d\xi' d\gamma'\right)$$

To make the first integrand independent of g choose

$$w(\xi, \gamma) = w(\xi + \gamma)$$

then

$$v_\infty(s, g) = F\left(\rho_\xi \rho_\gamma \int_{-\infty}^{+\infty} \int_{-\infty}^{+\infty} w(\xi' + \gamma')\, f_u(s + g - \xi', -\gamma')\, d\xi' d\gamma'\right)$$

Figures/coordinate_transform_1.eps	Figures/coordinate_transform_2.eps

Figure 79: a) The neuron in PMv integrates the contributions from all neurons in PP with a weight $w(\xi, \gamma)$ depending on their 'preferred' location (ξ, γ). Their receptive fields are represented by circles. b) For a different stimulus (s', g') the each of the PP-neurons responds differently. But for each neuron at (ξ, γ) there is a neuron at (ξ', γ') with $\xi' + \gamma' = \xi + \gamma$ that responds like the neuron (ξ, γ) did for stimulus (s, g). The output of the PMv-neuron depends only on $s + g$ if the weight for the neuron (ξ', γ') is equal to the weight of neuron (ξ, γ), i.e., if the weight $w(\xi, \gamma)$ depends only on $\xi + \gamma$.

Note:

- In [51] it is discussed that the required connectivity $w(\xi + \gamma)$ can be obtained in a natural learning procedure: baby follows its own random hand motion [60].

7.3   Recurrent Networks[24]

Recurrent networks are harder to analyze than feed-forward networks. Consider first linear neural dynamics, $F(u) = u$.

---

[24]DA 7.4

7.3.1   Linear Recurrent Networks

Need to consider N *coupled* odes for the components of $\mathbf{v}$

$$\tau_r \frac{d\mathbf{v}}{dt} = -\mathbf{v} + \underbrace{\mathbf{W}u}_{\text{input } \mathbf{h}} + \mathbf{M}\mathbf{v} \tag{49}$$

Solve in terms of the eigenvectors $\mathbf{e}_\mu$ of $\mathbf{M}$

$$\mathbf{M}\mathbf{e}_\mu = \lambda_\mu \mathbf{e}_\mu$$

with eigenvalues λ_μ.

For general matrices $\mathbf{M}$ the eigenvalues and the eigenvectors can be complex, $\lambda \in \mathbb{C}$.

Assume: $\mathbf{M}$ is symmetric, $M_{ij} = M_{ji}$

- eigenvalues $\lambda_\mu \in \mathbb{R}$

- eigenvectors $\mathbf{e}_\mu$ mutually orthogonal

$$\mathbf{e}_\mu \cdot \mathbf{e}_\nu = \delta_{\mu\nu} \tag{50}$$

- all vectors $\mathbf{v}$ can be written as a linear combination of the eigenvectors

$$\mathbf{v}(t) = \sum_{\mu=1}^{N_v} v_\mu(t)\, \mathbf{e}_\mu \tag{51}$$

  for any fixed t with N_v the number of components of $\mathbf{v}$. $v_\mu(t)$ is the time-dependent amplitude of the eigenmode $\mathbf{e}_\mu$.

Insert expansion (51) into (49)

$$\tau_r \sum_\mu \frac{dv_\mu}{dt}\mathbf{e}_\mu = -\sum_\mu (1-\lambda_\mu)\, v_\mu \mathbf{e}_\mu + \mathbf{h}$$

Use orthogonality (50) to project the equation onto $\mathbf{e}_\nu$

$$\tau_r \frac{dv_\nu}{dt} = -(1-\lambda_\nu)\, v_\nu + \mathbf{e}_\nu \cdot \mathbf{h} \tag{52}$$

Now we have only a single ode. Its solution is given by

$$v_\nu(t) = \frac{\mathbf{e}_\nu \cdot \mathbf{h}}{1-\lambda_\nu} + A_\nu e^{-\frac{1-\lambda_\nu}{\tau_r}t}$$

Using the initial condition

$$v_\nu(0) = \mathbf{e}_\nu \cdot \mathbf{v}(0)$$

111

we get

$$A_\nu = \mathbf{e}_\nu \cdot \mathbf{v}(0) - \frac{\mathbf{e}_\nu \cdot \mathbf{h}}{1 - \lambda_\nu}$$

The full solution is then given by the sum over all the eigenmodes with their respective amplitudes

$$\mathbf{v}(t) = \sum_{\nu=1}^{N_\nu} \left(\frac{\mathbf{e}_\nu \cdot \mathbf{h}}{1 - \lambda_\nu} + A_\nu e^{-\frac{1-\lambda_\nu}{\tau_r}t} \right) \mathbf{e}_\nu \tag{53}$$

The evolution of the components v_ν of $\mathbf{v}$ depends on the associated eigenvalue λ_ν

- For $\lambda_\nu < 1$:

  – a steady state is reached at large times

  $$v_\nu(t) \to v_\nu^\infty \equiv \frac{\mathbf{e}_\nu \cdot \mathbf{h}}{1 - \lambda_\nu} \qquad \text{for} \qquad t \to \infty$$

  – for $\lambda_\nu < 0$ the output component v_ν^∞ is reduced compared to the input component

  – for $0 < \lambda_\nu < 1$ the output component v_ν^∞ is larger than the input component $\mathbf{e}_\nu \cdot \mathbf{h}$: selective amplification of components of $\mathbf{h}$

  – for $\lambda_\nu \to 1$ the approach to the steady state becomes infinitely slow

  $$\tau_\nu = \frac{\tau}{1 - \lambda_\nu} \to \infty$$

  (critical slowing down)

- For $\lambda_\nu > 1$:

  – no steady state is reached

    * v_ν diverges exponentially within this linear approximation
    * nonlinearity F may lead to saturation

- For $\lambda_\nu = 1$:

  – it is easier to determine solution directly from (52)

  $$\tau_r \frac{dv_\nu}{dt} = \mathbf{e}_\nu \cdot \mathbf{h}$$

  i.e.

  $$v_\nu(t) = \mathbf{e}_\nu \cdot \mathbf{h} \frac{t}{\tau}$$

  – no saturation, *linear* growth

– more generally, for $\mathbf{h} = \mathbf{h}(t)$

$$v_\nu(t) = \frac{1}{\tau_r} \int_{t_0}^{t} \mathbf{e}_\nu \cdot \mathbf{h}(t') dt'$$

network functions as an *temporal integrator* of its input

Notes:

- temporal integration is needed, e.g., to obtain positions from a velocities

    – to compensate head orientation on visual input need to obtain head orientation from rotation measured in vestibular system.

- $\lambda > 0$ implies *excitatory recurrent* inputs: self-excitation

7.3.2 Oculomotor Control during Eye Saccades

In many animals eye position is fixed for a period of time and then a sudden jump ('saccade') to a new position is made.

Even with closed eyes the eye position relative to the object remains fixed during head rotations.

How is the eye position controled?

Figures/KaSc00.f17-2.ps
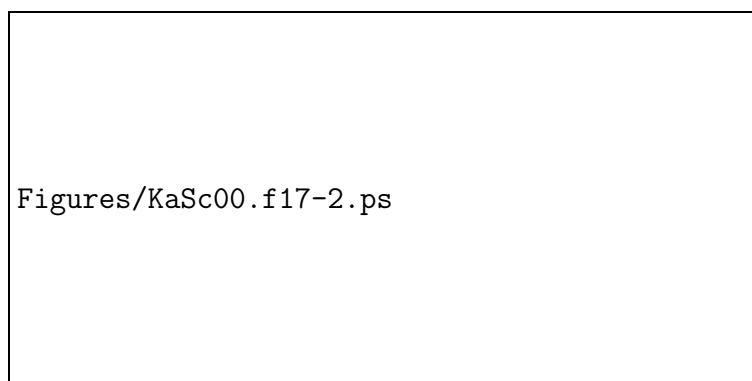
Figure 80: Sketch indicating location of medulla and other parts of the brain stem [38].

Different types of neurons are involved (located in parts of the medulla at the end of the spinal cord)

- neurons firing tonically: firing rate proportional to eye position
- neurons firing bursts during saccades

- both neurons feed into the motor neurons:
  motor neurons have pulse-step behavior

Note:

- If position neurons fail (by lesion, e.g.), animal can still make a saccade to a new
  eye position but the eye relaxes back to its rest position afterwards

a)
```
Figures/McFu92.f4.ps
```
b)

```
Figures/McFu92.f8.ps
```
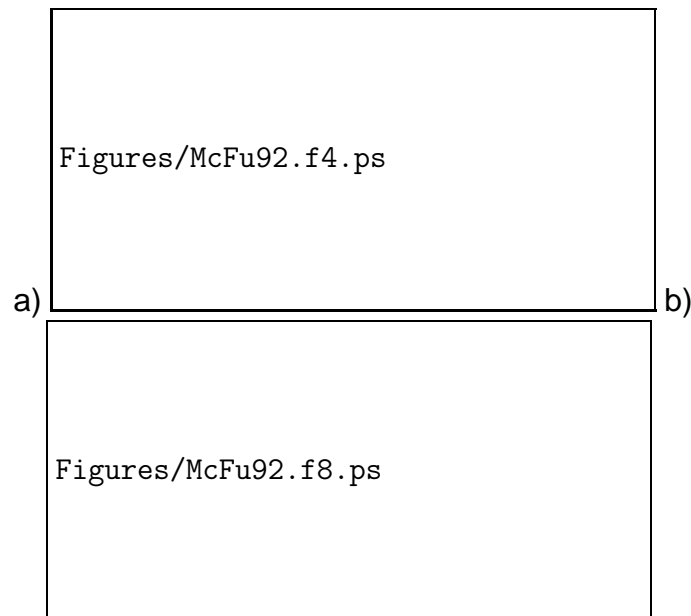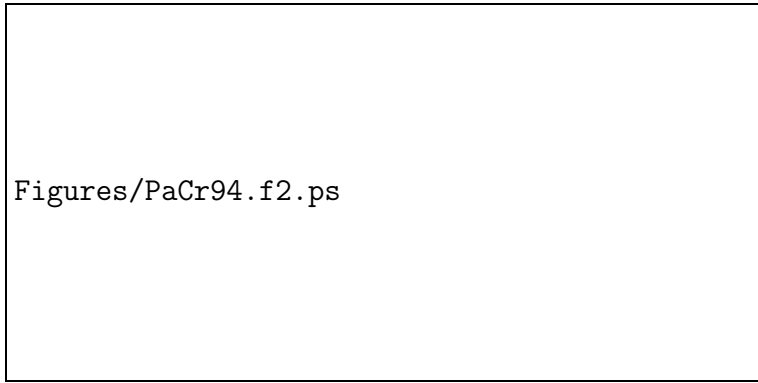
Figure 81: a) Burst-position neuron (A,C) and position neuron (B,D) in the monkey medulla (HE=horizontal eye position, HT=horizontal target position, FR=firing rate). b) The duration of the bursts is strongly correlated with the duration of the saccades and usually precedes them by $\sim 10ms$ (solid bars in inset for burst-position cells, open bars for position cells) [47].

```
Figures/PaCr94.f2.ps
```

Figure 82: Neurons in goldfish medulla. coding for eye position (A,B) or eye velocity (D). A) spontaneous eye movement. Firing rate (FR) correlated with left eye position (LE). B) Sinusoidal head rotation (in the dark) with compensating eye movement. Firing rate correlated with eye position, not eye velocity. D) Sinusoidal head rotation. Firing rate correlated with eye velocity. (LE=left eye position, $\dot{LE}$=left eye velocity, $\dot{H}$=head velocity) [48].

Position neurons need to **integrate** velocity information, e.g. from vestibular system about head rotation

Model for an integrator:

- single neuron with excitatory autapse (synapse of neuron onto itself)

- network with excitatory recurrent connections

Integrator needs to receive input corresponding to the motor commands (efference copy[25]) to update the position.

---

[25]Efference copies inform the brain also about expected sensory input (finger touching hand) to distinguish sensory signals created by the animal itself rather than by external influence. Efference copies presumably underly the observation that one cannot tickle oneself.

Figures/SeLe00a.f3.ps

Figures/SeLe00a.f1.ps
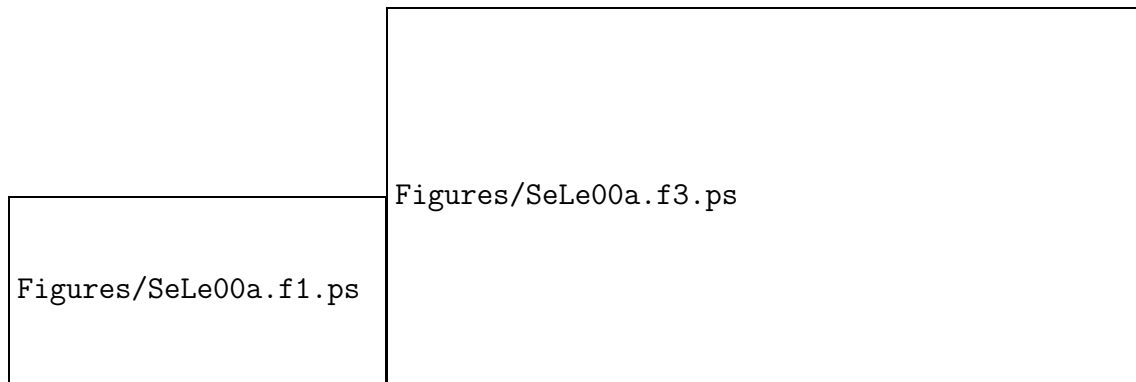
Figure 83: a) Network model for integrator in okulomotor control via recurrent excitation. The integrator network receives efference copies of the motor control signals (excitatory and inhibitory bursts) to update the stored eye position. b) Results from the integrator model of [52].

For these integrators exact integration requires

$$\lambda_\nu = 1$$

For $\lambda_\nu < 1$ the eye position would slowly relax back to center position

For $\lambda_\nu > 1$ the eye position would diverge to the sides

The relaxation/divergence occurs with the time-constant

$$\tau_\nu = \frac{\tau_r}{1 - \lambda_\nu}$$

Experimentally one finds that the eye position relaxes with a time constant

$$\tau_{relax} = \mathcal{O}(10s)$$

(in goldfish [52]) and

$$\tau_r = 5ms \ldots 100ms$$

For this type of integrator to be sufficient one would need the relevant eigenvalue to be precisely tuned,

$$|\lambda_\nu - 1| = \frac{\tau_r}{\tau_{relax}} = \frac{1}{2000} \ldots \frac{1}{100}.$$

So far, it is not clear whether there are mechanisms that would allow such a precise tuning of the synaptic strengths.

7.3.3   Limulus Vision. Contrast Enhancement

Output of the retina is not simply a pixelated picture of the visual scene:
The receptive fields of retinal ganglion cells have a spatial center-surround structure

and in addition temporal structure (Fig.64)

$\Rightarrow$ non-trivial computations are performed already in the retina

Simple example: contrast enhancement by lateral inhibition

Figures/mach_band_david_anson_bw_no_separator.ps

Figures/mach_band_david_anson_bw_with_separator.ps
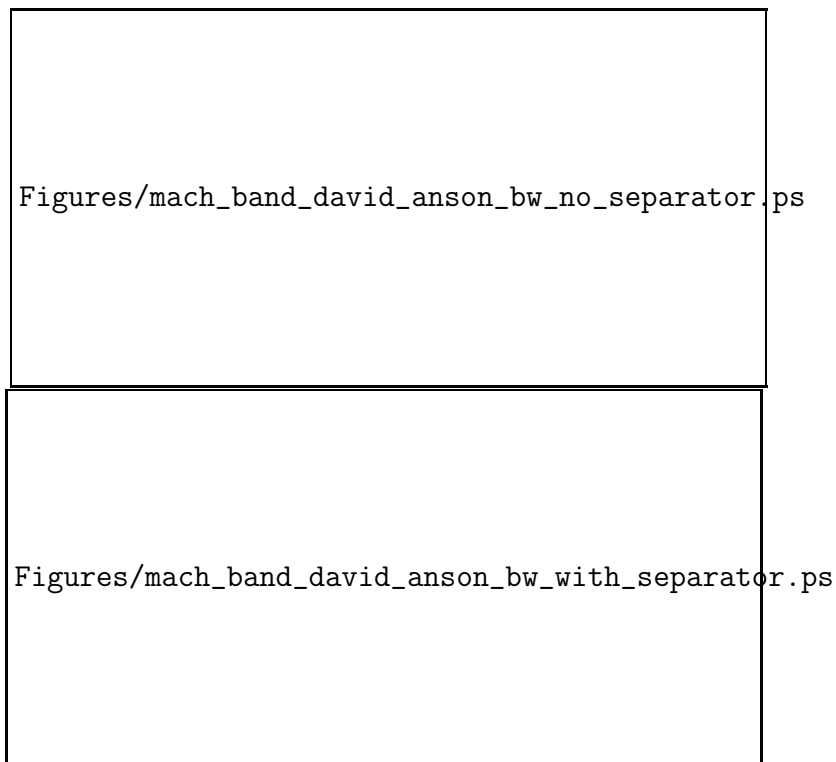
Figure 84: Mach bands. Contrast enhancement by lateral inhibition.

The vertebrate (and mammalian) retina is very complex (Fig.85).

Figures/KaSc00.f26-6.ps
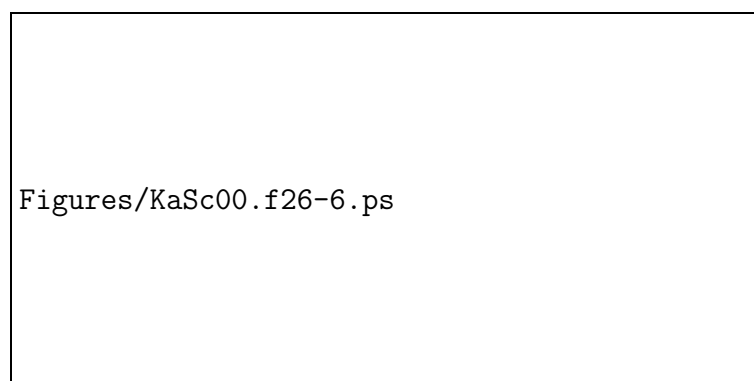
Figure 85: Many different types of cells contribute to the function of the retina, among them horizontal cells that provide lateral inhibition [38].

Consider simpler visual system: Limulus (horse-shoe crab)

```
Figures/horseshoe-crab.jpg
```

```
Figures/Horseshoe-crab-eye-detail.jpg
```
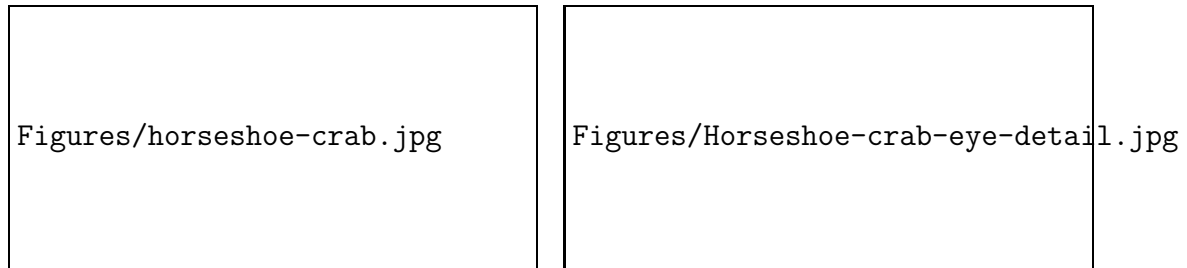
Figure 86: Horseshoe crab and its compound eye

The compound eye consists of $\mathcal{O}(1000)$ ommatidia. Each ommatidium has an individual lens and is functioning as 1 pixel.

Vision in Limulus was in particular studied by H.K. Hartline, starting in the 1930s (Nobel Prize 1967 [25]).

```
Figures/Ha69.f1.ps
```
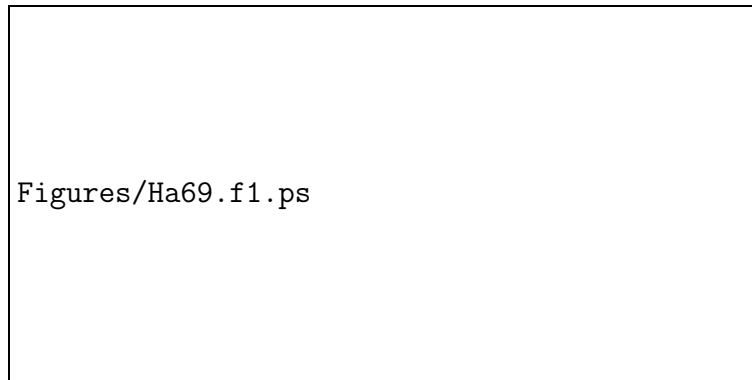
Figure 87: Electrical activity in single optic nerve. Stimulation with 3 different intensities [25].

```
Figures/HaRa57.f1.ps
```

```
Figures/HaRa57.f2.ps
```
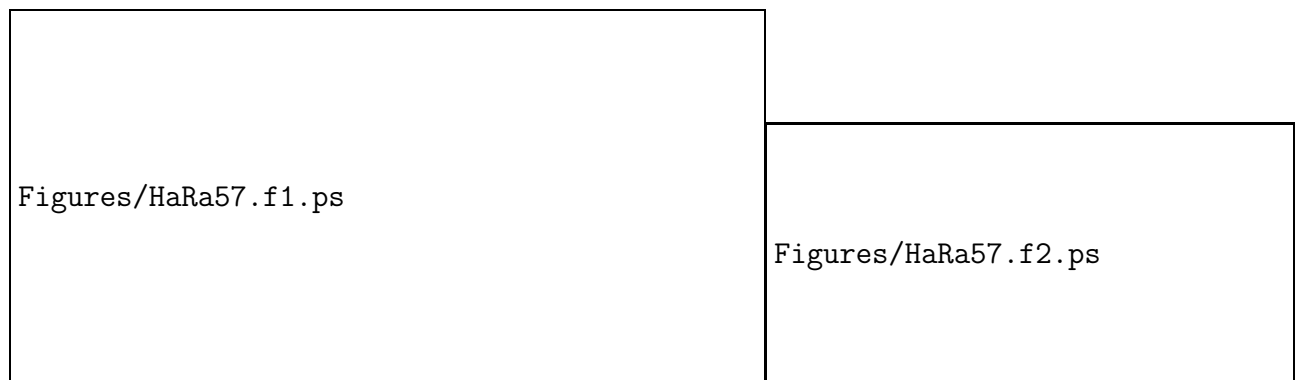
Figure 88: Stimulated ommatidia inhibit each other reciprocally with threshold [26].

The output from a given ommatidium depends on the stimulation of the ommatidia in its surround:

- lateral inhibition

- linear in the firing rate of the inhibiting ommatidium

- threshold: minimal firing rate needed for inhibition

Note:

- The inhibition is not driven directly by the stimulus to the other ommatidium but by the output of the other ommatidium: recurrent network

Simple Rate Model:

$$\tau_r \frac{dv_i}{dt} = -v_i + F(I_{s,i}(t))$$

$$\tau_s \frac{dI_{s,i}}{dt} = -I_{s,i} + \underbrace{h_i}_{\text{light stimulus}} - \sum_j w_{ij} [v_j - v_{thresh}]_+$$

Note:

- It is found that the synaptic strength w_{ij} depends on the distance between the ommatidia.

Focus on stationary state:

$$v_i^\infty = F(I_s^\infty) \qquad I_s^\infty = h_i - \sum_j w_{ij} \left[v_j^\infty - v_{thresh} \right]_+$$

thus

$$v_i^\infty = F \left(h_i - \sum_j w_{ij} \left[v_j^\infty - v_{thresh} \right]_+ \right)$$

Simplifications

- one-dimensional continuum of neurons: $v_i \Rightarrow v(x)$

- to avoid boundaries assume periodic domain $-\pi < x \leq +\pi$

- observation: suppression of firing is linear in the firing rate of the suppressing neuron
  $\Rightarrow$ equations become linear

- distance dependence of synaptic strength:

$$w_{ij} \Rightarrow g\, M(x - x') = \begin{cases} g & x - \Delta \leq x' \leq x + \Delta \\ 0 & \text{otherwise} \end{cases}$$

Thus

$$v_\infty(x) = h(x) - g \int_{-\pi}^{+\pi} M(x - x')v_\infty(x')dx' \tag{54}$$

To solve this integral equation note

- equation is linear

- **–** corresponds to matrix equation (49)
- **–** solve using eigenvectors, i.e. eigenfunctions, satisfying[26]

$$\int_{x-\pi}^{x+\pi} M(x - x') e_n(x') dx' = \lambda_n e_n(x)$$

- equation is translation invariant: $M(x, x') = M(x - x')$
  $\Rightarrow$ eigenfunctions are Fourier modes

$$e_n^{(c)}(x) = \cos nx \qquad e_n^{(s)} = \sin nx$$

Determine eigenvalues:

$$
\begin{aligned}
\int_{x-\pi}^{x+\pi} M(x - x') \cos nx' \, dx' &= \int_{x-\Delta}^{x+\Delta} \cos nx' \, dx' = \\
&= \frac{1}{n} \left(\sin n \, (x + \Delta) - \sin n \, (x - \Delta) \right) \\
&\quad \frac{2}{n} \cos nx \, \sin n\Delta
\end{aligned}
$$

$$\int_{x-\pi}^{x+\pi} M(x - x') \sin nx' \, dx' = \int_{x-\Delta}^{x+\Delta} \sin nx' \, dx' = \frac{2}{n} \sin nx \, \sin n\Delta$$

Thus

$$\lambda_0 = 2\Delta \qquad \text{for eigenvector} e_0^{(c)} = 1$$

$$\lambda_n = \frac{2}{n} \sin n\Delta \qquad \text{for } e_n^{(c)} = \cos nx \text{ and for} e_n^{(s)} = \sin nx \qquad n > 0$$

Expand $v_\infty(x)$ and $h(x)$ into Fourier series

$$v_\infty(x) = \sum_{n=0}^{\infty} v_n^{(c)} \cos nx + \sum_{n=1}^{\infty} v_n^{(s)} \sin nx \qquad h(x) = \sum_n h_n^{(c)} \cos nx + h_n^{(s)} \sin nx$$

and insert into (54)

$$
\begin{aligned}
\int_{x-\pi}^{x+\pi} M(x - x') v_\infty(x') \, dx' &= \sum_{n=1}^{\infty} \int_{x-\pi}^{x+\pi} M(x - x') \left(v_n^{(c)} \cos nx' + v_n^{(s)} \sin nx' \right) dx' = \\
&= \sum_{n=1}^{\infty} \lambda_n v_n^{(c)} \cos nx + \lambda_n v_n^{(s)} \sin nx
\end{aligned}
$$

Using the orthogonality of different trigonometric functions (e.g. $\int_{\pi}^{+\pi} \cos nx \cos mx dx = \delta_{nm}$)

one can collect all $\cos nx$ and $\sin nx$ separately to get

$$v_n^{(c,s)} = \frac{1}{1 + g\lambda_n} h_n^{(c,s)}$$

---

[26]cf. DA Chap. 7.4

Consider small step in luminosity

$$h(x) = \begin{cases} 1 - \delta & x < 0 \\ 1 + \delta & x > 0 \end{cases}$$

with expansion

$$h^{(s)}_{2n+1} = \frac{4\delta}{(2n+1)\pi} \qquad n = 0, 1, 2 \ldots$$

$$h^{(s)}_{2n} = 0 \qquad h^{(c)}_n = 0 \qquad n = 0, 1, 2, \ldots$$

$$h^{(c)}_0 = 1$$

Thus

$$v_\infty(x) = \frac{1}{1 + 2g\Delta} + \sum_{n=0}^{\infty} \frac{1}{1 + g\frac{2}{2n+1}\sin(2n+1)\Delta} \frac{4\delta}{\pi(2n+1)} \sin(2n+1)x \qquad (55)$$

a) Figures/mach_plot.eps   b) Figures/visual_lateral.1.eps
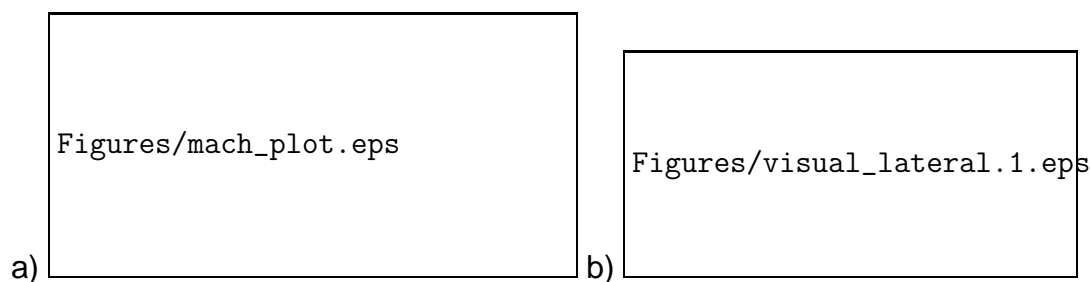
Figure 89: Mach band: lateral inhibition enhances small differences in luminosity ($g\Delta = 1$). a) solution (55) b) qualitative sketch.

Note:

- differences between pixels are enhanced by lateral inhibition
    - Mach bands
    - contrast enhancement

a) Figures/Ha69.f13a.ps   b) Figures/KnTo70.f6.ps
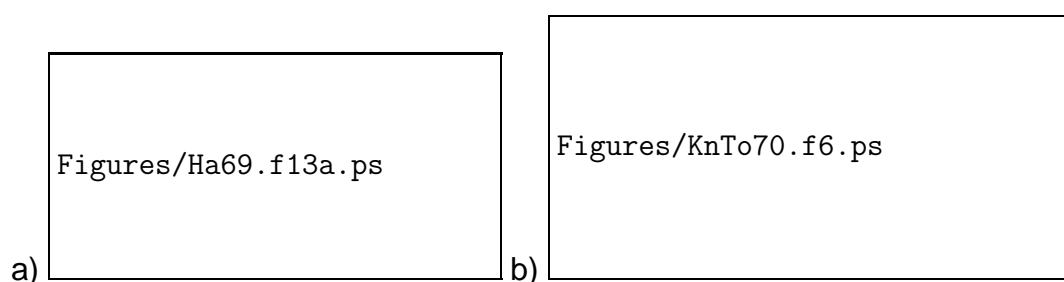
Figure 90: a) Sharpening of on-transient by delayed lateral inhibition. Upper curve: response if only a single ommatidium is illuminated. Lower non-monotonic curve: illumination covers also neighbors, which provide delayed inhibition [25]. b) Temporal shape of lateral interaction: short excitation followed by longer inhibition [40].

Dynamical behavior:

- Lateral inhibition arises with a delay
  initially strong response of all cells, then inhibition kicks in $\Rightarrow$ firing of cells decrease $\Rightarrow$ inhibition decreases $\Rightarrow$ firing rate increases again after a delay
  $\Rightarrow$ non-monotonic approach to steady state

- In addition self-inhibition:
  rises very quickly, decays then more slowly than lateral inhibition

Could model lateral interaction with a double-exponential as for the slow synapse (cf. (30))

- rapidly decaying excitation

- slowly decaying inhibition

$$I_{s,i} = h_i + I_{s,u}^{(e)} + I_{s,i}^{(i)}$$

$$\tau_e \frac{dI_{s,i}^{(e)}}{dt} = -I_{s,i}^{(e)} + \sum_j w_{ij}^{(e)} \left[v_j(t) - v_{thresh}^{(e)} \right]_+$$

$$\tau_i \frac{dI_{s,i}^{(i)}}{dt} = -I_{s,i}^{(i)} - \sum_j w_{ij}^{(i)} \left[v_j(t) - v_{thresh}^{(i)} \right]_+$$

7.3.4 Persistent States

Consider again nonlinear recurrent network (17)

$$\tau \frac{d\mathbf{v}}{dt} = -\mathbf{v} + \mathbf{F} \left(\mathbf{h} + \mathbf{M}\mathbf{v} \right)$$

So far we did not investigate any possible role for the nonlinearity $\mathbf{F}$

Consider for simplicity minimal model:

- single neuron with sigmoid firing-rate function with threshold v_θ

$$\tau \frac{dv}{dt} = -v + F(h + mv) \qquad F(h + mv) = \frac{1}{1 + e^{-(h+m(v-v_\theta))}}$$

Can combine threshold and feed-forward input: $v_{th} = (v_\theta - h)/m$

$$\tau \frac{dv}{dt} = -v + \frac{1}{1 + e^{-m(v-v_{th})}} \tag{56}$$

123

Steady states $v = v_\infty$ satisfy the transcendental equation

$$v_\infty = \frac{1}{1 + e^{-m(v_\infty - v_{th})}}$$

Cannot be solved in terms of simple functions: use graphical approach

- small m:
  straight line intersections sigmoid in exactly 1 point: single steady state (fixed point)

- large m:

  - large positive v_{th}: single fixed point with $v_\infty \approx 0$
  - large negative v_{th}: single fixed point with $v_\infty \approx 1$
  - intermediate values of v_{th}: three fixed points simultaneously
    can show
      * 'outer' fixed points $v_\infty^{(1)} \approx 0$ and $v_\infty^{(3)} \approx 1$ are linearly stable
      * intermediate fixed point $v_\infty^{(2)}$ is linearly unstable: solution exists, but any
        small perturbation will push v away from $v_\infty^{(2)}$ to either $v_\infty^{(1)}$ or $v_\infty^{(3)}$

Easier visualization of dynamics using a potential

$$\tau \frac{dv}{dt} = -\frac{dU}{dv} \qquad \text{with} \qquad U(v) = \frac{1}{2}v^2 - \int_{-\infty}^{v} \frac{1}{1 + e^{-m(v' - v_{th})}} dv'$$

Consider large m and approximate F by a step function

$$F(v) = \begin{cases} 1 & \text{for } v > v_{th} \\ 0 & \text{for } v < v_{th} \end{cases}$$

then
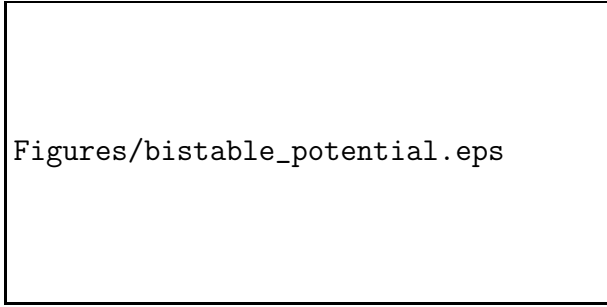
$$U(v) = \begin{cases} \frac{1}{2}v^2 - (v - v_{th}) & \text{for } v > v_{th} \\ \frac{1}{2}v^2 & \text{for } v < v_{th} \end{cases}$$

Minima at

$$v = 1 \quad \text{for} \quad v_{th} < 1$$
$$v = 0 \quad \text{for} \quad v_{th} > 0$$

Thus:

$$\begin{aligned} v_{th} < 0 \quad &\text{single minimum at} \quad v_\infty^{(1)} = 1 \\ 0 < v_{th} < 1 \quad &\text{two minima at} \quad v_\infty^{(1)} = 0 \qquad v_\infty^{(3)} = 1 \\ 1 < v_{th} \quad &\text{single minimum at} \quad v_\infty^{(3)} = 0 \end{aligned}$$

Figures/bistable_potential.eps

Figure 91: Potential $U(v)$ for three values of v_{th}.

During the evolution the value of the potential $U(v)$ cannot increase

$$\frac{dU(v(t))}{dt} = \frac{dU(v)}{dv}\frac{dv}{dt} = -\left(\frac{dU}{dv}\right)^2 \leq 0$$

'Particle with position v is sliding down the potential landscape U'

Thus:

- eventually the neuron will always go into a steady state

- neuron can be active $v_\infty \approx 1$ even without any input h: *persistent activity*

- neuron can be *bistable*:
  depending on initial conditions the neuron will go into the steady state $v_\infty^{(1)}$ or $v_\infty^{(3)}$
  neuron can function as a *memory*

Working memory used to remember items for a brief time (e.g. phone numbers,...)

Figures/delay1.eps	Figures/delay2.eps	Figures/delay3.eps
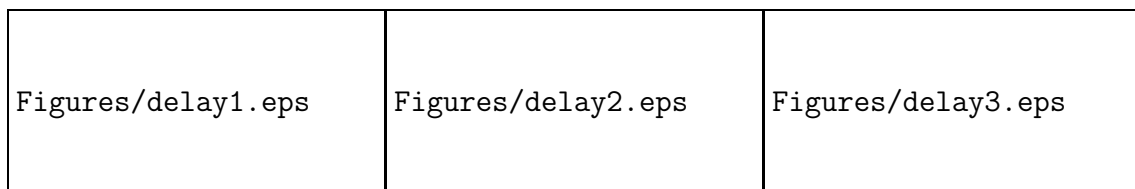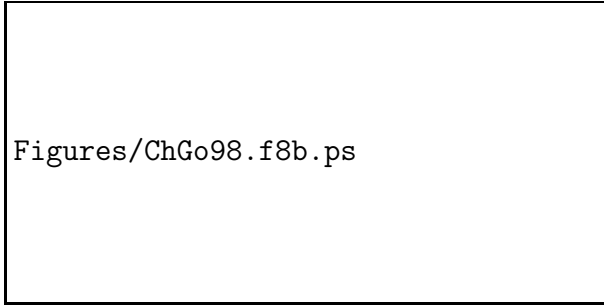
Figure 92: Delayed memory task. The cue (red circle) tells the monkey which of the two blue buttons it is to press after the delay, i.e. when the red go-signal comes on.

Figure 93: Firing rate of a population of neurons in prefrontal cortex in rhesus macaque monkeys. Neurons fire persistently during the delay period while the stimulating cue is off. The neurons stop firing when the monkey makes a saccade to the goal indicated by the cue [5].

7.3.5 Associative Memory[27]

We would like to store multiple patterns in a network.

Simplify the system and its dynamics yet further by considering a network of N McCulloch-Pitts neurons [46]

- neurons are ON ($v = +1$) or OFF ($v = -1$)

- input: sum of weighted inputs

- step function $F(x) = sgn(x)$

- discrete time steps: iteration $v_i \rightarrow v_i'$

$$v_i' = sgn\left(\sum_j M_{ij} v_j\right) \tag{57}$$

Figure 94: State space of a network consisting of 3 McCulloch-Pitts neurons.

Note:

---

[27][27] Ch.2

- the space of possible states are the corners of an N-dimensional hypercube

- the dynamics consists in hopping from one corner to another

Goal:

- find $\mathbf{M}$ such that given k patterns $\hat{\mathbf{v}}^{(s)}, s = 1 \ldots k$, are *stable* fixed points of the iteration (57)

Consider symmetric $\mathbf{M}$, $M_{ij} = M_{ji}$, with vanishing diagonal[28], $M_{ii} = 0$,

Introduce the energy function

$$E = -\frac{1}{2} \sum_i \sum_j M_{ij} v_i v_j$$

The energy is non-increasing under the iteration (57):
when some component v_l changes to

$$v_l' = sgn \left(\sum_j M_{ij} v_j \right) \equiv v_l + \Delta v_l$$

the energy change is (using $M_{ii} = 0$)

$$\Delta E = -\Delta v_l \sum_j M_{lj} v_j$$

Then

$$\begin{aligned}
\Delta E &= -sgn \left(\sum_r M_{lr} v_r \right) \sum_r M_{lr} v_r + v_l \left(\sum_r M_{lr} v_r \right) \\
&= -\left| \sum_r M_{lr} v_r \right| + \underbrace{v_l}_{=\pm 1} \sum_r M_{lr} v_r
\end{aligned}$$

Thus

$$\Delta E = \begin{cases} -2 \left| \sum_r M_{lr} v_r \right| & \text{for} sgn \left(\sum_r M_{lr} v_r \right) = -sgn \left(v_l \right) \qquad v_l \text{ did change} \\ 0 & \text{for } sgn \left(\sum_r M_{lr} v_r \right) = sgn \left(v_l \right) \qquad \text{no change in } v_l \end{cases}$$

Moreover, E is bounded from below since $v_l = \pm 1$

Note:

- for any such $\mathbf{M}$ and any initial conditions the dynamics always leads to a fixed point

---

[28]Diagonal elements need not be chosen to vanish, but the performance is somewhat better that way [27].

- discrete motion in a discrete energy landscape

- no energy exists in general if $\mathbf{M}$ is not symmetric

How to choose the coupling matrix $\mathbf{M}$ to store k specific patterns, i.e. to have specific patterns as stable fixed points?

Single pattern: Consider $\hat{\mathbf{v}} = (\hat{v}_1, \ldots, \hat{v}_N)$,

$$sgn\left(\sum_j M_{lj}\hat{v}_j\right) = \hat{v}_i$$

Try

$$M_{ij} = \begin{cases} \alpha\hat{v}_i\hat{v}_j & \text{for } i \neq j \\ 0 & \text{for } i = j \end{cases}$$

Then each term in the energy sum has the same sign for that pattern $\hat{\mathbf{v}}$ making the energy extremal for that pattern

$$E(\hat{\mathbf{v}}) = -\frac{1}{2}\sum_i\sum_j M_{ij}\hat{v}_i\hat{v}_j = -\frac{1}{2}\alpha\sum_{ij}\hat{v}_i^2\hat{v}_j^2 \underbrace{=}_{M_{ii}=0} -\frac{1}{2}\alpha\left(N^2 - N\right)$$

Consider the iteration (57)

$$\sum_j M_{ij}\hat{v}_j = \alpha\hat{v}_i\sum_{i\neq j=1}^N \hat{v}_j^2 = \alpha\left(N-1\right)\hat{v}_i$$

Choose $\alpha = 1/\left(N-1\right)$. Then $\hat{\mathbf{v}}$ is a fixed point of the iteration.

What happens if some of the components of the initial conditions $\tilde{\mathbf{v}}$ do not agree with $\hat{\mathbf{v}}$? E.g. $\tilde{\mathbf{v}}$ agrees with $\hat{\mathbf{v}}$ only in the first m components,

$$\tilde{\mathbf{v}} = (\hat{v}_1, \hat{v}_2, \ldots \hat{v}_m, -\hat{v}_{m+1}, \ldots, -\hat{v}_N)$$

Then[29]

$$\sum_j M_{lj}\tilde{v}_j = \sum_{j=1}^m M_{lj}\hat{v}_j - \sum_{j=m+1}^N M_{lj}\hat{v}_j = \frac{1}{N}\hat{v}_l\left(m - (N-m)\right) = \frac{1}{N}\left(2m - N\right)\hat{v}_l$$

Thus, for $m > N/2$ the sign of this sum is the same as for $\hat{\mathbf{v}}$
$\Rightarrow \tilde{\mathbf{v}}$ is also mapped to $\hat{\mathbf{v}}$.

Notes:

- $\hat{\mathbf{v}}$ is an attractor

---

[29]Strictly speaking, since $M_{ll} = 0$ one needs to distinguish between $l \leq m$ and $l > m$. But it makes only a small difference. For $l \leq m$ one gets $(N-1)^{-1}(2m - N - 1)$ whereas for $l > m$ one gets $(N-1)^{-1}(2m - N + 1)$.

- the mapping $\mathbf{M}$ first *projects*[30] the vector $\mathbf{v}$ onto $\hat{\mathbf{v}}$ and then scales up the vector again to full size.

- for initial conditions within the *basin of attraction* the iteration corrects incorrect components of the initial condition

- initial conditions that contain too many 'errors' do not converge to the attractor, they are outside the basin of attraction of this attractor and in the basin of attraction of another attractor

- following the work of John Hopfield [31] this type of associative memory has been studied extensively from a computational perspective.

Thus:

- The network serves as *associative memory* (content-addressable memory): the memorized state $\hat{\mathbf{v}}$ is retrieved (reached) even if it is only partially remembered in the initial condition

Multiple patterns. Consider $\hat{\mathbf{v}}^{(\mu)}$, $1 \leq \mu \leq k$, and try

$$M_{ij} = \frac{1}{N} \sum_{\mu} \hat{v}_i^{(\mu)} \hat{v}_j^{(\mu)}$$

Is each pattern indeed a fixed point of the iteration?
Start the iteration at one of the patterns $\hat{\mathbf{v}}^{(\nu)}$

$$\sum_j M_{ij} \hat{v}_j^{(\nu)} = \frac{1}{N} \sum_\mu \hat{v}_i^{(\mu)} \sum_j \hat{v}_j^{(\mu)} \hat{v}_j^{(\nu)} = \hat{v}_i^{(\nu)} + \underbrace{\frac{1}{N} \sum_{\mu \neq \nu} \sum_j \hat{v}_i^{(\mu)} \hat{v}_j^{(\mu)} \hat{v}_j^{(\nu)}}_{\text{cross-talk}}$$

Thus,

- analogous to the case of a single stored memory $\mathbf{M}$ first projects $\mathbf{v}$ onto the subspace spanned by the patterns $\hat{\mathbf{v}}^{(\mu)}$ and then scales the vector up again via the nonlinearity

- if

$$\frac{1}{N} \left| \sum_{\mu \neq \nu} \sum \hat{v}_i^{(\mu)} \hat{v}_j^{(\mu)} \hat{v}_j^{(\nu)} \right| < 1$$

the sign of $\sum_j M_{ij} \hat{v}_j^{(\nu)}$ is the same as that of $\hat{v}_j^{(\nu)}$
$\Rightarrow$ the pattern $\hat{\mathbf{v}}^{(\nu)}$ is correctly retrieved.

---

[30]$\mathbf{M}$ can be written as $\mathbf{M} = \hat{\mathbf{v}} \hat{\mathbf{v}}^t$, with $\hat{\mathbf{v}}^t$ being a row vector and $\hat{\mathbf{v}}$ as column vector.

- again the iteration can complete the pattern if the initial condition $\mathbf{v}^{(init)}$ differs not too much from $\hat{\mathbf{v}}^{(\nu)}$

- because of the cross-talk the error tolerance is reduced

- expect that the cross-talk becomes more significant for larger numbers of stored patterns
  $\Rightarrow$ the network has only a finite capacity k_{max} for storing patterns, which depends on the error rate accepted. For random patterns one can show

$$k_{max} \approx 0.14 \cdot N$$

- the network has often also 'spurious memories', i.e. attractors that do not correspond to the k stored patterns

    - because of symmetry $v_i \rightarrow -v_i$ inverted pattern is always also an attractor
    - some mixtures of patterns like $v_i = \pm\hat{v}_i^{(\mu_1)} \pm \hat{v}^{(\mu_2)} \pm \hat{v}_i^{(\mu_3)}$ are also attractors (mixtures composed of even number of patterns could add up to 0 and cannot be in the state space.

- if the patterns to be stored are orthogonal to each other, $\sum_j \hat{v}_j^{(\mu)} \hat{v}_j^{(\nu)} = \delta_{\mu\nu}$, the cross-talk vanishes: no error in the iteration

    - **but:** for $k = N$ one has, using matrix notation $(\mathbf{V})_{i\mu} \equiv \hat{v}_i^{\mu}$,

$$\text{cross-talk:} \quad \mathbf{V}^t \mathbf{V} = \mathbf{I} \qquad \Rightarrow \qquad \mathbf{V}^t = \mathbf{V}^{-1}$$

$$\text{weight matrix:} \quad \mathbf{V}\mathbf{V}^t = \mathbf{V}\mathbf{V}^{-1} = \mathbf{I}$$

    thus the weight matrix is diagonal and the network preserves *any* input: no memory at all.
    i.e. since retrieval corresponds to projection onto the subspace spanned by the stored patterns: N orthogonal vectors span the whole space $\rightarrow$ the projection becomes the identity.

    - for $k < N$ the performance does improve if the patterns are orthogonal
      often preprocessing is employed to make the patterns of interest more orthogonal

Note:

- If the network 'learns' one pattern at a time

$$M_{ij}^{(\mu+1)} = M_{ij}^{(\mu)} + \frac{1}{N}\hat{v}_i^{(\mu+1)}\hat{v}_j^{(\mu+1)}$$

the weight update resembles Hebb's rule ('neurons that fire together wire together'):

- weight is strengthend if pre- and post-synaptic neuron are active

- weight is weakened if only one of them is active

- **but:**

  * weight is also strengthened when neither neuron is active
  * weight can be positive or negative: same synapse can switch from excitatory to inhibitory or vice versa
  * model can be modified to make it physiologically more reasonable

8 Statistical Approach

In particular in cortex

- variability of spiking (cf. Fig.55)

  - deterministic variability or noise?
  - relevant for function or 'nuisance'?

- during short intervals only small number of spikes, which fluctuates strongly between trials
  $\Rightarrow$ imprecise and unreliable transmission of information

- need to merge multiple sources/types of sensory inputs:
  multi-sensory integration: how to weigh different sources of information

Gain insight into working of brain by considering illusions, i.e. situations in which the brain seemingly 'draws incorrect conclusions'

Examples:

- unreliable information: moving rhombi at low contrast
  `http://www.cs.huji.ac.il/~yweiss/Rhombus/`

- merging information for disambiguation: Necker cube with additional information
  `http://www.cut-the-knot.org/Curriculum/Geometry/Necker.shtml`
  `http://www.dogfeathers.com/java/necker.html`

- barber pole illusion
  `http://www.psychologie.tu-dresden.de/i1/kaw/diverses%20Material/www.illusionworks.com/html/barber_pole.html`

In particular at low contrast: imprecise information due to low spike rate:
interpret the spiking of the neuron as information about the *probability* of a certain sensory input, say.

Consider simple example: neuron sensing the position s of an object (prey, say)

Goal for the brain area that is reading that unreliable information:
What is the probability for the prey to be at a certain position s under the condition that a certain neuron spikes during a brief time Δt ($r = 1/\Delta t$),

$$P(s|r)$$

What information does the neuron provide directly?
the neuron has a tuning curve, i.e. $\bar{r} = f(s)$

Assuming a Poisson distribution for the spiking of the neuron as a function of its mean firing rate $\bar{r}$ one obtains for the probability of the neuron to spike during a brief intervat Δt

$$P(r|s) = \frac{1}{1!} \left(\bar{r}\Delta T\right)^1 e^{-\bar{r}\Delta t} \approx \bar{r}\Delta t = f(s)\,\Delta t$$

How do we convert between these two probabilities?

Consider joint probability

$$P(r,s) = P(r|s)P(s) = P(s|r)P(r)$$

Which implies Bayes' Theorem[31]

$$\underbrace{P(s|r)}_{\text{Posterior}} = \frac{1}{P(r)} \underbrace{P(r|s)}_{\text{Likelihood}} \underbrace{P(s)}_{\text{Prior}}$$

Notes:

- Prior: probabiliy distribution of stimuli independent of whether the neuron spikes or not
  The prior reflects the knowledge (expectation) that the system (animal) has a priori about its environment.
  It may have learned the prior on different time scales

  - under evolutionary control (long time scales)
  - through previous input, e.g.
    * memories stored from previous exposures
    * previous spikes of the same neuron (affecting neural spiking via facilia-tion and/or depression) e.g. ambient light

- Posterior: probability distribution of the stimulus incorporating the fact that the neuron spiked
  Best 'guess' for the position of the prey presumably at the maximum of the posterior (MAP=maximum a posteriori estimate)

$$\left.\frac{dP(s|r)}{ds}\right|_{s_{max}} = 0$$

  subsequent brain areas may use this best guess to base decisions on

---

[31] Thomas Bayes, mathematician and Presbyterian minister (1702-1761).

- $P(r)$ does not affect the dependence on the stimulus: we can usually ignore it

Examples:

i) Gaussian tuning curve $f(s) \propto e^{-(s-s_0)^2/2\sigma^2}$

ii) Gaussian tuning curve with linear prior: e.g., prey is approaching from the right $\Rightarrow$ shift in s_{max}

iii) successive measurement by the same neuron: for interpretation of second spike use the posteriori obtained from the first spike as prior $\Rightarrow$ sharpening of distribution.

a)
```
Figures/bayes_tuning.eps
```
b)
```
Figures/bayes_two_spikes.eps
```
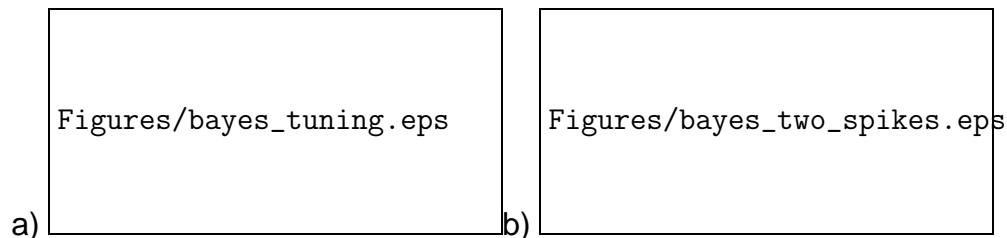
Figure 95: a) Posteriori for Gaussian tuning curve and linear prior. b) Flat initial prior, posterior of first and second spike used as prior for second and third spike, respectively.

iv) two neurons:
if the spiking of the two neurons is given by two *independent* Poisson processes

$$P(s|r_1, r_2) = \frac{1}{P(r_1, r_2)} P(r_1, r_2|s)P(s) \approx \frac{1}{P(r_1, r_2)} P(r_1|s)P(r_2|s)P(s)$$

a)
```
Figures/bayes_two_neurons_closer.eps
```
b)
```
Figures/bayes_two_neurons_further.eps
```
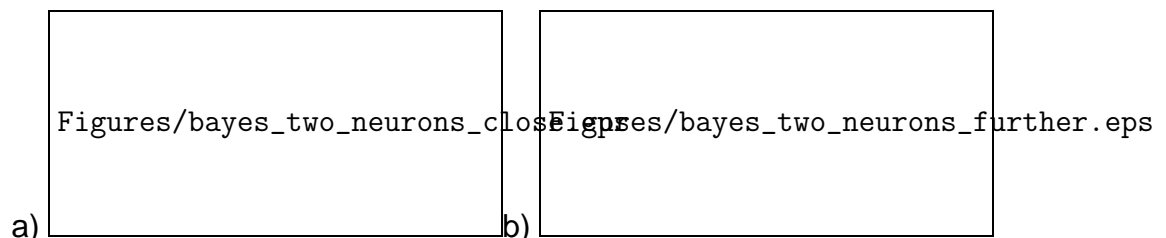
Figure 96: Two neurons with Gaussian tuning curve and different preferred location. a) equal widths. b) unequal widths.

When combining the information from two neurons, the peak is shifted towards the preferred location of neuron with narrower likelihood (which has more precise information).

Note:

- In the case of the Necker cube the likelihood for both configurations are exactly the same as is the prior

  - both configurations have also equal posteriors and the percept switches.
  - integration of additional information necessary to disambiguate the percept.

8.1   Bayes and the Cutaneous Rabbit

A tactile illusion:
stimulate mechanically the skin with brief pulses (2 ms) sequentially at two locations (cf. Fig.97a)

Perception:
...There is a smooth progression of jumps up the arm, as if a tiny rabbit were hopping from wrist to elbow...[22]

...In one experiment it was possible to induce a vivid hopping that traveled up one arm, across the neck, and down the other arm by the use of five contacts, two widely separated on each arm and one on the nape of the neck...[22]

The touch can even be perceived at locations that are anesthetized.

Figures/Go07a.f1A.ps	Figures/Go07a.f1B.ps	Figures/Go07a.f1C.ps
a)	b)	c)
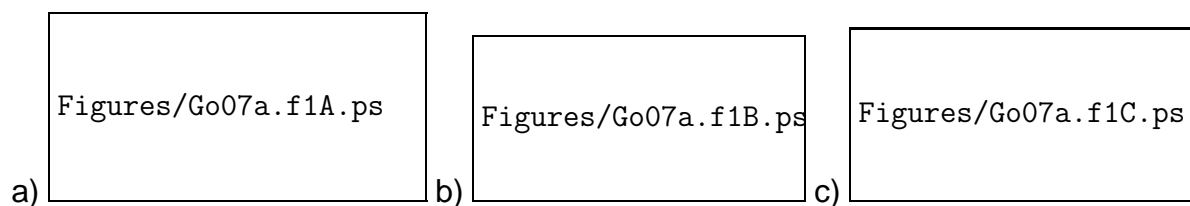
Figure 97: Sketch of stimulation protocol (positions in cm, time in seconds). a) Rabbit can be interpreted as *length contraction.* b) τ-effect: the more rapidly traversed of two equal distances is perceived as shorter. c) Two-arm comparison τ-effect: different lengths are perceived as the same if theu are traversed in different times [23]

Can these illusions be understood as arising from a rational model for the perception of the brain?

Need a high-level model:
consider a *Bayesian observer*, i.e. model probabilities for response and percept:

- describe perceived trajectory as

$$x = b + mt$$

  with perceived endpoints

$$x(0) = b \qquad x(\Delta t) = b + m\Delta t$$

- for simplicity consider two neurons with Gaussian receptive fields centered at the true endpoints of the trajectory, x_1 and x_2, respectively,

$$f_i(x) \propto \frac{1}{\sigma_s} e^{-(x-x_i)^2/2\sigma_s^2}, \qquad i = 1, 2$$

- Likelihood of the activation pattern D of these neurons if the trajectory was given by $x = b + mt$ and the time interval was Δt, [32]

$$P(D|m,b) \propto \frac{1}{\sigma_s} e^{-(b-x_1)^2/2\sigma_s^2} \frac{1}{\sigma_s} e^{-(b+m\Delta t - x_2)^2/2\sigma_s^2}$$

  the values m and b can be considered as *hypotheses* about the trajectory

- assume: eventual percept of the trajectory is given by the maximum ('mode') of the probability for the trajectory given the stimulus-evoked neural activation pattern D

$$P(m,b|D).$$

  m_{max} and b_{max} would constitute the most likely hypotheses about the trajectory. i.e. use maximum a posteriori (MAP) estimate.

- to obtain $P(m,b|D)$ in terms of $P(D|m,b)$ use Bayes' theorem

$$P(m,b|D) \propto P(D|m,b)\, P(m,b)$$

- we need a prior $P(m,b)$:
  assume:

  - the initial point could be anywhere (flat prior for b)
  - small velocities are more likely than large velocities

$$P(m,b) \propto 1 \cdot \frac{1}{\sigma_v} e^{-m^2/2\sigma_v^2}$$

- combined

$$P(m,b|D) \propto \frac{1}{\sigma_s} e^{-(b-x_1)^2/2\sigma_s^2} \frac{1}{\sigma_s} e^{-(b+m\Delta t - x_2)^2/2\sigma_s^2} \cdot 1 \cdot \frac{1}{\sigma_v} e^{-m^2/2\sigma_v^2}$$

Figures/Go07a.f2B.ps
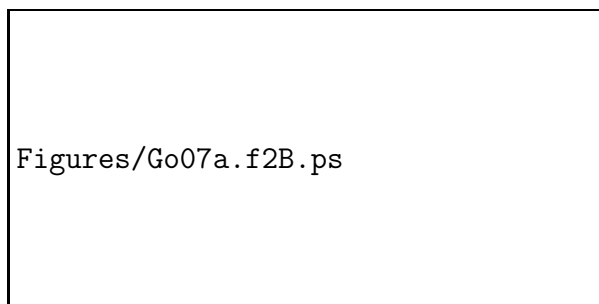
Figure 98: Probability distributions of the model in terms of initial position and velocity (a) or initial and end position (b). Factual values inidicated by cross [23].

---

[32] naive Bayes: assume that the conditional probability of the response of the two sensory modalities are independent of each other, i.e. can factorize the joint conditional probability. 'noise of the two modality is uncorrelated'

If the brain operates using the MAP estimate then the perceived trajectory should correspond to m_{max} and b_{max} that maximize $P(m, b|D)$

Determine maximum by minimizing exponent

$$\frac{\partial}{\partial b} \ln\left(P(m, b|D)\right) = -\frac{1}{\sigma_s^2}\left((b_{max} - x_1) + (b_{max} + m_{max}\Delta t - x_2)\right) = 0$$

$$b_{max} = \frac{1}{2}\left(x_1 + x_2 - m_{max}\Delta t\right)$$

$$\frac{\partial}{\partial m} \ln\left(P(m, b|D)\right) = -\frac{1}{\sigma_s^2}\left(b_{max} + m_{max}\Delta t - x_2\right)\Delta t - \frac{1}{\sigma_v^2}m_{max} = 0$$

$$b_{max} = -\frac{\sigma_s^2}{\Delta t \, \sigma_v^2}m_{max} - m_{max}\Delta t + x_2$$

yielding

$$m_{max} = \frac{\Delta x}{\Delta t}\frac{1}{1 + \frac{2}{(\lambda\Delta t)^2}}$$

and

$$b_{max} = x_1 + \Delta x\frac{1}{2 + (\lambda\Delta t)^2}$$

with

$$\lambda = \frac{\sigma_v}{\sigma_s}$$

characterizing the reliability of the position information and the degree of bias towards low velocities.

Maximum of posterior is at a smaller velocity

Consequently the perceived lengths is contracted (since times are kept fixed)

$$\Delta x' \equiv m_{max}\Delta t = \Delta x\,\frac{1}{1 + \frac{2}{(\lambda\Delta t)^2}}$$

i.e.

$$\frac{\Delta x'}{\Delta x} = \frac{1}{1 + \frac{2}{(\lambda\Delta t)^2}}$$

The initial point is perceived as shifted towards the final point by

$$b_{max} - x_1 = \Delta x\frac{1}{2 + (\lambda\Delta t)^2}$$

This model has a single fit parameter λ:

- large λ: high spatial acuity and/or low expectation for slow motion

- small λ: low spatial acuity and/or strong expectation for slow motion

Figures/Go07a.f3A.ps

a)   b)

Figures/Go07a.f3B.ps
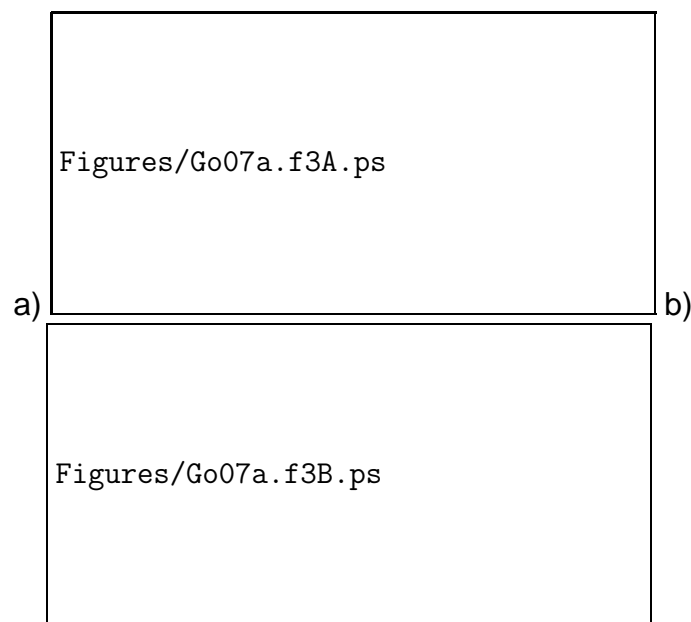
Figure 99: a) Perceived length contraction as a function of duration of trajectory. True distance between taps is $10cm$, perceived distance is l'. b) Two-arm τ-effect: ratio of lengths that yield the same perceived length as a function of the ratio of the durations of the trajectories ($\Delta t_2 = 1s - \Delta t_1$). Value for λ was fit separately for a) and b). [23]

Two-arm τ-effect: different lengths are perceived as equal if the durations are different

$$\frac{\Delta x_1'}{\Delta x_2'} = 1 = \frac{\Delta x_1 \frac{1}{1+\frac{2}{(\lambda \Delta t_1)^2}}}{\Delta x_2 \frac{1}{1+\frac{2}{(\lambda \Delta t_2)^2}}}$$

In the experiment a specific protocol was used ($t_{max} = 1s$)

$$\Delta t_2 = t_{max} - \Delta t_1$$

Rewrite length ratio in terms of

$$\nu = \frac{\Delta t_2}{\Delta t_1}$$

to yield

$$\frac{\Delta x_1'}{\Delta x_2'} = \frac{1 + \frac{2(1+\nu)^2}{\lambda^2 t_{max}^2}}{1 + \frac{2(1+\nu)^2}{\lambda^2 t_{max}^2 \nu^2}}$$

Notes:

- model provides coherent rationalization of

137

- **–** perception of length contraction
- **–** τ-effect (dependence of perceived distance on time between stimuli)
- **–** κ-effect (dependence of perceived time between stimuli on distance between them)

- merges the expectation of slow movements with the observed imprecisely determined positions

- reasonable success suggests that

  - **–** the brain may be using such probabilities in the information processing
  - **–** the brain may be employing optimal merging of unreliable information in Bayes fashion

- how could probabilities be encoded?
  one can show that for Poisson-like spike statistics [61]

  - **–** neural populations can encode probabilities
  - **–** implementing Bayes' theorem, which requires multiplying two probability distributions, can be achieved by adding the activities of the neurons encoding the two distributions

- this gives a function to the high variability of cortical spiking activity

8.2   Integration of Multi-Sensory Information[33]

- How should possibly conflicting information from different sensory inputs be combined?

- How does the brain do it?

Experimental study of the integration of haptic and visual information

- visual information about the height of a bar via three-dimensional image:

  - **–** to modify the reliability of that information the images are corrupted by various degrees of noise

- haptic (touch) information provided by simulated force feed-back

- the haptic and visual information disagree with each other by $\mathcal{O}(10\%)$

---

[33]following [16]

a)

b)
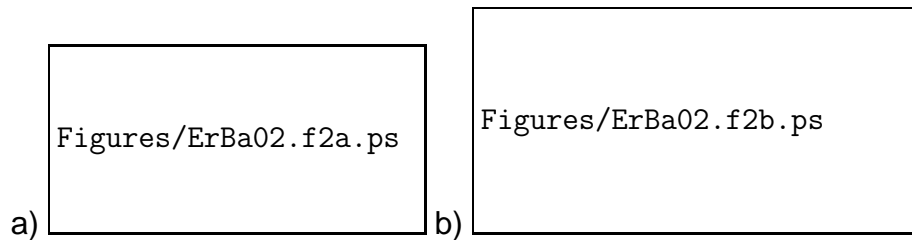
Figure 100: a) Set-up: three-dimensional image of a bar and simulated force feed-back from a bar of possibly different height. b) Stereoscopic image of bar without and with noise [16].

Theoretical treatment:

Assume independent Gaussian likelihoods for the visual and the haptic information

$$P_v(r_v|S) \quad \propto \quad \frac{1}{\sigma_v} e^{-\frac{(S-S_v)^2}{2\sigma_v^2}}$$

$$P_h(r_h|S) \quad \propto \quad \frac{1}{\sigma_h} e^{-\frac{(S-S_h)^2}{2\sigma_h^2}}$$

thus

$$P_{vh}(r_v, r_h|S) \propto \frac{1}{\sigma_v \sigma_h} e^{-\frac{(S-S_v)^2}{2\sigma_v^2}} e^{-\frac{(S-S_h)^2}{2\sigma_h^2}}$$

Assume a constant prior

$$P(S) = P_0$$

Posterior

$$P_{vh}(S|r_v, r_h) \propto P_{vh}(r_v, r_h|S) \, P_0$$

Note:

- Since the prior is constant:
  maximum a posteriori estimate (MAP) is equivalent to a maximum likelihood estimate (MLE)

Rewrite in terms of a single Gaussian

$$\frac{(S-S_v)^2}{\sigma_v^2} + \frac{(S-S_h)^2}{\sigma_h^2} = \frac{1}{\sigma_{vh}^2}(S - S_{vh})^2 + c_0$$

with

$$\frac{1}{\sigma_{vh}^2} = \frac{1}{\sigma_v^2} + \frac{1}{\sigma_h^2} \qquad \Leftrightarrow \qquad \sigma_{vh}^2 = \frac{\sigma_v^2 \sigma_h^2}{\sigma_v^2 + \sigma_h^2} \tag{58}$$

$$S_{vh} = w_v S_v + w_h S_h \qquad \text{with} \qquad w_v = \frac{\sigma_{vh}^2}{\sigma_v^2} \qquad w_h = \frac{\sigma_{vh}^2}{\sigma_h^2} \tag{59}$$

Note:

- if the uncertainty in the two responses is not equal, the response of the input that is less uncertain, i.e. with σ^2 smaller, is to be weighted more.

To test whether humans use MLE in this context one needs to know S_{vh} as well as S_v and S_h and the associated uncertainties, σ_v^2, σ_h^2, and σ_{vh}^2

Measure uncertainty via psychometric function:

- have subjects repeatedly compare the height of the test stimulus with that of comparison stimuli, which have various heights

- psychometric function $\Psi(S)$: relative frequency of the subjects ranking the comparison stimulus (variable height) to be higher than that of a test stimulus (height 55mm)

- point of subjective equality (PSE) = 50% level:

$$\Psi(S_{PSE}) = 0.5$$

- discrimination threshold $T_{v,h}$: $\Psi(S_{PSE} + T_{v,h}) = 0.84$
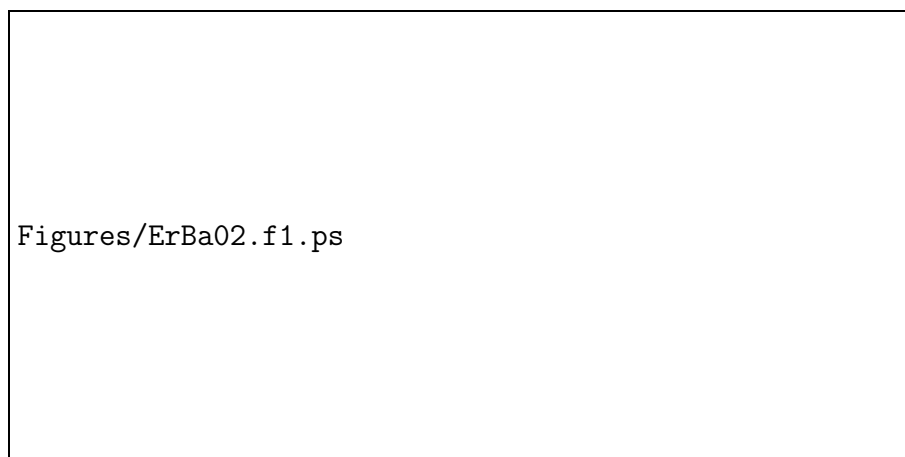
Figure 101: Sketch of the likelihoods (top) and of the psychometric function (bottom) for two values of the ratio σ_h^2/σ_v^2 with fixed discrepancy Δ between the visual and haptic bar height. Top: solid line gives estimated height based on combined information. Bottom: The psychometric function gives the fraction of trials in which the comparison stimulus (variable height) is perceived as higher than the test stimulus (fixed average height $\frac{1}{2}(S_v + S_h) = 5.5cm$) [16].

- the cumulative Gaussian (error function) gives a good fit of Ψ (Fig.102). For that function one has

$$T_{v,h} = \sigma_{v,h}$$

this determines the individual σ_h^2 and σ_v^2 for the different noise levels in the visual input.

Figures/ErBa02.f3a.ps
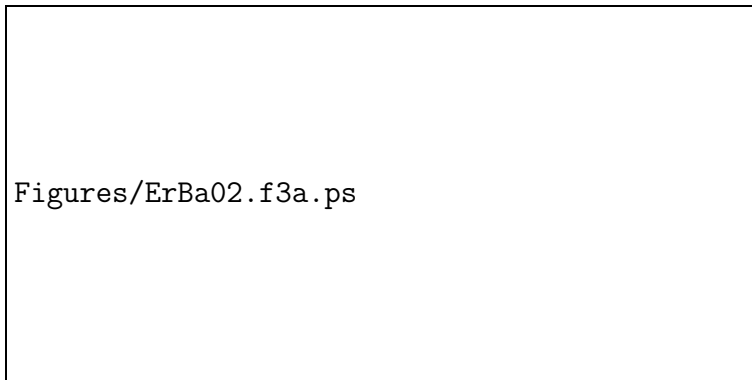
Figure 102: Measured psychometric function for estimates based on haptic or visual information alone (visual information corrupted by noise) [16]

Figures/ErBa02.f3b.ps
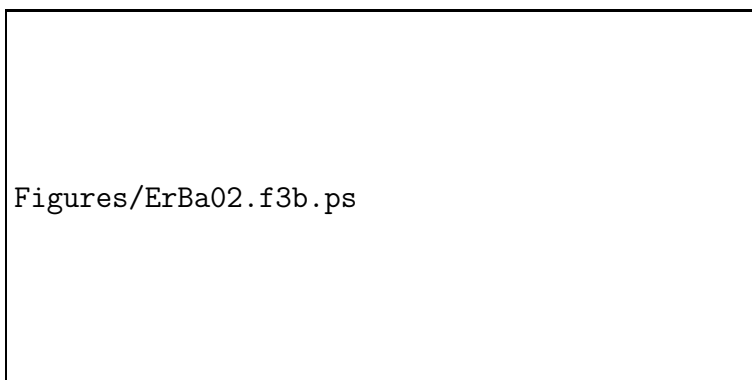
Figure 103: Noise dependence of the combined visual-haptic height estimate [16]

- the measured $\sigma_{v,h}^2$ give the theoretically optimal weights $w_{v,h}$ for the integration

$$w_v = \frac{\sigma_{vh}^2}{\sigma_v^2} \qquad w_h = \frac{\sigma_{vh}^2}{\sigma_h^2}$$

- experimentally determined weights from (59) using $w_h = 1 - w_v$

$$w_v = \frac{S_{vh} - S_h}{S_v - S_h}$$

- quite good agreement with the optimal weights (Fig.104)

Note:

- the weights must adjust within the 1 second of the presentation, since noise levels vary random from one presentation to the next.

```
Figures/ErBa02.f3c.ps
```
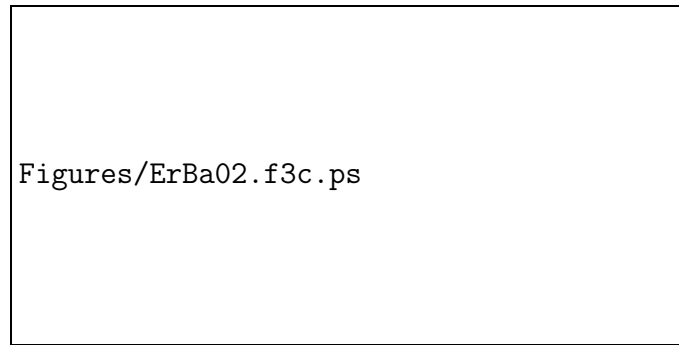
Figure 104: Measured and MLE-optimal weights entering the combined estimate as a function of noise level [16]

- integration of visual and haptic information reduces the variance (58), which lowers the threshold for discrimination ($T_{vh} = \sigma_{vh}$)

```
Figures/ErBa02.f3d.ps
```
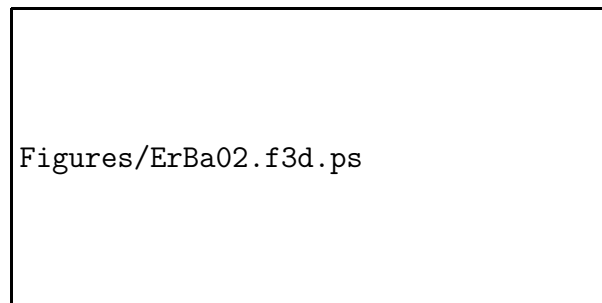
Figure 105: The threshold for combined visual-haptic height discrimination is lower than each individual threshold [16].

Not quite class-appropriate example of an illusion arising from the merging of unreliable auditory with precise, but incorrect visual information
http://www.youtube.com/watch?v=7-ZnPE3G_YY

List of Figures

A   Basic Concepts of Numerical Methods for Differential Equations

Consider differential equations of the type

$$\frac{d\mathbf{y}}{dt} = \mathbf{F}(t, \mathbf{y}) \qquad \mathbf{y}(t = 0) = \mathbf{y}_0$$

In general $\mathbf{y}$ is a vector: coupled equations.

Note:

- all higher-order equations can be written as systems.
  E.g.

$$\frac{d^2 y}{dt^2} = F(t, y, \frac{dy}{dt})$$

  can be written as

$$\frac{dy}{dt} = v$$
$$\frac{dv}{dt} = F(t, y, v)$$

For simplicity we consider scalar equations

$$\frac{dy}{dt} = F(t, y)$$

For numerical approximation *discretize* time

$$y_n \equiv y(t_n)$$

We need then

For small time steps Δt we can perform a Taylor expansion

$$
\begin{aligned}
y_{n+1} &= y(t_n + \Delta t) = \\
&= y(t_n) + \Delta t \left. \frac{dy}{dt} \right|_{t_n} + \frac{1}{2} \Delta t^2 \left. \frac{d^2 y}{dt^2} \right|_{t_n} + \dots
\end{aligned}
$$

We cannot keep all terms in the expansion: truncate

$$y_{n+1} = y_n + \Delta t\, F(t_n, y_n) + \mathcal{E}_{local}(\Delta t, t_n) \tag{60}$$

where the error $\mathcal{E}_{local}(\Delta t, t_n)$ contains all the omitted terms.

This is the *forward Euler*[34] *scheme.*

Expect

$$\mathcal{E}_{local}(\Delta t, t_n) = \mathcal{O}(\Delta t^2) = a(t_n)\Delta t^2 + b(t_n)\Delta t^3 + \dots$$

Note:

---

[34]*Leonhard Euler (1707-1783)*

- in each time step the scheme makes an error $\mathcal{O}(\Delta t^2)$: this is the *local* error

- to obtain $y(t_{max}) = y(N\Delta t)$ we need to make N steps
  in these N steps the error could accumulate to a *global* error

$$\mathcal{E}_{global} = \sum_{n=1}^{N} \mathcal{E}_{local}(\Delta t, t_n) \approx \sum_{n=1}^{N} a(t_n)\Delta t^2 \approx N\bar{a}\Delta t^2 = \bar{a}t_{max}\Delta t$$

  expect that the error decreases *linearly* when Δt is increased.

- if $\mathcal{E}_{global} \to 0$ for $\Delta t \to 0$ a scheme is called *convergent*

- The Euler scheme is called a *first-order* accurate scheme.

- To obtain accurate solutions the Euler scheme requires very small Δt: slow.
  Higher-order schemes with $\mathcal{E}_{global} = \mathcal{O}(\Delta t^n)$ with $n = 2, 3, 4, ..$ can be much more efficient (faster) to obtain accurate solutions. Examples are Runge-Kutta, Crank-Nicholson, predictor-corrector,... [49]

Example:

$$\frac{dy}{dt} = \lambda y$$

with exact solution

$$\tilde{y}(t) = y(0)e^{\lambda t}$$

Note:

- for $\lambda < 0$ the solution decays to 0 for any initial condition

Euler scheme

$$y_{n+1} = y_n + \Delta t\, \lambda y_n = (1 + \Delta t\lambda)\, y_n = (1 + \Delta t\lambda)^2\, y_{n-1} = \ldots$$

i.e.

$$y_n = (1 + \Delta t\lambda)^n\, y(0)$$

Does this solution decay for any Δt if $\lambda < 0$?

$$|y_n| = |\,(1 + \Delta t\lambda)^n\,|\,|y(0)| = |\,(1 + \Delta t\lambda)\,|^n\,|y(0)|$$

Thus: the solution decays only if $|1 + \Delta t\lambda| < 1$,

$$-1 < 1 + \Delta t\lambda < +1$$

For $\lambda < 0$ this is only the case if

$$\Delta t < \Delta t_{max} \equiv \frac{1}{|\lambda|}$$

The forward Euler scheme has a *stability limit.*

For $\Delta t > \Delta t_{max}$:

- solution grows exponentially in magnitude with the number of time steps (although exact solution decays to 0)

- in each time step the solution switches sign

- the scheme is **unstable** for these large time steps: the numerical solution has nothing to do with the true solution of the differential equation.

Thus:

- the numerical solution of an equation can only be trusted if it converges as $\Delta t \to 0$ i.e. one has to solve the differential equation for sequentially smaller values of Δt and the solution is to change less and less as Δt becomes smaller and smaller

$$\mathcal{E}_{global} \sim \Delta t^p \qquad p = 1 \text{ for Euler}$$

$$\ln \mathcal{E}_{global} \sim p \ln \Delta t$$

  p is given by slope on log-log-plot. Always check whether the scheme obtains the correct slope over at least a decade in Δt

- unstable schemes typically generate solutions that oscillate with each time step *independent* of the size of the step:
  halving the time step doubles the frequency of the oscillations

- any oscillation that corresponds to a true solution of the differential equation will have a period that is

  - independent of Δt for small Δt
  - significantly larger than Δt (to resolve an oscillation one needs on the order of 10 time steps/period).

Choice of time step:

- accuracy: time step needs to be small enough to resolve fastest change in the true solution

- stability: scheme needs to remain stable

Stiff problems:

- true solution evolves on a slow time scale: would allow large Δt

- system has very rapid modes that decay and are not visible in the final solution: requires small Δt

Example (see homework):

$$\frac{dy}{dt} = \lambda y + A \sin \omega t \qquad \lambda < 0 \qquad |\lambda| \gg \omega$$

after a rapid decay during a time $1/|\lambda|$ the solution evolves slowly with frequency ω.

In the Taylor formula expand around t_{n+1}

$$y_n = y_{n+1} - \Delta t \left. \frac{dy}{dt} \right|_{t_{n+1}} + \mathcal{O}(\Delta t^2)$$

yielding the scheme

$$y_{n+1} = y_n + \Delta t \, F(y_{n+1}, t_{n+1}) \tag{61}$$

This is the *backward Euler* scheme, which is also first-order accurate.

In our simple *linear* example we get:

$$y_{n+1} = y_n + \Delta t \lambda \, y_{n+1}$$

which is easily solved for y_{n+1}

$$y_{n+1} = \frac{1}{1 - \Delta t \lambda} y_n$$

Consider magnitude of the solution

$$|y_n| = \frac{1}{|1 - \Delta t \lambda|^n} |y(0)|$$

thus, $|y_n| \to 0$ with $n \to \infty$ for *arbitrarily* large values Δt if $\lambda < 0$.

The backward Euler scheme is *unconditionally stable.*

Note:

- of course, for very large Δt the solution may not be very accurate, but no instability will arise.

- choice of time step purely based on the desired accuracy of the solution.

But:

- the scheme (61) is *implicit*:
  the unknown y_{n+1} appears also on the right-hand side inside the function $F(y, t)$
  the equation is an implicit equation for y_{n+1}, which may be difficult to solve if $F(y, t)$ is nonlinear in y.

- implicit schemes typically require additional effort (e.g. Newton iteration method for solving the nonlinear equation)

For more details about numerical schemes see, e.g. *Numerical Recipes* [35]*[49]* or the lecture notes for *ESAM 346 Modeling and Computation in Science and Engineering*[36]
.

---

[35] *Numerical Recipes* $http://www.nr.com$

[36] ESAM 346 Modeling and Computation in Science and Engineering `http://people.esam.northwestern.edu/~riecke/Vorlesungen/346/Notes/notes.346.pdf`

B Linear Response Kernel using Functional Derivatives

In a more fancy fashion the optimal kernel describing the linear linear response of a neuron can be derived using *functional derivatives* (cf. Sec.6.2.2).

E is a *functional* of $D(\tau)$

$$E\{D(\tau)\} = \frac{1}{T} \int_0^T \left(r_0 + \int_0^\infty D(\tau)s(t'-\tau)d\tau - r(t') \right)^2 dt'$$

For functions minima are characterized by a vanishing derivative. Analogously, minima of functionals can be found elegantly by using the *functional derivative.* One can avoid the explicit use of functional derivatives by converting the integral into a sum (see Appendix 2.9A in [10])

At a minimum the functional derivative vanishes

$$\frac{\delta E\{D(\tau)\}}{\delta D(\tau)} = 0$$

Basic property of functional derivatives

$$\frac{\delta D(\tau)}{\delta D(\tau')} = \delta(\tau - \tau') \qquad \text{Dirac } \delta - \text{function}$$

In short, this is analogous to

$$\frac{\partial x}{\partial x} = 1 \qquad \frac{\partial y}{\partial x} = 0$$

or for a function that depends on the components v_i of a vector one has

$$\frac{\partial v_i}{\partial v_j} = \delta_{ij}$$

Using this basic property

$$
\begin{aligned}
\frac{\delta E\{D(\tau)\}}{\delta D(\tau')} &= \frac{1}{T} \int_0^T \frac{\delta}{\delta D(\tau')} \left(r_0 + \int_0^\infty D(\tau)s(t'-\tau)d\tau - r(t') \right)^2 dt' \\
&= \frac{1}{T} \int_0^T \left\{ 2 \left(r_0 + \int_0^\infty D(\tau)s(t'-\tau)d\tau - r(t') \right) \cdot \right. \\
&\qquad \left. \cdot \int_0^\infty \left(\underbrace{\left(\frac{\delta}{\delta D(\tau')} D(\tau) \right)}_{\delta(\tau-\tau')} s(t'-\tau) \right) d\tau \right\} dt' \\
&= \frac{2}{T} \int_0^T \left(r_0 + \int_0^\infty D(\tau)s(t'-\tau)d\tau - r(t') \right) s(t'-\tau')dt' \\
&\overset{!}{=} 0 \quad \text{at a minimum}
\end{aligned}
$$

NOTES:

- discuss also some of the networks stuff in Rolls&Treves (good for homework simulations and to get a feeling for these kind of networks)

- check out book by Trappenberg (Tr09)[58]

- look at book by Cox (GaCo10)[19]

- also Ermentrout and Terman [15]

- include also population coding: Fisher information etc.

- other simple spiking models in addition to Izhikevich (e.g. Gerstner: Badel 2008). Put something like that in the homework? Fit things.

- LNP and GLM (i.e. LNP with feedback of spike history for refractory effects). cf. Alonso paper DeJi10